AN ELECTRON-DIFFRACTION INVESTIGATION OF THE MOLECULAR STRUCTURE OF GASEOUS PENTAFLUOROSULFUR HYPOFLUORITE (SOF_6)

by

ROGER ALLEN CRAWFORD

A THESIS

submitted to

OREGON STATE COLLEGE

in partial fulfillment of
the requirements for the
degree of

DOCTOR OF PHILOSOPHY

June 1959

APPROVED:

Redacted for Privacy

Assistant Professor of Chemistry

In Charge of Major

Redacted for Privacy

Chairman of Department of Chemistry

Redacted for Privacy

Chairman of School Graduate Committee

Redacted for Privacy

Dean of Graduate School

Date Thesis is presented June 12, 1958

Typed of Lilah Potter

ACKNOWLEDGEMENT

These studies were carried out under the guidance of Dr. Kenneth W. Hedberg. I wish to thank Dr. Hedberg for the invaluable assistance, constructive suggestions and encouragement given me during the course of this research project. I am also indebted to Drs. Schomaker and Sturdivant of California Institute of Technology and Dr. S. Crane of G. M. Gianini Company for the information given me concerning the power supply. Lastly, I wish to thank my wife for her continued patience and encouragement throughout this research project.

TABLE OF CONTENTS

LIST OF FIGURES

LIST OF FIGURES - Cont.

AN ELECTRON-DIFFRACTION INVESTIGATION OF THE MOLECULAR STRUCTURE OF GASEOUS PENTAFLUOROSULFUR HYPOFLUORITE (SOF_6)

INTRODUCTION

The diffraction of electrons has constituted one of the most powerful methods for investigations of the structure of gaseous molecules. This method has had the advantage of a simple experiment giving, for simple molecules, accurate measures of interatomic distances in a relatively short time. The first paper (by Wierl) describing the technique appeared in 1931 (29, p. 521-564); included were results for twenty compounds. This was followed, in the next nine years, by reports on over one hundred fifty substances (24, p. 296-301). Such activity, of course, rapidly depleted the number of simple molecules of unknown structure, and in very recent years effort has been given to improving the experiment and through the improved data (both quality- and quantity-wise) to studies of dynamic properties of molecules and to even more accurate determinations of molecular geometries. Allen and Sutton (1, p. 46-72) have compiled data giving interatomic distances and molecular structure for many compounds that have been studied using gaseous electron diffraction.

An electron-diffraction apparatus of advanced design is currently under construction at this college. The diffraction unit itself (comprising the diffraction chamber, electron gun, pumping system, and miscellaneous apparatus) is being designed by Dr. Hedberg and the regulated high-voltage power supply has been constructed by this author. The power supply is similar to the one now in operation at the California Institute of Technology; however, our unit has several design modifications which make it more versatile. The power supply is discussed in this thesis.

This thesis gives an account of the investigation of the compound pentafluorosulfur hypofluorite (SOF_6) which was prepared by Dudley, Cady and Eggers (12, p. 1553-1556). The diffraction data for this compound were gathered by Dr. Hedberg using the California Institute of Technology apparatus. The last part of this thesis describes the programming of the Alwac III-E digital computer for the lengthy calculations necessary in structural analysis by gaseous electron diffraction.

SERIES REGULATED POWER SUPPLY

The series-regulated power supply has the function of delivering a maximum of 30 milliamperes at approximately -50 kilovolts d-c and was designed to regulate this voltage to ± 25 volts. This highly regulated output, used as the supply for the electron gun in the diffraction apparatus, will produce an electron beam of essentially constant wavelength necessary for accurate diffraction work.

The block diagram shown in Figure I is a schematic representation of the power supply. In order to render this overall discussion more meaningful, the functions of these components are first described briefly, later followed by constructional details and a more complete account of their operation.

The control panel serves three main functions. These are 1) to supply power to electron tubes in the various units, 2) to supply power to the high-voltage transformer after a short time delay which permits the electron tube filaments to come to operating temperature and, 3) to act as a safety device such that if something goes wrong, for example a short circuit, the entire system will shut off. The second function protects the kenotrons and series-regulator tube against high voltage

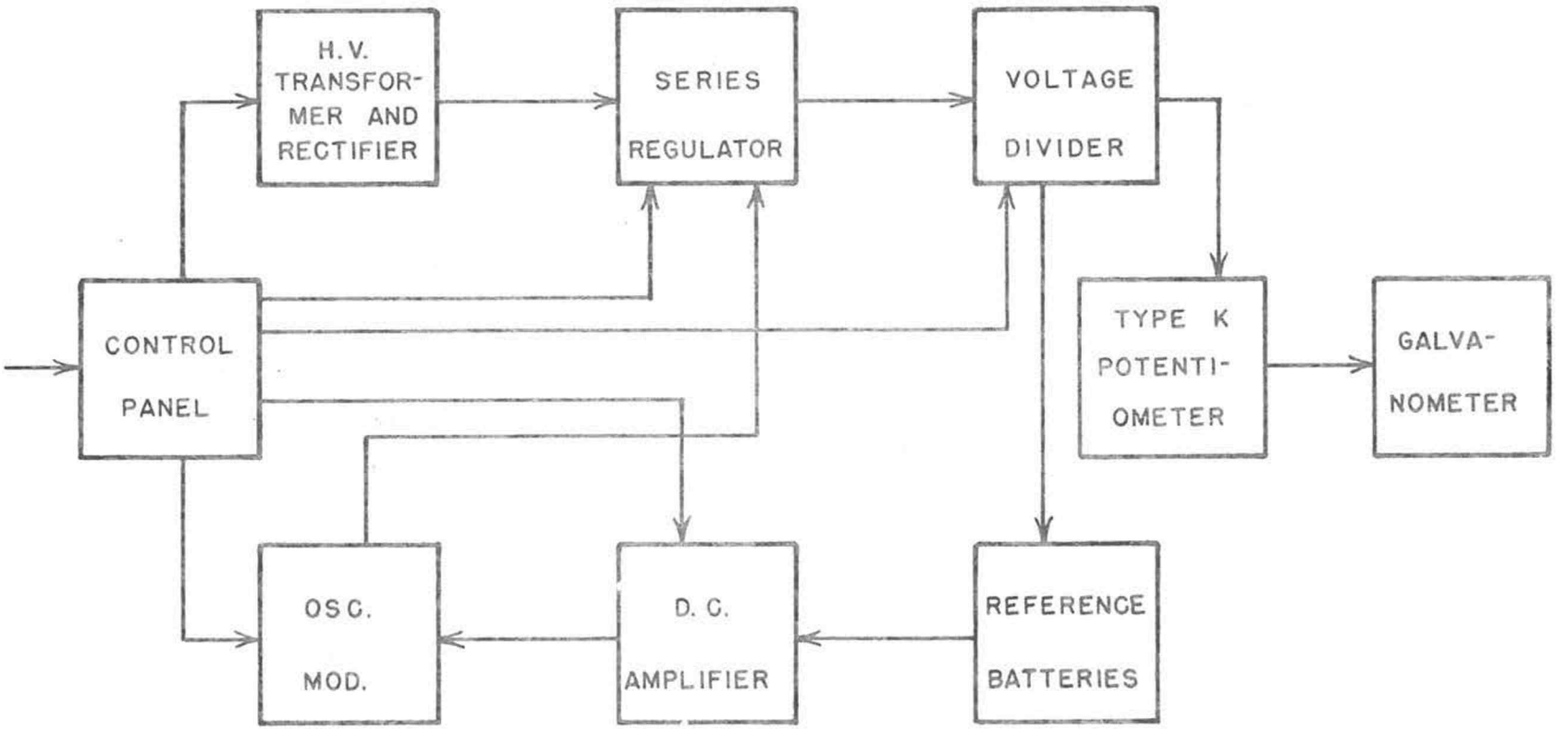

FIGURE I

BLOCK DIAGRAM

SERIES REGULATED POWER SUPPLY

discharge and the third function protects the power supply as a whole against excessive loads.

The high-voltage transformer and rectifier has the sole purpose of converting the 220 volts a-c to pulsating d-c at -50,000 volts. These are the maximum input and output voltages.

The series-regulator must convert the pulsating d-c to a filtered low per cent ripple d-c. Also, in conjunction with the other blocks, it must maintain the output at a constant d-c level under varying load conditions.

The voltage divider samples the output voltage and directs this sampled voltage two places. One destination is a potentiometer which compares the sample with a standard cell and relays this difference signal to a galvanometer to permit visual observation of voltage variations. The sample voltage is also compared with reference batteries and any variation is impressed on the D.C. amplifier as an error signal. The voltage divider could be called the detector in the feedback loop.

The reference batteries comprise nine 0-22½-45 volt d-c dry cells connected in series.

The D.C. amplifier is a conventional high-gain amplifier and serves only to greatly amplify the error

signal.

The oscillator-modulator has the function of transforming the d-c error signal to an r-f error signal. This r-f error signal is communicated to the series-regulator tank where the actual correction of the error takes place.

CONTROL PANEL

Figure II is a simplified wiring schematic of the control panel, Figures III and IV are wiring diagrams and Table I is a component list. The following discussion will be restricted to Figure II where A and C are the 'hot' leads, N is neutral and G is chassis ground.

When the master wall switch (not shown) is thrown, power is available at the upper left two contacts of relay 1 and at the main power switch through a safety device, the water interlock switch. This device assures that sufficient water is flowing through the cooling coils of the diffusion pumps operating the diffraction unit: failure of the water circulation shuts off the power supply. When the main power start button is depressed, the neon light is lighted and the coil of relay 1 is actuated. Since the lower contacts of the main power switch have continuity until the stop button

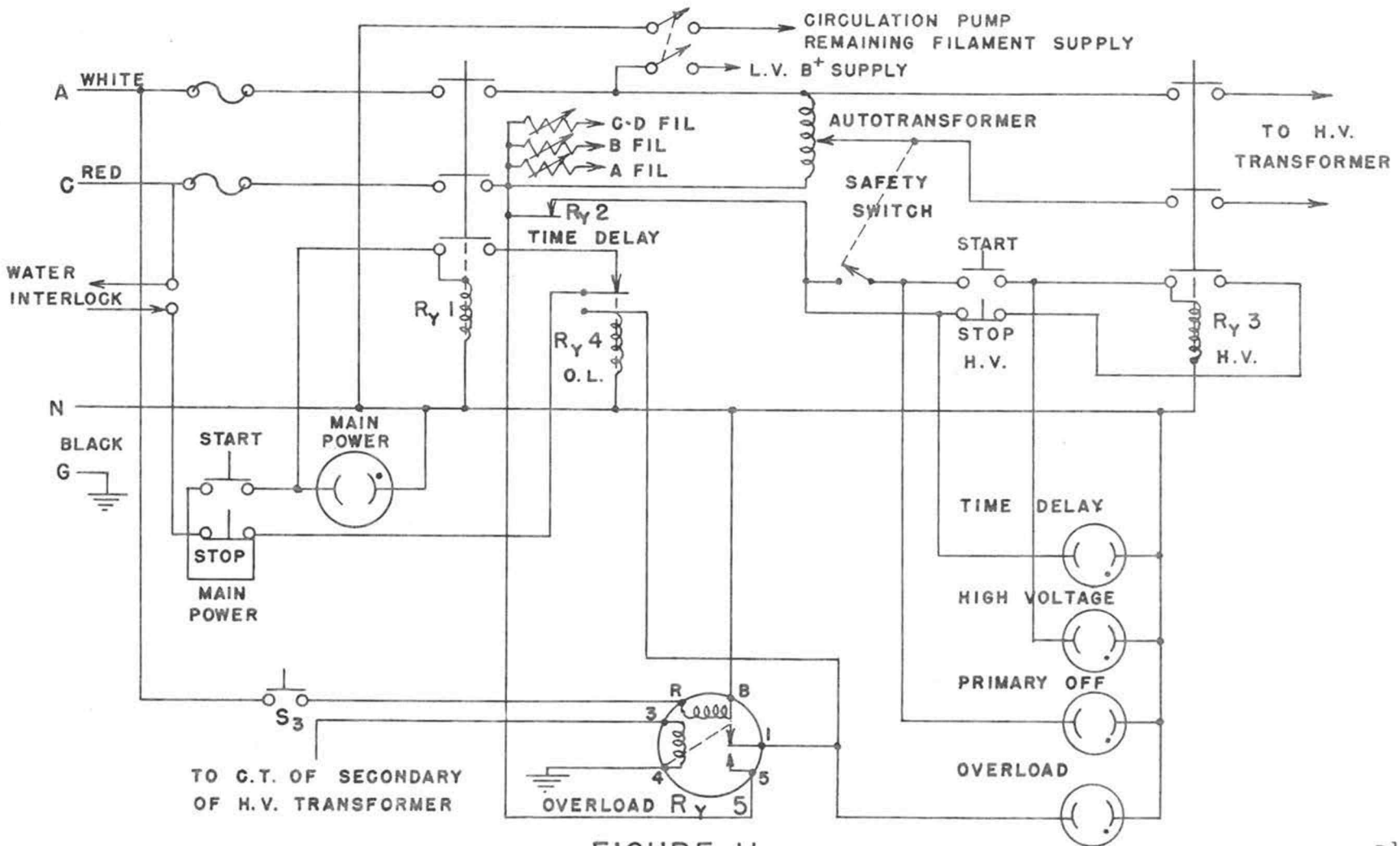

FIGURE II

CONTROL PANEL - STATIC STATE

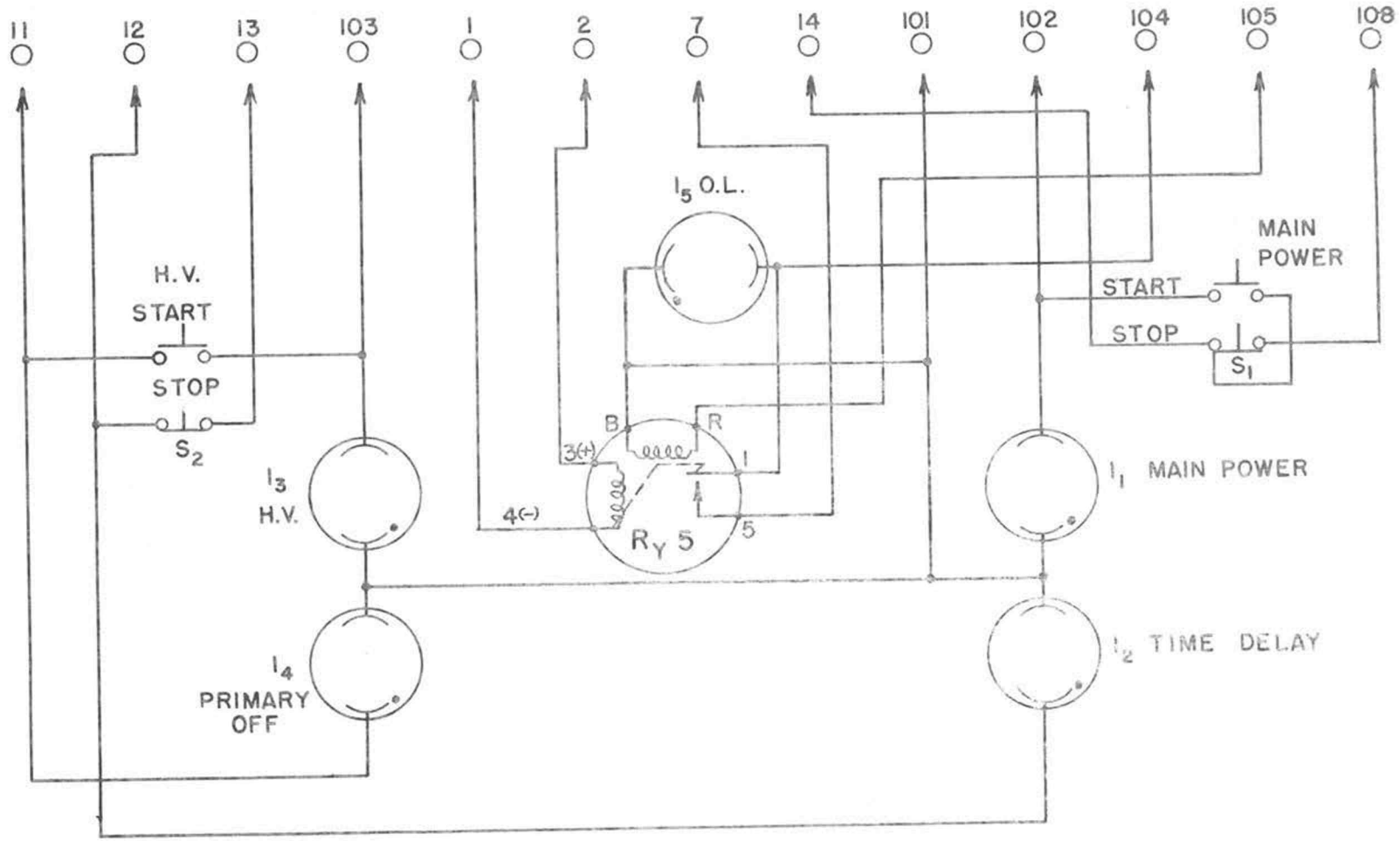

FIGURE III
CONTROL PANEL - FIRST DECK

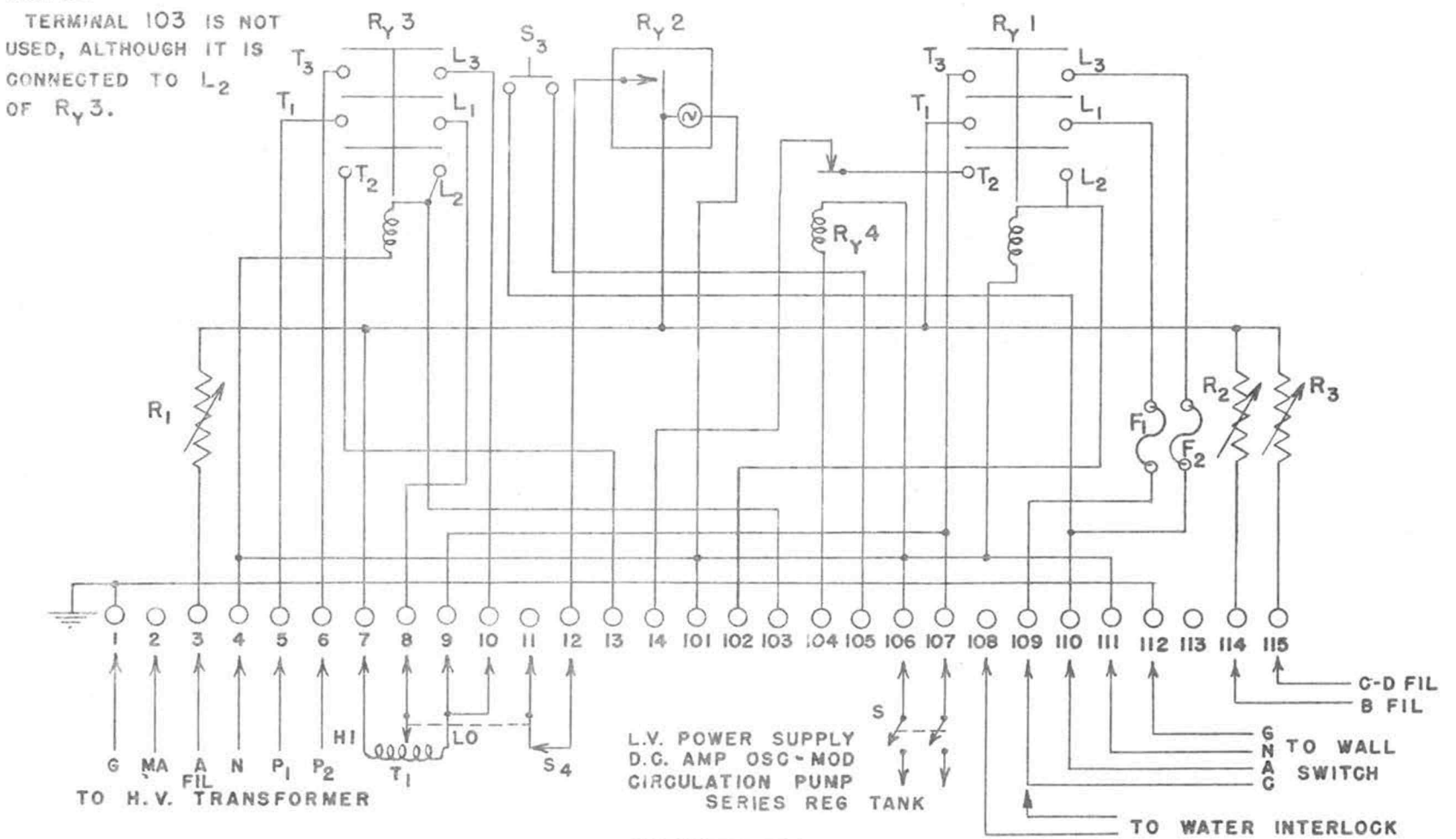

FIGURE IV

CONTROL PANEL - SECOND DECK

TABLE I

PARTS LIST FOR CONTROL PANEL

Item	Description	No. Needed
F_1	Fuse, cartridge, 15 amp. 250 volt a-c.	1
F_2	Fuse, cartridge, 10 amp. 250 volt a-c.	1
I_1, I_2, I_3 I_4, I_5	Neon glow lamp, NE-45, $\frac{1}{4}$ watt, 110 volts a-c.	5
R_1, R_2	Resistor, adjustable power, wire wound, 10 ohms, 100 watts.	2
R_3	Resistor, adjustable power, wire wound, 4 ohms, 100 watts.	1
Ry_1, Ry_3	Contactor, Square D, class 8502, type C01, series A, 110 volts a-c coil, 2P. with holding contacts	2
Ry_2	Cramer time delay, type 330, S.P. maximum time 80 seconds, 115 volts a-c, 60 cps.	1
Ry_4	Relay, Guardian, series 200, 115 volts a-c, SPDT, N.C.	1
Ry_5	Relay, Weston Sensitrol, model 705 type 5, 0-30 ma. make contact on increasing current, solenoid 120 volts a-c.	1
S_1, S_2	Station, push button, Square D, class 9001, type BB-4, 110 volts a-c, 60 cps.	2
S_3	Switch, push button, Mallory no. 2001, SPST, N.O. non-locking.	1
S_4	Micro-switch, $\frac{1}{2}$ amp. at 115 volts a-c (physically located on auto-transformer).	1

TABLE I - Cont.

Item	Description	No. Needed
S_5	Switch, DPDT, 15 amps. 125 volts a-c.	1
T_1	Autotransformer, Powerstat, type 236, panel mount, 2.2 KVA. (physically located directly below control panel).	1

is depressed, relay 1 remains actuated (via relay 4) after releasing the start button. The actuation of relay 1 closes three sets of contacts through which power is supplied to the filaments of various tubes (the rectifier tubes or kenotrons, tubes in the series-regulator circuitry, the D.C. amplifier and oscillator-modulator), to the low-voltage d-c power supplies, and to the circulation pump located in the voltage divider tank. After about 40 seconds, the time delay (relay 2) is closed allowing power to go to the safety switch located on the autotransformer and to the lower right contact of relay 3. The safety switch is a device which prevents actuation of the high voltage start switch unless the autotransformer setting corresponds to zero output. Were it possible to throw the high-voltage start switch with the autotransformer at an arbitrary setting, damagingly large surge currents might result. When the autotransformer setting corresponds to zero output, the high-voltage start button can actuate relay 3 and power becomes available to the high-voltage transformer. Once relay 3 is actuated, the safety switch is by-passed. Another safety device which has been incorporated is the overload meter and relay which protects the power supply against excessive d-c loads. The actuating coil is connected to the center tap of the high-voltage transformer,

requiring all d-c current through one-half of the high voltage transformer to go through the meter. If current becomes excessive, pin 1 and pin 5 of the overload meter (relay 5) are shorted together and 110 volts a-c are applied to relay 4. When relay 4 actuates, continuity to relay 1 is broken and the system is turned off. The overload meter will remain in shorted condition until the restoring switch, S_3, is pushed.

In order to increase the versatility of the power supply a pair of switches have been incorporated in the control unit which enable the output to be taken as regulated or unregulated. When an unregulated output is desired (such as is often the case when an x-ray tube is being powered) power to the unnecessary voltage divider, series-regulator, D.C. amplifier, and the oscillator-modulator may be interrupted by DPST switch S_5. Another switch (not shown) effectively by-passes the water interlock: it is then unnecessary to have water flowing in the diffusion pumps of the electron-diffraction apparatus.

TRANSFORMER-RECTIFIER

The transformer-rectifier unit used in this power supply is a Standard X-Ray Company unit modified by the author to meet the varying use requirements. These

modifications amount to changing the standard Gratz four-valve full-wave rectifier circuit employed in the original unit (Figures V and VI) to a two-tube full-wave end-grounded circuit. A simplified schematic of the altered rectifier circuit is shown in Figure VII. The original circuit was capable of delivering an output of 100 kilovolts at 200 milliamperes with a 220 volt a-c, 60 cps, single-phase input. The principal components of the unit are the high voltage diodes or valves ("kenotron" is the General Electric Co. trade name) with their filament transformers, and the high-voltage transformer. The filaments of the valves require about 12-14 amperes at 12 volts for proper operation and the elements of the tubes are spaced to prevent any significant conduction at peak inverse voltages of the order of 140 kilovolts. The valve filament transformers are rugged devices carrying primary-secondary insulation sufficient to withstand peak inverse voltages from the high-voltage transformer. One of these is designed to supply two valves, two others each one valve; a fourth transformer is present in the tank and was used originally to supply the filament of an x-ray tube. (This transformer may be used with an x-ray tube in the rewired set-up also, but its output measured to be 12 volts at 110 volts input, will

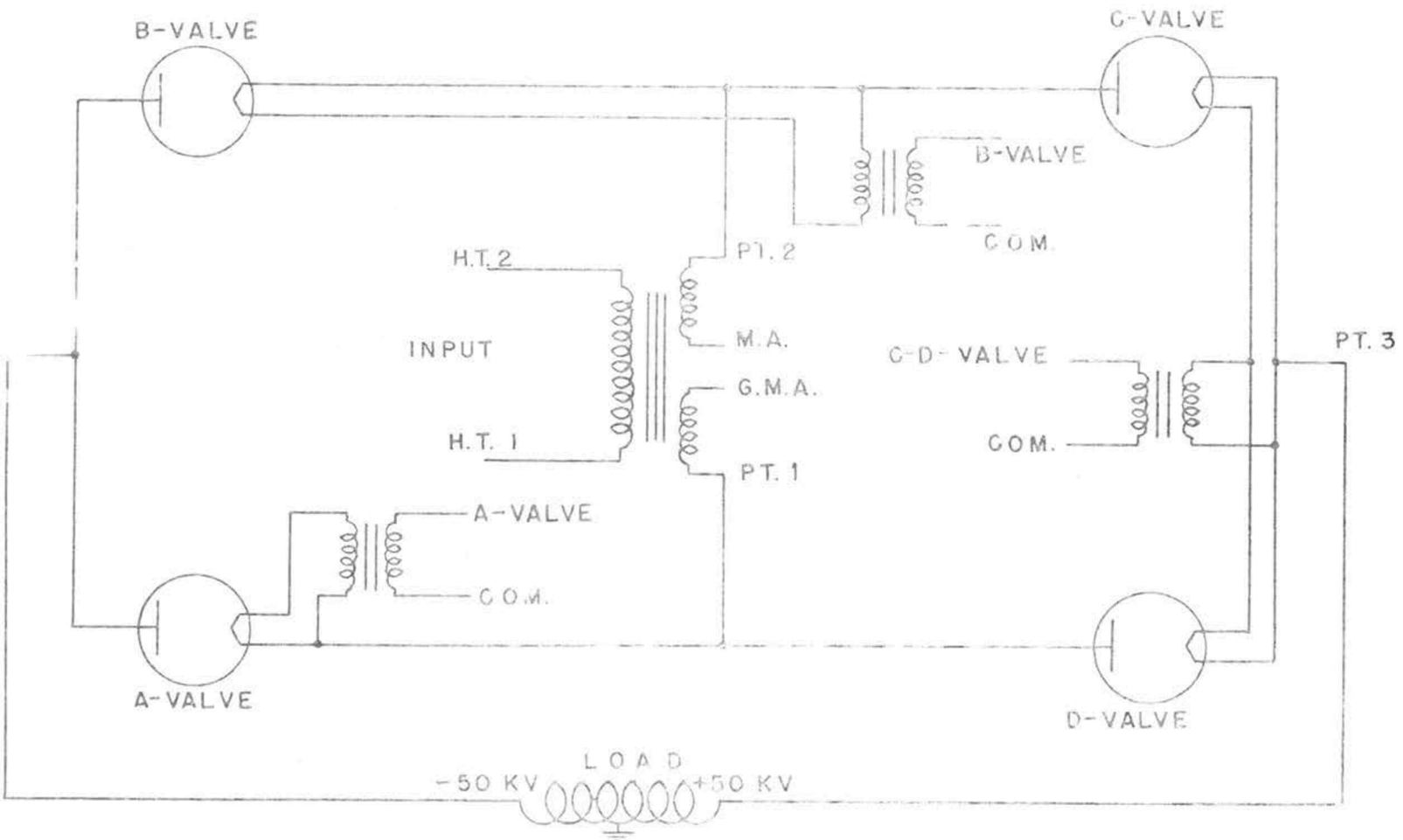

FIGURE V
SIMPLIFIED ORIGINAL CIRCUIT

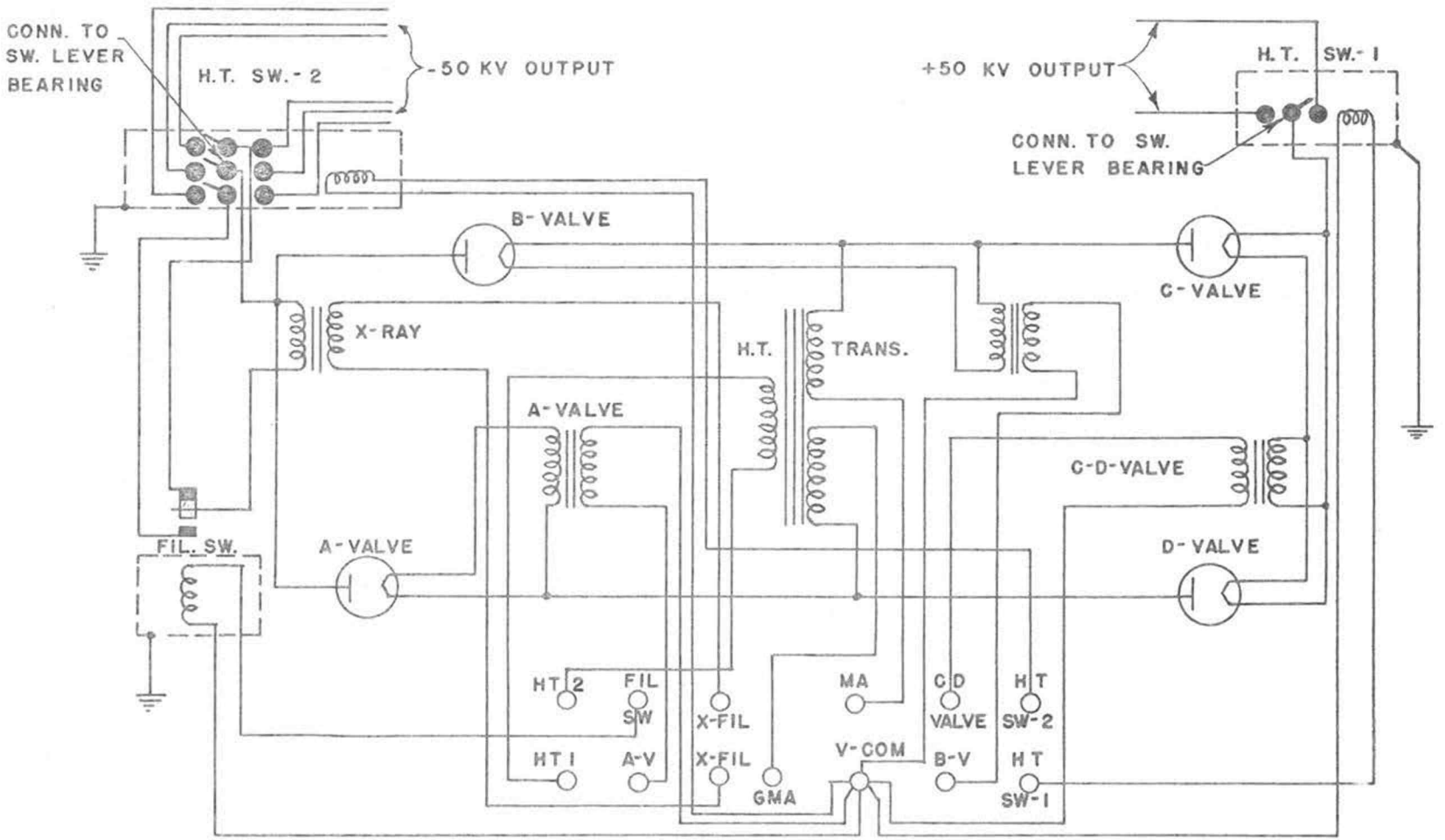

FIGURE VI

X-RAY TRANSFORMER - WIRING DIAGRAM

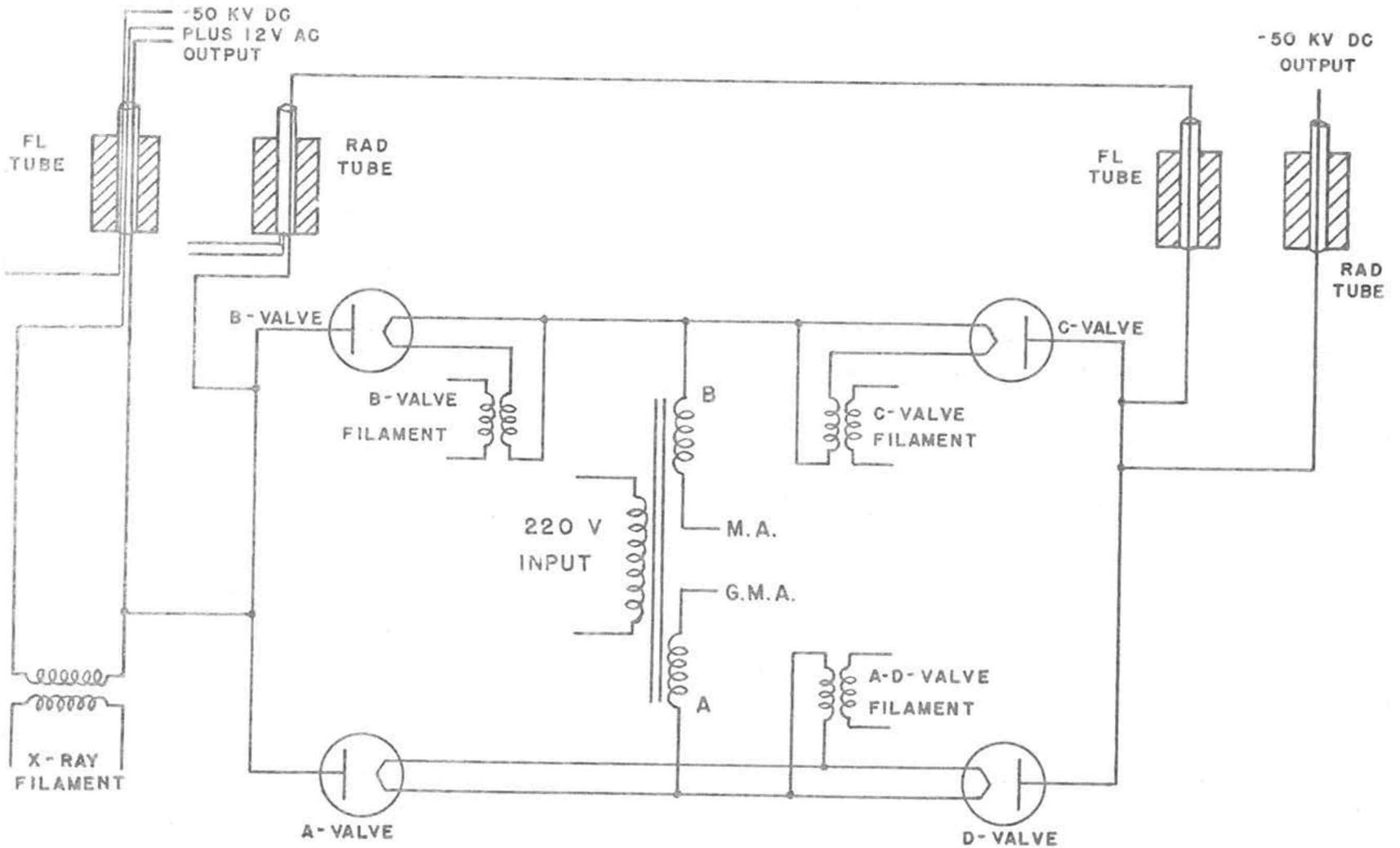

FIGURE VII
MODIFIED X-RAY TRANSFORMER

first have to be modified with a resistor or auto-transformer in order to correspond to the 6 volt requirement of modern x-ray tubes.) The high voltage transformer is a single-phase iron core device with a center-tapped secondary which is usually grounded to the tank. The transformer output in the original circuit was thus ± 50 kilovolts with respect to ground.

The details of the rewiring are as follows. First, the anode and filament clamps were reversed for the C- and D-valves so that all filaments are now connected to the high-voltage transformer. Second, the filament transformer which operated the C- and D-valves in the Gratz circuit was rewired to supply the A- and D-valves, this pair being chosen instead of the B- and C-valve pair only because of convenience of location. (Physically this was accomplished by taking one lead from the filament transformer secondary over the high voltage transformer, and by connecting the second to the high voltage transformer output terminal: that is, the metal plate which surrounds the transformer.) Third, the original B-valve filament transformer was converted to supply the C-valve by connecting the non-common lead of the secondary to the non-common side of the C-valve filament. Fourth, the output leads of the original A-valve transformer were connected to the B-valve filament. These

leads, incidentally, had to be carefully positioned to avoid danger of shorting the high voltage transformer secondary. Lastly, a change was made with respect to the output leads of the transformer-rectifier unit. The two output leads of the original circuit were converted to a common output by use of an external high-voltage cable and two of the four bushings (see Figure VII); the external connection was made necessary by the spacing limitations inside the tank.

The top of the transformer-rectifier tank contains thirteen low-voltage terminals, two of which are inoperable in the rewired set-up; high-tension switches 1 and 2 (H.T. Sw. 1 and H.T. Sw. 2) are now used only in their normal positions. These switches should not be confused with high-tension terminals 1 and 2 (H.T. 1 and H.T. 2) which are the 220 volt a-c input terminals. The position of the filament switch (Fil. Sw.) is of no significance. Comparing Figures II and IV with Figure VI, it is seen that the original filament transformer designation is still retained thus conforming with the terminal designation on top of the transformer-rectifier tank. This was done to simplify the inter-unit wiring procedure.

The operation of the rewired unit may be described briefly. The center tap of the secondary of the high-voltage transformer is at ground potential (via the

overload milliammeter) so that valve pairs A and D, and B and C stand at voltages 180° out of phase. These valve pairs are made conducting only when their filaments are at negative potential with respect to their plates, a circumstance achieved 60 times per second. Since both halves of the input signal are used, the output is full-wave rectified with a 120 cps ripple. Maximum rms output voltage is about -50 kilovolt with respect to ground. This type of circuit has aptly been termed a voltage-halving circuit (27, p. 137-138).

OSCILLATOR-MODULATOR

The purpose of the oscillator-modulator is to convert a d-c error signal to an r-f error signal. Figure VIII is a simplified schematic of the Hartley shunt feed circuit used. The Hartley oscillator is very good for this purpose in that the circuit elements are not critical (8, p. 487-491). This circuit employs a single LC tuned tank (C_1 and L_1) and the 180 degree phase requirement is obtained by connecting the grid to one end of the tank and the plate to the other. L_2 is the shunt and is a radio frequency choke which has a low d-c resistance and a high r-f impedence. C_3 is a by-pass capacitor which blocks the d-c path to the cathode. This capacitor must be large enough to offer low impedence to

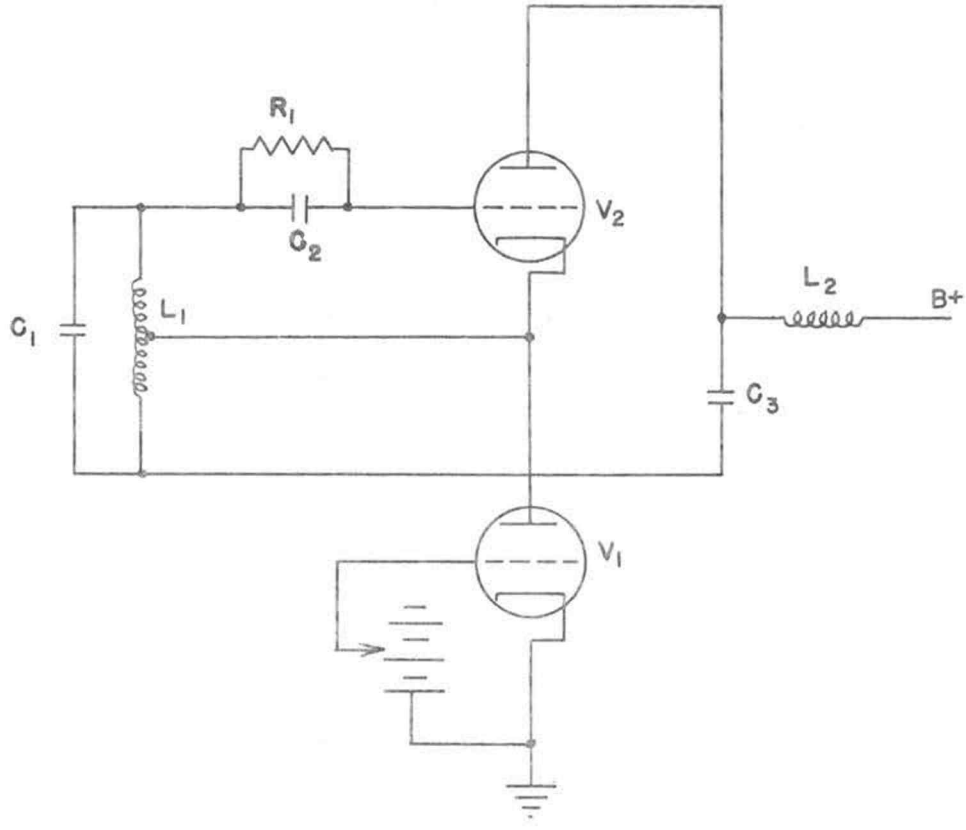

FIGURE VIII

HARTLEY SHUNT
FEED OSCILLATOR

the r-f signal. Resistor R_1 provides self bias for tube V_2 and C_2 is the usual capacitor in the grid circuit to couple the r-f signal to the grid. The Hartley oscillator does suffer from one disadvantage. Since there is no low impedence path to the cathode, the output becomes non-sinusoidal in strongly oscillating circuits, that is, contains harmonics.

If tube V_1 were removed from the circuit and the cathode of V_2 grounded (see Figure VIII), the oscillator would oscillate with a constant amplitude; however, its purpose is instead to provide a variable amplitude which is a direct function of the error signal. V_1 then serves as the current regulator for V_2, the current through V_1 being determined by the bias on V_1. If the bias on V_1 is increased (that is, the grid becomes more negative with respect to the cathode), the current through V_1 and series connected V_2 decreases. The decreased current in V_2 is followed by a proportional decrease in the amplitude of the r-f signal. Similarly, decreased bias on V_1 is followed by an increased r-f signal amplitude. Figure IX is the wiring diagram of the oscillator-modulator and Table II is a list of the components.

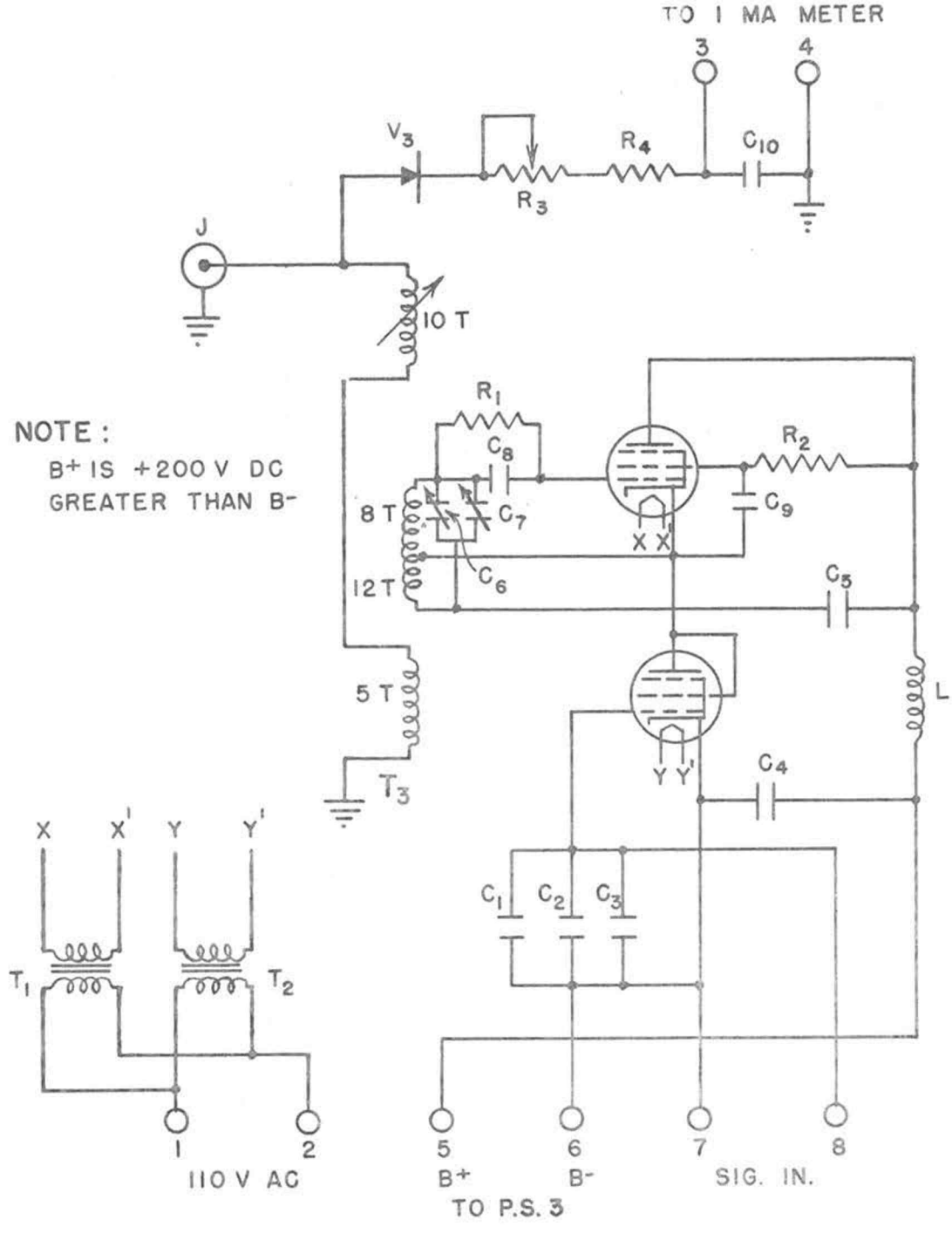

FIGURE IX

OSCILLATOR- MODULATOR

TABLE II

COMPONENTS FOR OSCILLATOR-MODULATOR

Item	Description	No. Needed
C_1,C_2	Capacitor, oil dielectric, 10 mfd., 1000 V.d-c	2
C_3	Capacitor, oil dielectric, 4 mfd., 1000 V.d-c	1
C_4,C_5,C_9	Capacitor, paper, 0.01 mfd.	3
C_6	Capacitor, air, variable, 140 mmfd.	1
C_7	Capacitor, air, variable, 250 mmfd.	1
C_8	Capacitor, paper, 500 mmfd.	1
C_{10}	Capacitor, paper, 0.001 mfd.	1
J	Receptacle, coaxial, type N. Amphenol no. 82-24	1
R_1	Resistor, composition, 27 K ohms, 2 watt	1
R_2	Resistor, w.w. 10 K ohms, 20 watts	1
R_3	Potentiometer, w.w. 10 K ohms	1
R_4	Resistor, composition, 43 K ohms, 2 watt	1
T_1,T_2	Transformer, filament, Thordarson 21F10	2
T_3	Transformer, primary- 2¼ inch diameter, 20 turns tapped at 8 turns, 18 wire. secondary- 2¼ inch diameter, 5 turns in series with 10 turns wound on 1⅛ inch cylinder, 18 wire	1
V_1,V_2	Tube, electron 6L6	2

TABLE II - Cont.

Item	Description	No. Needed
V_3	Tube, germanium diode, Kemtron 1N60	1
PS 3	Lambda regulated power supply, model 28 200-325 V.d-c, 0-100 ma.	1

DIRECT-COUPLED AMPLIFIER

The D.C. amplifier is a simple high-gain amplifier and since the circuitry is so basic it will not be discussed. The source of the d-c voltage to this unit, as well as the oscillator-modulator, is two Lambda power supplies. Figure X is the wiring diagram and Table III is a list of components.

VOLTAGE DIVIDER

The voltage divider has the task of accurately sampling the output voltage. It consists of a bank of precision resistors, connected in series, with a total resistance of 50 megohms. Figure XI shows the wiring diagram and Figure XII is a photograph of the set-up. Incorporated in the voltage divider tank is a stirring motor to assure uniform temperature throughout. It can be assumed that the temperature-resistance coefficient of each resistor is the same; therefore, the resistance ratio between any two resistors may be kept constant by keeping the temperature uniform. A uniform temperature insures that the voltage used for regulation will represent exactly the same fraction of the total voltage at all times.

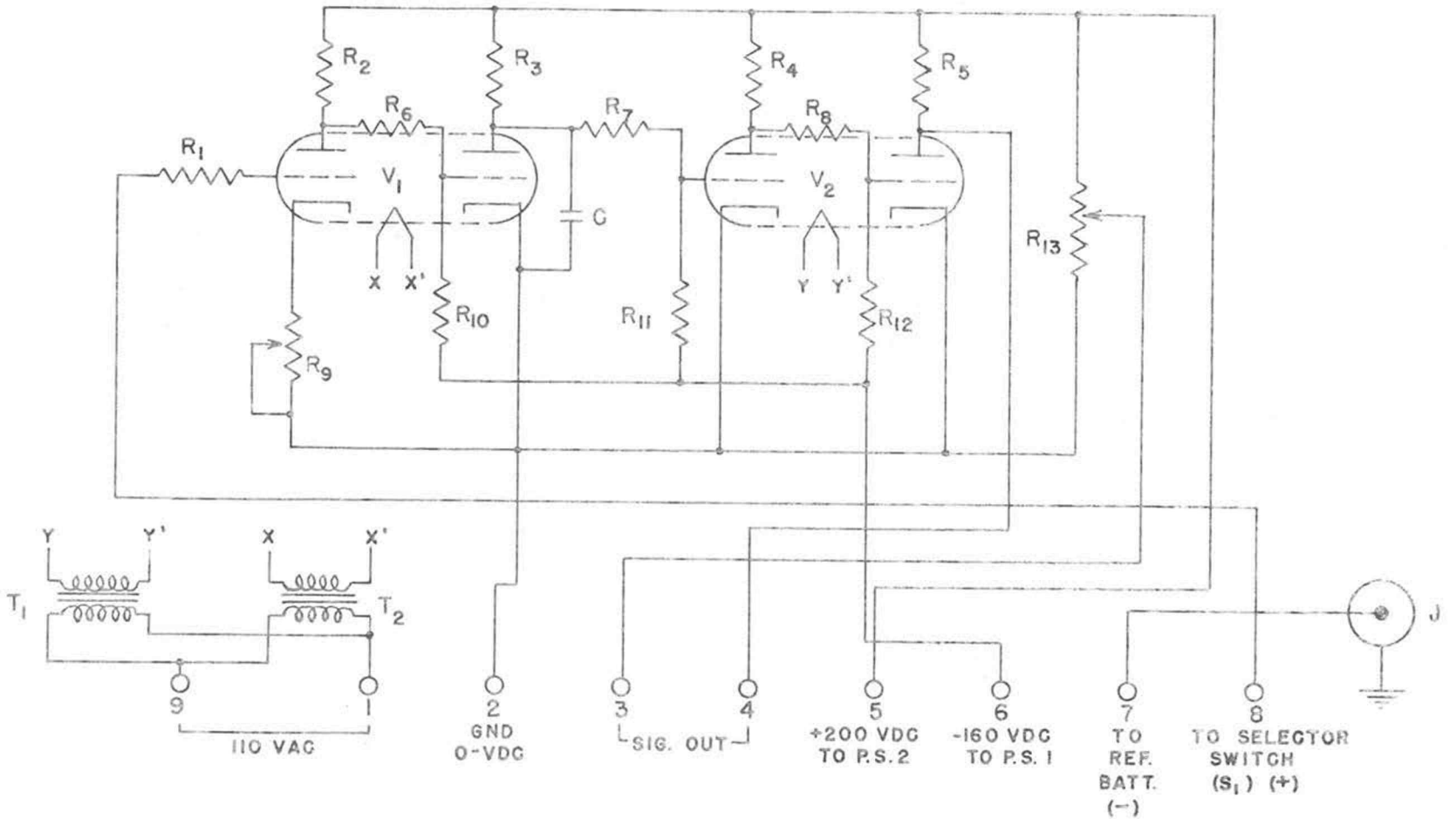

FIGURE X

D. C. AMPLIFIER

TABLE III

COMPONENTS FOR D. C. AMPLIFIER

Item	Description	No. Needed
C	Capacitor, paper, 0.002 mfd., 600 v.	1
J	Receptacle, coaxial, type N, Amphenol no. 82-24	1
R_1	Resistor, composition, 2.2 M ohms, 2 watt	1
R_2,R_3 R_4,R_5	Resistor, composition, 15 K ohms, 2 watt	4
R_6,R_7,R_8	Resistor, composition, 82 K ohms, 1 watt	3
R_9	Potentiometer, w.w., 1 K ohms, 4 watt	1
R_{10},R_{11} R_{12}	Resistor, composition, 120 K ohms, 5%, 1 watt	3
R_{13}	Potentiometer, w.w., 0.1 M ohms, 4 watt	1
V_1,V_2	Tube, electron, 6SN7	2
T_1,T_2	Transformer, filament, Thordarson 21F10	2
PS 1	Lambda regulated power supply, model 29, 100-200 V.d-c, 0-100 ma.	1
PS 2	Lambda regulated power supply, model 28, 200-325 V.d-c, 0-100 ma.	1
S_1	Switch, selector, Cinema Engineering Co., CES-1C2-18D with knob and dial (physically located by autotransformer)	1

NOTE:

$R_1, R_2, R_3, \& R_4$: RESISTORS - 1%
SHALLCROSS PRECISION-
ENCLOSED IN PORCELAIN TUBES.

B: BUSHING.

$J_1, J_2, \& J_3$: RECEPTACLES, AMPHENOL,
TYPE N.

ALL VOLTAGES ARE WITH RESPECT TO
GROUND WITH -50 KV INPUT.

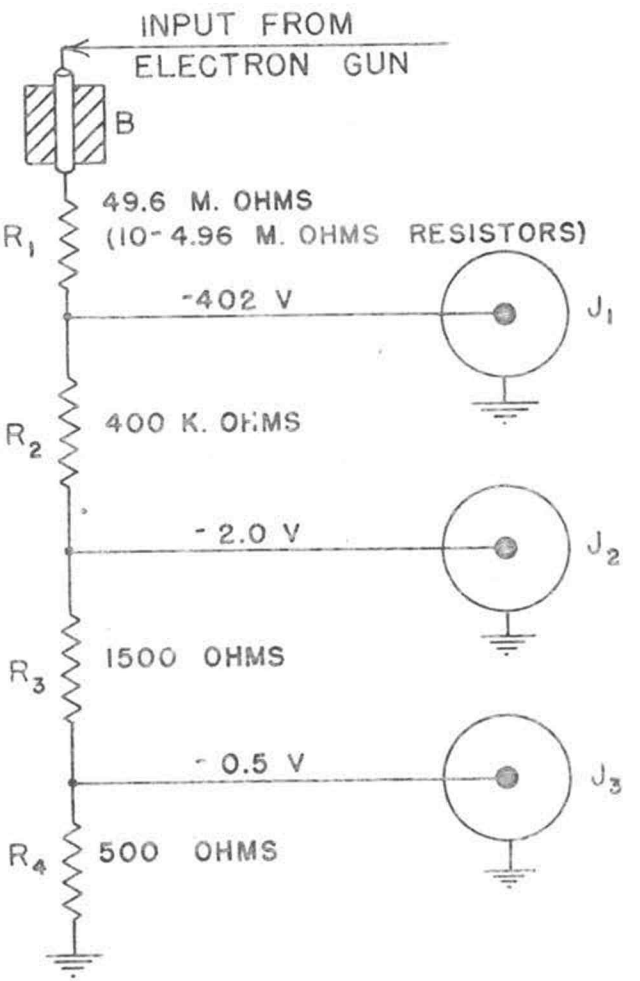

FIGURE XI
VOLTAGE DIVIDER

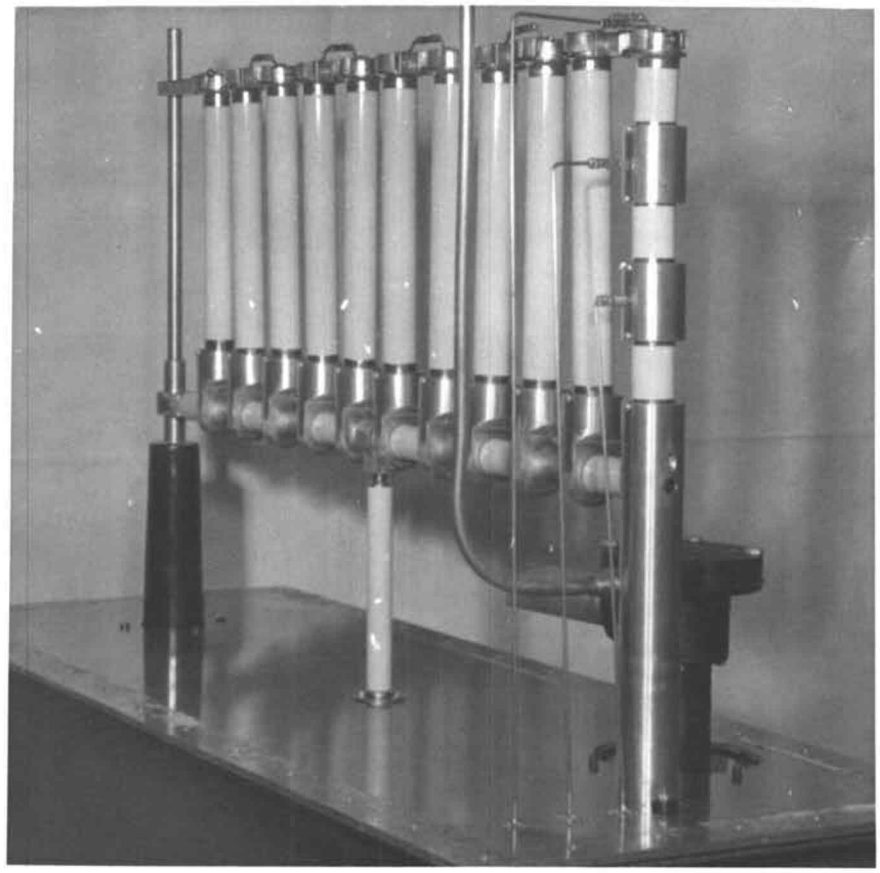

FIGURE XII

VOLTAGE DIVIDER TANK

SERIES-REGULATOR

The wiring diagram of the series-regulator is shown in Figure XIII and the list of components is given in Table IV. Figures XIV and XV are photographs of the unit.

The high-voltage input (received at J_2) is the pulsating d-c output of the transformer-rectifier unit. A considerable part of the 120 cps ripple is removed by capacitor C_5, which has a time constant of about 12.5 seconds (0.25 mfd. times 50 megohms); a very much smaller part is removed by capacitor C_4, which has the same capacitance of C_5, but operates in a low resistance circuit. The r-f signal is received at J_1 from the oscillator-modulator and communicated to the series-regulator tube circuitry (enclosed by the dotten lines) via r-f transformer T_1, of which the primary is at d-c ground potential and the secondary is at -50 kilovolts d-c. Tube V_1 is made conducting by the negative portion of the signal and an r-f choke in conjuntion with two capacitors (C_1 and C_3) removes the ripple before the signal is impressed on the grid of the regulator tube V_2. Tube V_2 is self-biased via resistor R_4 and meter M to the cathode of tube V_2. An error signal varies the bias on V_2 which causes a change in plate resistance in a direction to correct the error.

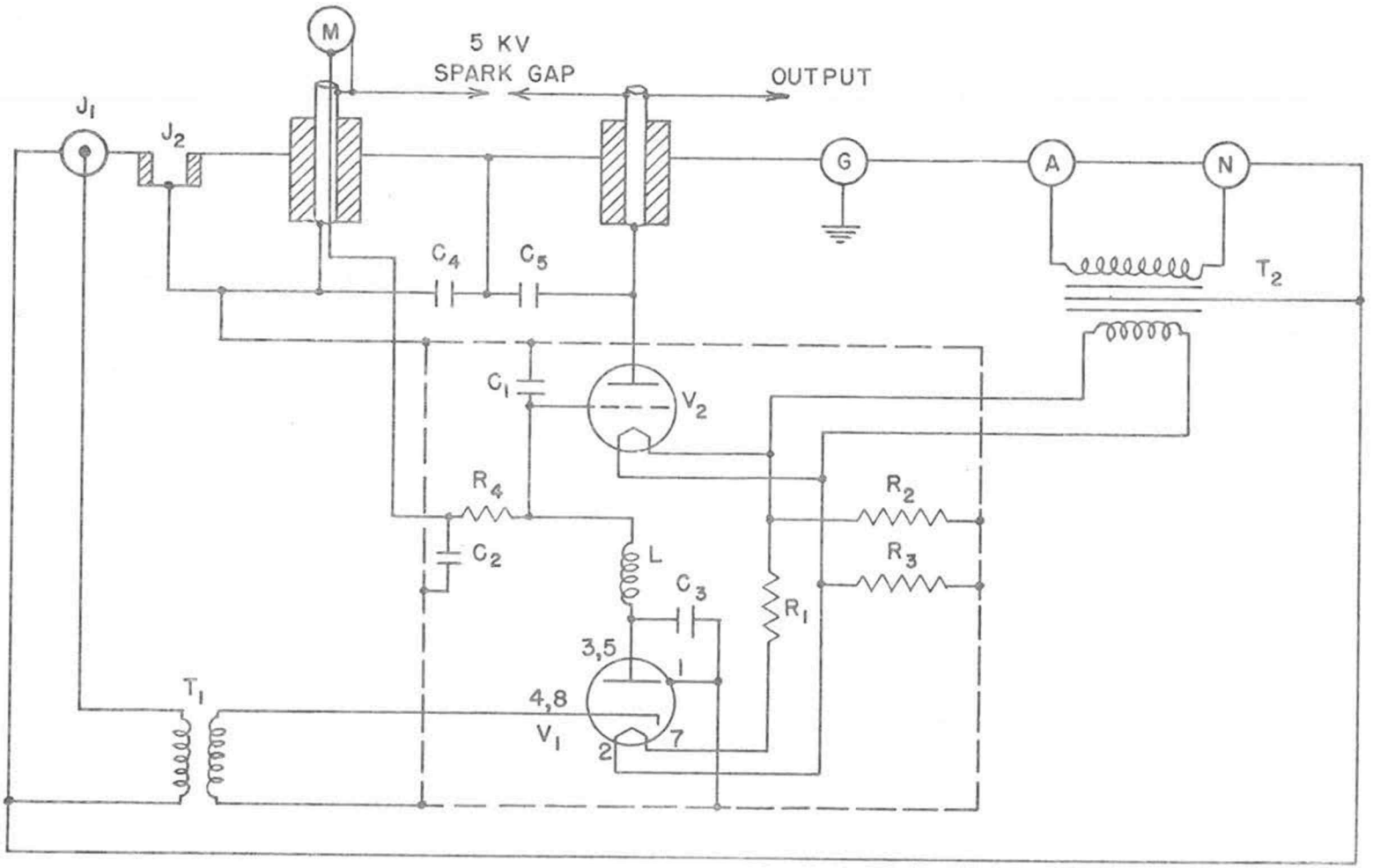

FIGURE XIII

SERIES REGULATOR

TABLE IV

COMPONENTS FOR SERIES-REGULATOR

Item	Description	No. Needed
C_1	Capacitor, ceramic 150 mmfd.	1
C_2	Capacitor, bathtub 0.5 mfd., 400v.	1
C_3	Capacitor, ceramic 130 mmfd.	1
C_4,C_5	Capacitor, paper dielectric, 0.25 mfd., 50 KV insulation, G. E. No. 14F455	2
J_1	Receptacle, coaxial, type N, Amphenol No. 82-24	1
J_2	Receptacle, high voltage, G. E. No. 1003258C1	1
L	Choke, r-f, 2.5 mh., 75 ma.	1
R_1	Resistor, w.w., 4 ohms, 10 watts	1
R_2,R_3	Resistor, w.w., 40 ohms, 10 watts	2
R_4	Resistor, w.w., 0.7 M ohms, 0.1%, 1 watt, Shallcross precision	1
T_1	Transformer, air core, 50 KV insulation, coils wound on teflon cylinders which are mounted on macarta cores, adjustable coupling, primary- 12 turns of no. 18 wire, secondary- 36 turns of no. 18 wire, teflon cylinders are 1½ inch in diameter	1
T_2	Transformer, filament, 7.5 volts a-c, 60 cps, 50 KV insulation, 100 VA, Del Electronics Inc.	1
V_1	Tube, electron, 6H6	1

TABLE IV - Cont.

Item	Description	No. Needed
V_2	Tube, electron, 450TH, Eitel McCullough Inc.	1
M	Meter	

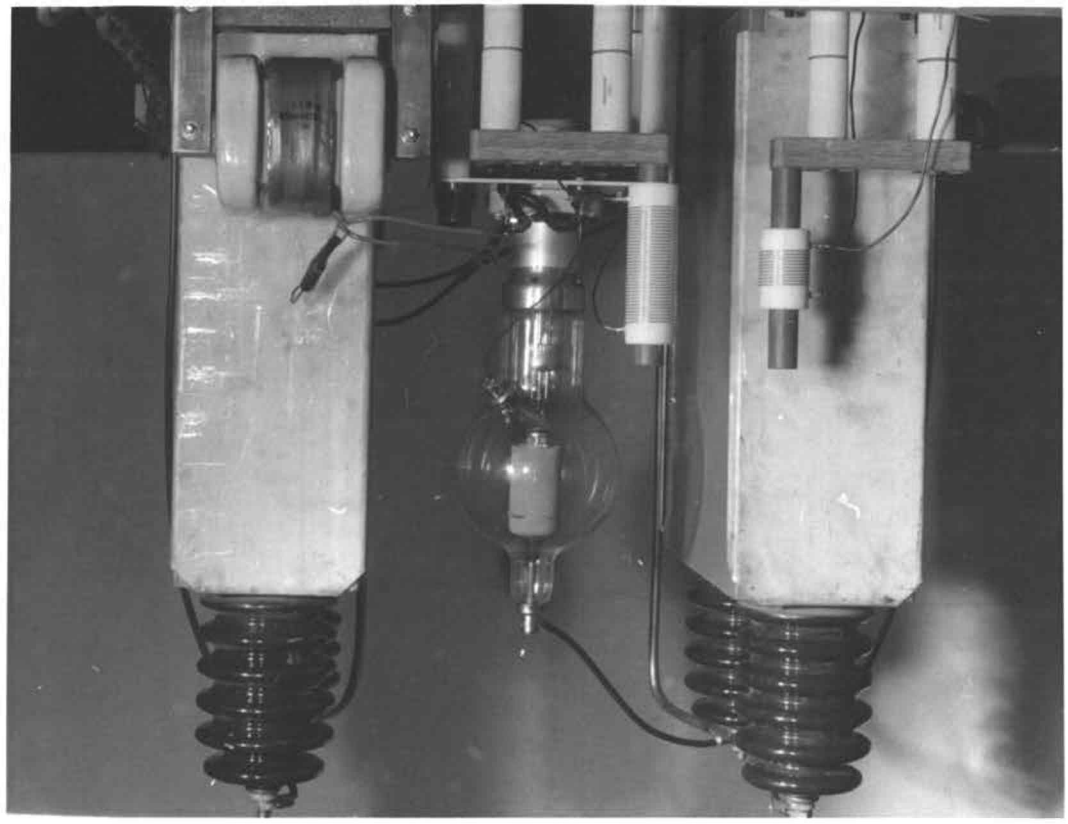

FIGURE XIV

SERIES REGULATOR TANK

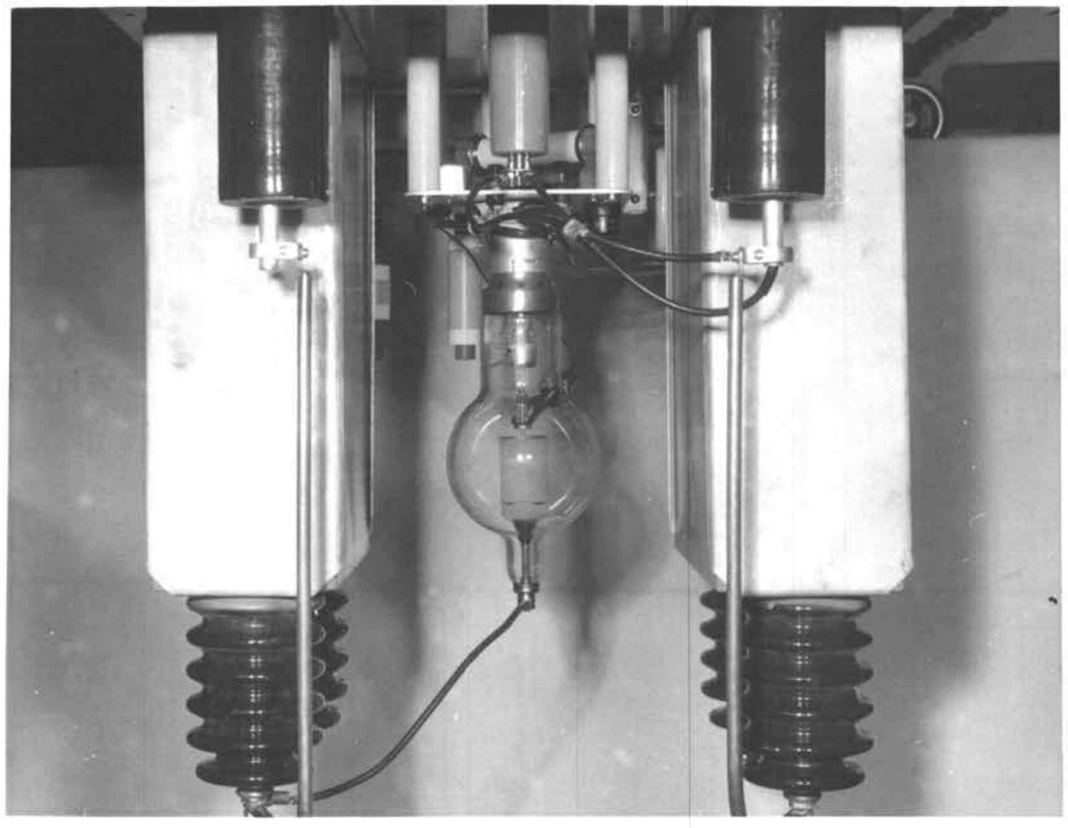

FIGURE XV

SERIES REGULATOR TANK

Resistors R_2 and R_3 serve to maintain the cathodes of V_1 and V_2 at a suitable d-c potential and resistor R_1 provides 6 volts a-c for the filament of tube V_1. The 5 kilovolt spark gap serves to protect the series-regulator tube V_2.

OPERATIONAL DESCRIPTION

The operation of the power supply may be traced using the simplified schematic shown in Figure XVI. If the voltage at the electron gun should become more negative, the error voltage, proportionally reduced in numerical value by the 49.6 M.ohm resistors, is led to the D.C. amplifier which provides a much amplified negative-going error signal (but positive with respect to ground) as input to the cathode of the first tube of the oscillator-modulator. Since the grid voltage of the tube is constant, the negative signal decreases the bias and the resultant increased conduction causes the amplitude of the 2 megacycle signal to increase. The output of the oscillator-modulator is coupled, via an isolation transformer of which the secondary winding is at -50 kilovolts d-c, to the diode in the series-regulator tank. The signal is rectified by the diode and the negative envelope filtered by the LC network.

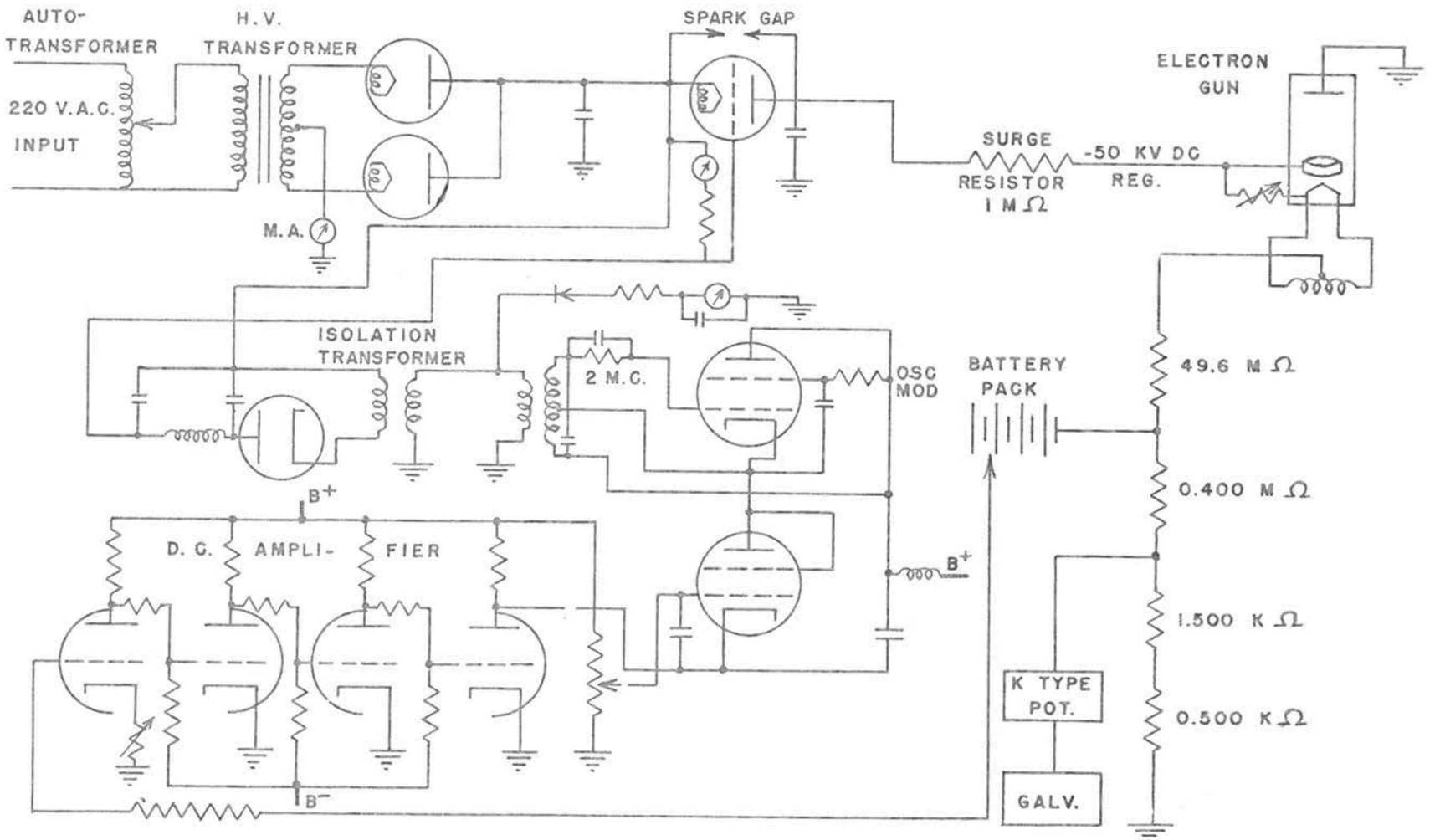

FIGURE XVI

SERIES REGULATED POWER SUPPLY

Since the negative envelope is used, the grid of the series-regulator tube becomes more negative increasing the plate resistance and the voltage drop across the tube. Since more voltage is dropped across the tube, the voltage at the electron gun becomes less negative acting to correct the original error. It must be remembered that this circuit will correct only for transient voltage changes. Drift is corrected by use of the autotransformer and visual observation of the galvonometer.

INVESTIGATION OF THE MOLECULAR STRUCTURE OF PENTAFLUOROSULFUR HYPOFLUORITE BY ELECTRON DIFFRACTION

THEORETICAL

ELASTIC SCATTERING. Since electron diffraction from gases is nearly always done with fast electrons (30-50 kilovolt), the following development of the scattering theory deals only with this case.

It is advantageous to consider elastic scattering by an atom first and then extend this to randomly oriented molecules. Consider a monochromatic beam of electrons in field free space impinging on a small region of high electrostatic field. The electrons are scattered and the distribution of scattered electrons is observed at a great distance from the atom. Let r represent this distance and Θ the angle which the scattered electrons make with the incident beam. If N is the number of electrons in the incident beam which passes a unit area per unit time, then the number of scattered electrons impinging on the area dS at angle Θ in unit time is given by the solid angle formula (6, p. 233-236)

$$N I_{(\theta)}\, dS/r^2 = N I_{(\theta)}\, d\Omega \qquad (1)$$

where $I(\theta)$ is a function to be calculated. $I(\theta)$ is obtained by use of the wave equation

$$\nabla^2 \psi_{(x,y,z)} + \frac{8\pi^2 m}{h^2}\left(W - V_{(x,y,z)}\right)\psi_{(x,y,z)} = 0$$

or simply

$$\nabla^2 \psi + \frac{8\pi^2 m}{h^2}(W - V)\psi = 0 \qquad (2)$$

ψ is the wave function which is a complex function describing the amplitude and phase of the wave at any point. ∇^2 is the operator which is $\frac{\partial^2}{\partial x^2} + \frac{\partial^2}{\partial y^2} + \frac{\partial^2}{\partial z^2}$ in cartesian coordinates. W is the kinetic energy of the electrons and is constant, that is, the electrons have the same energy before and after collision. W can be determined from the accelerating potential used in the experiment. V is the potential energy of the interaction between the electron and the charged atom and is considered to be only a function of r.

Figure XVII (6, p. 234) is a convenient set of coordinates; the primed coordinates refer to the atoms and the unprimed to the electron wave. The infinite

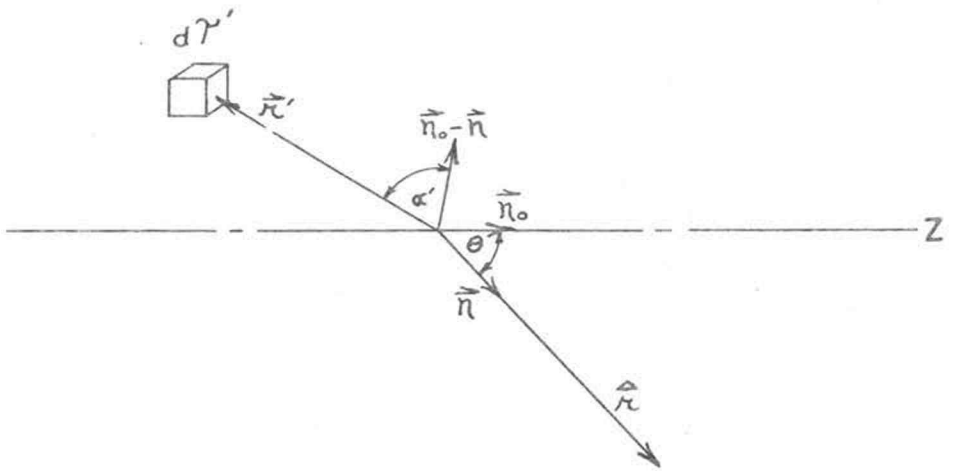

FIGURE XVII

COORDINATES FOR ATOMIC SCATTERING

plane wave is traveling along Z. From the de Broglie relationship $\lambda = h/mv$, one obtains

$$\frac{8\pi^2 m W}{h^2} = k^2 = \frac{4\pi^2}{\lambda^2}$$

and equation (2) becomes

$$(\nabla^2 + k^2)\psi = \frac{8\pi^2 m V}{h^2}\psi \qquad (3)$$

Now if $f_{(x,y,z)}$ be a known function, the most general solution of

$$(\nabla^2 + k^2)\psi = f_{(x,y,z)}$$

is (22, pp. 106-115)

$$\psi_{(x,y,z)} = G_{(x,y,z)} - \frac{1}{4\pi}\iiint \frac{e^{ik|\vec{r}-\vec{r}'|}}{|\vec{r}-\vec{r}'|} f_{(x',y',z')}\, dx'dy'dz' \qquad (4)$$

where $G_{(x,y,z)}$ is the general solution of

$$(\nabla^2 + k^2)G = 0$$

If ψ is any solution of equation (2), then equation (4) becomes (6, p. 234)

$$\Psi_{(x,y,z)} = G_{(x,y,z)} - \frac{1}{4\pi}\int \frac{e^{ik|\vec{r}-\vec{r}'|}}{|\vec{r}-\vec{r}'|}\cdot\frac{8\pi^2 m}{h^2}V'\Psi' d\tau' \qquad (5)$$

where

$$d\tau' = dx'dy'dz'$$
$$V' = V(x',y',z')$$
$$\Psi' = \Psi(x',y',z')$$

If Ψ is an adequate description of the electron waves, $G_{(x,y,z)}$ defined by

$$G_{(x,y,z)} = e^{ikz} \qquad (6)$$

must represent the incident plane wave and the integral of equation (5) the diffracted wave. For $\vec{r} >> \vec{r}'$ (the circumstance prevailing in the electron diffraction experiment) this integral becomes $r^{-1} e^{ikr} f(\theta)$ leading to the equation

$$\Psi = e^{ikz} + r^{-1} e^{ikr} f(\theta) \qquad (7)$$

Using the relationship (6, p. 234)

$$|\vec{r}-\vec{r}'| \cong r - \left(\frac{\vec{r}}{r}\right)\cdot\vec{r}'$$

$f(\Theta)$ becomes

$$f_{(\theta)} = -\frac{2\pi m}{h^2}\int e^{-ik\frac{\vec{r}}{r}\cdot\vec{r}'} V'\psi' d\tau' \qquad (8)$$

The solution to the scattering problem thus involves the integration of equation (8).

The evaluation of the integral of equation (8) is achieved by the use of an approximation, the Born approximation, occasioned by the nature of ψ'. The function ψ' is composed of two parts, a ψ_o' and a part similar to the integral of equation (8). The Born approximation consist of neglecting the integral part of ψ', that is

$$\psi' \cong \psi_o' = e^{ikz'} \qquad (9)$$

which may be interpreted in physical terms as assuming only a single scattering process within the atom with no shift in phase occurring. The Born approximation has found ample experimental justification in the case of molecules containing atoms of not too different atomic numbers; however, when the molecule contains atoms of quite different atomic numbers a more elaborate theory is necessary (13, p. 667-671). Let $z' = \vec{n}_o \cdot \vec{r}'$ where $\vec{n}_o$ (see Figure XVII) is the unit vector along the Z

axis. Since $\left(\frac{\vec{r}}{r}\right) = \vec{\eta}$ is also a unit vector, equation (8) becomes

$$f(\theta) = -\frac{2\pi m}{h^2}\int e^{ik\left[z' - \left(\frac{\vec{r}}{r}\right)\cdot\vec{r}'\right]} V' d\tau'$$

$$= -\frac{2\pi m}{h^2}\int e^{ik(\vec{\eta}_0\cdot\vec{r}' - \vec{\eta}\cdot\vec{r}')} V' d\tau'$$

$$= -\frac{2\pi m}{h^2}\int e^{ik(\vec{\eta}_0 - \vec{\eta})\cdot\vec{r}'} V' d\tau' \qquad (10)$$

With reference to Figure XVII, it is seen that θ is the angle between $\vec{\eta}$ and $\vec{\eta}_0$, hence,

$$|\vec{\eta}_0 - \vec{\eta}|^2 = |\vec{\eta}_0|^2 + |\vec{\eta}|^2 - 2|\vec{\eta}_0||\vec{\eta}|\cos\theta$$

$$= 2 - 2\cos\theta$$

$$|\vec{\eta}_0 - \eta| = \sqrt{2}(1 - \cos\theta)^{1/2}$$

$$|\vec{\eta}_0 - \eta| = 2\sin\theta/2 \qquad (11)$$

which leads to

$$(\vec{\eta}_0 - \vec{\eta})\cdot\vec{r}' = (2\sin\theta/2)\, r'\cos\alpha' \qquad (12)$$

where α' is the angle between $\vec{r}'$ and $(\vec{\eta}_0 - \vec{\eta})$. Equation (10) thus becomes

$$f(\theta) = -\frac{2\pi m}{h^2}\int e^{i2k(\sin\theta/2)r'\cos\alpha'} V' d\tau' \qquad (13)$$

Since everything is now in terms of the atom, the primes will be dropped except where needed for clarity. Taking $\vec{\eta}_0 - \vec{\eta}$ as the polar axis and changing to spherical coordinates gives

$$f(\theta) = -\frac{2\pi m}{h^2}\int_0^{\infty}\int_0^{\pi}\int_0^{2\pi} e^{i2k(\sin\theta/2)r\cos\alpha} r^2 V(r)\sin\alpha\, d\beta\, d\alpha\, dr \qquad (14)$$

where β is the azimuthal angle and α is the latitude. β may be integrated immediately to obtain

$$f(\theta) = -\frac{4\pi^2 m}{h^2}\int_0^{\infty}\int_0^{\pi} e^{i2k(\sin\theta/2)r\cos\alpha} r^2 V(r)\sin\alpha\, d\alpha\, dr \qquad (15)$$

Recalling that $k = 2\pi/\lambda$ and introducing a new constant $s = \frac{4\pi}{\lambda}\sin\theta/2$ equation (15) becomes

$$f(\theta) = -\frac{4\pi^2 m}{h^2}\int_0^{\infty}\int_0^{\pi} e^{isr\cos\alpha} r^2 V(r)\sin\alpha\, d\alpha\, dr \qquad (16)$$

The integration over α is accomplished as follows

$$\int_0^{\pi} e^{isr\cos\alpha} \sin\alpha \, d\alpha = -\frac{1}{isr} e^{isr\cos\alpha} \Big|_0^{\pi}$$

$$= +\frac{1}{isr}\left[e^{isr} - e^{-isr}\right]$$

but

$$\sin sr = +\frac{1}{2i}\left[e^{isr} - e^{-isr}\right]$$

so that

$$\int_0^{\pi} e^{isr\cos\alpha} \sin\alpha \, d\alpha = \frac{2\sin sr}{sr} \qquad (17)$$

The evaluation of $f(\theta)$ has thus been reduced to the solution of the equation.

$$f(\theta) = -\frac{8\pi^2 m}{h^2}\int_0^{\infty} \frac{\sin sr}{sr} V(r)\, r^2 \, dr \qquad (18)$$

The quantity V(r) may be expressed by the equation (6, p. 235)

$$V(r) = -\frac{Ze^2}{r} + e^2\int \frac{|\phi(r')|^2}{|\vec{r}-\vec{r}'|} d\tau' \qquad (19)$$

in which the first term represents the potential of the

impinging electron in the field of the nucleus of charge Ze and the second term the potential of the electron in the field of the extra-nuclear electrons which have probability distribution $|\phi(r')|^2$. It is convenient to employ equations (18) and (10) for respectively the first and second terms of equation (19). From equation (18)

$$\frac{8\pi^2 m}{h^2}\int_0^\infty \frac{\sin sr}{sr}\,\frac{Ze^2}{r}\,r^2\,dr = \frac{8\pi^2 mZe^2}{sh^2}\int_0^\infty \sin sr\,dr \tag{20}$$

is obtained, which may be evaluated as follows (21, p. 658-665).

$$\frac{8\pi^2 mZe^2}{sh^2}\int_0^\infty \sin sr\,dr = \left[\frac{8\pi^2 mZe^2}{sh^2}\right]\lim_{K\to 0}\int_0^\infty e^{-Kr}\sin sr\,dr$$

$$= \left[\frac{8\pi^2 mZe^2}{sh^2}\right]\lim_{K\to 0}\left(\frac{s}{s^2+K^2}\right)$$

$$= \frac{8\pi^2 me^2}{h^2}\,\frac{Z}{s^2} \tag{21}$$

By substituting the second part of equation (19) into equation (10) and using the equation

$$\int \frac{e^{ik(\vec{r}_0-\vec{r})\cdot\vec{r}'}}{|\vec{r}-\vec{r}'|}\,d\tau' = \frac{4\pi e^{ik(\vec{r}_0-\vec{r})\cdot\vec{r}'}}{k^2|\vec{r}_0-\vec{r}|^2} \tag{22}$$

derived by Bethe (4, p. 325-400) one obtains the expression

$$\frac{8\pi^2 m\epsilon^2}{h^2}\int \frac{|\phi(r')|^2 e^{ik(\vec{r}_0-\vec{r})\cdot\vec{r}'}}{k^2|\vec{r}_0-\vec{r}|^2}\,d\tau' \tag{23}$$

Again changing to spherical coordinates and using the relationships for $(\vec{r}_0-\vec{r})$, $\vec{r}'$ and $\underline{k}$ obtained earlier, expression (23) becomes

$$\frac{8\pi^2 m\epsilon^2}{h^2}\int_0^\infty\int_0^\pi\int_0^{2\pi} \frac{|\phi(r')|^2 e^{isr\cos\alpha}\, r^2\sin\alpha\, d\beta\, d\alpha\, dr}{s^2} \tag{24}$$

Integration over α and β is accomplished as described before yielding the expression

$$-\frac{8\pi^2 m\epsilon^2}{h^2}\int_0^\infty \frac{4\pi}{s^2}\,\frac{\sin sr}{sr}\,|\phi(r')|^2 r^2\,dr \tag{25}$$

Adding expression (21) to (25), one obtains

$$f(\theta) = \frac{8\pi^2 m e^2}{h^2}\left[\frac{Z - F(\theta)}{s^2}\right] \qquad (26)$$

where

$$F(\theta) = 4\pi\int_0^\infty |\phi(r')|^2 \frac{\sin sr}{sr} r^2 dr \qquad (27)$$

The complete solution to the Schrodinger equation is thus

$$\psi = e^{ikz} + \frac{8\pi^2 m e^2}{h^2} e^{ikr}\left[\frac{Z - F(\theta)}{s^2}\right] \qquad (28)$$

F is the atomic scattering factor for x-rays and has been tabulated for nearly all atoms (17, p. 470-476) and (23, p. 1-29). At large scattering angles, $F \rightarrow 0$ which means that the nucleus is responsible for most of the scattering. As $\theta \rightarrow 0$, $F(\theta) \rightarrow Z$ and $s \rightarrow 0$ in such a fashion that $(Z - F(\theta))/s^2$ approaches a finite value (23, p. 28).

Now that the wave function for the elastic scattering of electrons by atoms has been obtained, the theory may be extended to elastic scattering by molecules. Since molecules are aggregates of atoms, equation (28)

should apply provided that the potential function for a bound atom does not differ from that for an unbound atom. This, of course, is not strictly true; however, deviations from spherical symmetry occasioned by bond formation cannot matter much since the electron-electron scattering of fast electrons is of minor importance.

The theory of scattering from gaseous molecules is developed by first considering the effect from a simple molecule in fixed orientation and then averaging over all orientations. Implicit in the treatment is the independence of scattering from neighboring molecules. Figure XVIII (6, p. 236) shows a convenient coordinate system. Since the origin of the coordinates is not located at the center of any atom, the expression for the amplitude of the wave scattered by the $i^{\underline{th}}$ atom is given by the second term of equation (7) and becomes (6, p. 236)

$$\psi_i = \frac{e^{ik|\vec{r}-\vec{r}_i|}}{|\vec{r}-\vec{r}_i|} e^{ikz_i} f(\theta) \qquad (29)$$

As in the treatment of the scattering from an atom

$$|\vec{r}-\vec{r}_i| \cong r - \vec{\eta}\cdot\vec{r}_i$$

$$z_i = \vec{\eta}_o - \vec{\eta}$$

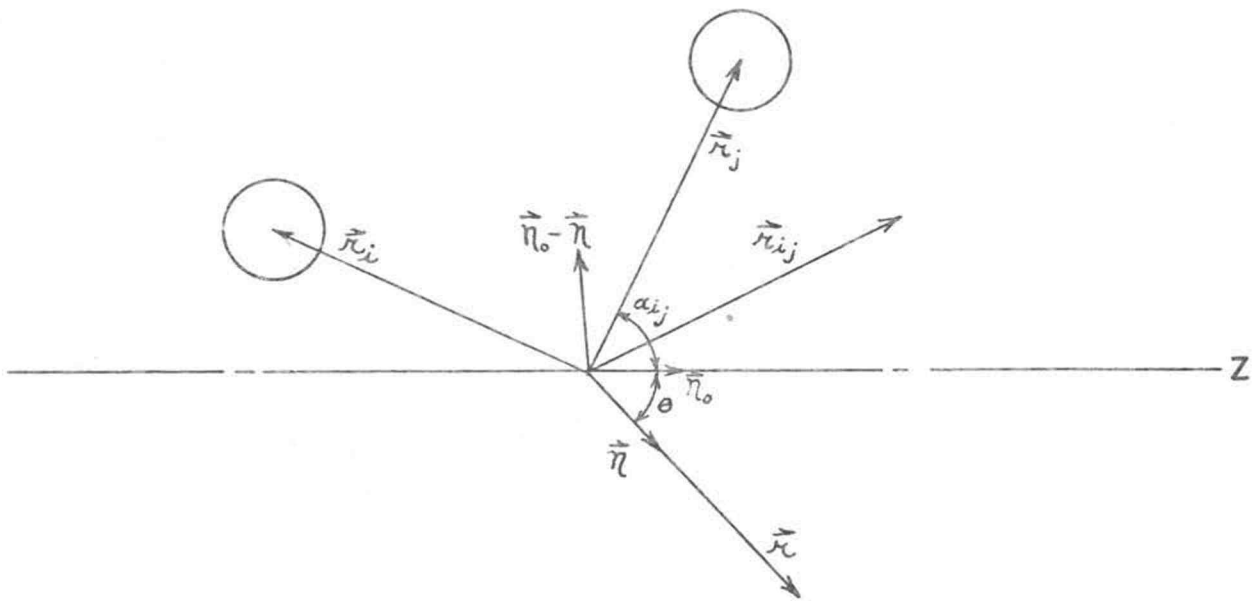

FIGURE XVIII

COORDINATES FOR MOLECULAR SCATTERING

where $\vec{n}$ and $\vec{n}_o$ are unit vectors along $\vec{r}$ and Z. Here $|\vec{r}-\vec{r}_i|$ is the distance from the center of the i$^{\underline{th}}$ atom to the point of observation; the new factor e^{ikZ_i} takes account of the difference in phase of the indicent wave at the center of the i$^{\underline{th}}$ atom relative to the origin. From equation (29) one obtains

$$\psi_i = \frac{e^{ik(r-\vec{n}\cdot\vec{r}_i)}\, e^{ikZ_i}}{r} f_i(\theta)$$

$$= \frac{e^{ikr}}{r}\, e^{ik(Z_i-\vec{n}\cdot\vec{r}_i)} f_i(\theta)$$

$$= \frac{e^{ikr}}{r}\, e^{ik(\vec{n}_o-\vec{n})\cdot\vec{r}_i} f_i(\theta) \qquad (30)$$

Equation (30) must be summed over all atoms in the molecule of fixed orientation to obtain the total scattering amplitude.

$$\psi = \sum_i \psi_i = \frac{e^{ikr}}{r} \sum_i e^{ik(\vec{n}_o-\vec{n})\cdot\vec{r}_i} f_i(\theta) \qquad (31)$$

Since the molecules are randomly oriented in the electron diffraction experiment, the scattered waves from different molecules will have a random phase relationship; therefore, the averaging over all possible orientations

must be done on the intensity $|\psi|^2$.

$$I = \psi\psi^* = \frac{e^{ikr}}{r}\frac{e^{-ikr}}{r}\left|\sum_i e^{ik(\vec{\eta}_0-\vec{\eta})\cdot\vec{r}_i} f_i\right|^2$$

$$= \frac{1}{r^2}\sum_i\sum_j f_i f_j e^{ik(\vec{\eta}_0-\vec{\eta})\cdot(\vec{r}_i-\vec{r}_j)}$$

$$= \frac{1}{r^2}\sum_i\sum_j f_i f_j e^{ik(\vec{\eta}_0-\vec{\eta})\cdot\vec{r}_{ij}} \qquad (32)$$

where ψ^* is the complex conjugate of ψ and $\vec{r}_{ij} = \vec{r}_i - \vec{r}_j$.

The averaging process is accomplished by changing to spherical polar coordinates (taking $\vec{\eta}_0 - \vec{\eta}$ as the polar axis) and integrating over the surface of a unit sphere (24, p. 298), that is, over the angle variables α and β ; the result is the mean intensity per unit solid angle from randomly oriented molecules.

$$I = \frac{1}{r^2}\sum_i\sum_j f_i f_j \frac{1}{4\pi}\int_0^{\pi}\int_0^{2\pi} e^{ik(\vec{\eta}_0-\vec{\eta})\cdot\vec{r}_{ij}} \sin\alpha\, d\beta\, d\alpha \qquad (33)$$

with

$$|\vec{\eta}_0 - \vec{\eta}| = 2\sin\theta/2$$

$$|\vec{r}_{ij}| = r_{ij}\cos\alpha_{ij}$$

$$s = \frac{4\pi}{\lambda}\sin\theta/2$$

equation (33) becomes

$$I = \frac{1}{r^2} \sum_i \sum_j f_i f_j \frac{1}{4\pi} \int_0^{\pi} \int_0^{2\pi} e^{is r_{ij} \cos \alpha_{ij}} \sin \alpha_{ij} \, d\beta \, d\alpha_{ij} \qquad (34)$$

which gives

$$I = \frac{1}{r^2} \sum_i \sum_j f_i f_j \frac{\sin s r_{ij}}{s r_{ij}} \qquad (35)$$

Except for the f_i, equation (35) was derived by Debye (11, p. 809-823) for the case of molecular scattering by x-rays.

When i = j, equation (35) reduces to

$$I = \frac{1}{r^2} \sum_i (f_i)^2 \qquad (36)$$

because

$$\lim_{x \to 0} \frac{\sin x}{x} = 1$$

When the f_i are included explicitly one obtains the solution to the problem of elastic scattering of electrons by molecules in its fullest form:

$$I = \left(\frac{8\pi^2 m e^2}{h^2} \right)^2 \frac{1}{r^2} \sum_i \sum_j \frac{(Z-F)_i (Z-F)_j}{s^4} \frac{\sin s r_{ij}}{s r_{ij}} \qquad (37)$$

INELASTIC SCATTERING. Several things may happen to a molecule during bombardment which result in a fraction of the beam being scattered inelastically: the bombarding electrons may leave the molecule in an excited electronic state, they may ionize the molecule, or they may change the vibrational or rotational state of the molecule. In all such processes the impinging electrons leave the scattering point with less energy and the scattered rays have correspondingly longer wavelengths. This radiation, in contrast to that scattered by elastic processes, is not coherent, a circumstances occasioned by the great number of energetically different molecular quantum states active in inelastic processes.

It is useful to have an idea of the angular distribution of inelastically scattered electrons in spite of the fact that the inelastic scattering is not related to the molecular structure: inelastic scattering contributes a background of which account must be taken when the data are reduced. No treatment has been given for this scattering effect from molecules as such; instead an approximate solution to the problem is based on the reasonable assumption that the inelastic scattering effect from a molecule will not differ much from the aggregate effect of the atoms comprising the molecule.

Further, since it has not been possible to calculate explicitly the incoherent intensity for atoms with $Z > 1$, these approximate solutions rest on extensions of the hydrogen atom results to polyelectronic atoms. For example, at large scattering angles the intensity for incoherent scattering by a hydrogen atom approaches the intensity that would be scattered by a Thomson electron (25, p. 3) and for an atom containing Z electrons, the total intensity is assumed to be ZI_e. The treatment described below is by Morse (20, p. 443-445) who extended Heisenberg's results for the incoherent scattering of x-rays by molecules (14, p. 737-740) to fast electrons.

Taking into account the change in wavelength which occurs in incoherent scattering, the scattered intensity from atoms may be written (20, p. 444)

$$I_{(\theta)} = A^2 \frac{k_n}{k_a} \left| \int \phi_n^* \phi_a \left(\frac{Z}{r_0} - \sum_{t=1}^{t=Z} \frac{1}{r_{0t}} \right) e^{i(k_n \vec{r} - k_a \vec{r}_0) \cdot \vec{r}_a} \, d\tau \, dV_0 \right|^2 \tag{38}$$

where

$$A = 2\pi m \epsilon^2 / h^2$$

r = coordinate of the atomic electron

a = coordinate of the bombarding electron

$k_n = 2\pi/\lambda_n$ = wave numbers after collision

$k_a = 2\pi/\lambda_a$ = wave numbers before collision

ϕ_n^* = wave function of atom after collision

ϕ_a = wave function of atom before collision

$\frac{Z}{r_o} - \sum_{t=1}^{t=Z} \frac{1}{r_{o,t}} = V_{(r)}$ = the potential function for the bombarding electron

By letting $k_n = k_a$ (valid for high energy electrons), the vector $\vec{S} = \vec{r} - \vec{r}_o$, and integrating over dV_o one obtains

$$I_{(\theta)} = \left(\frac{4\pi A}{s^2}\right)^2 \left| \int \phi_n^* \phi_a \left(Z - \sum_t e^{ik(\vec{S}-r_t)}\right) d\tau \right|^2 \qquad (39)$$

Expanding equation (39) and using the trigometric relation

$$\cos x = \frac{1}{2}\left(e^{ix} + e^{-ix}\right) \qquad (40)$$

one obtains

$$I_{(\theta)} = \left(\frac{4\pi A}{s^2}\right)^2 \int (\phi_n)^2 \left[Z - 2Z \cos k(\vec{S}\cdot\vec{r}_t) + \right.$$

$$\left. \sum_{s,t} e^{ik[\vec{S}\cdot(\vec{r}_s - \vec{r}_t)]} \right] d\tau \qquad (41)$$

Equation (41) is integrated in a manner somewhat similar to that already used giving

$$I_{(\theta)} = \left(\frac{4\pi\dot{A}}{s^2}\right)^2 \left(Z^2 - 2Z^2 F_1 + S\right) \qquad (42)$$

Now S has been found (20, p. 444) to be equal to

$$S = Z^2 F_1^2 + S_v \qquad (43)$$

where S_v is the incoherent scattering function first derived by Heisenberg (14, p. 737-740). Equation (42) becomes

$$I_{(\theta)} = \left(\frac{8\pi^2 m\epsilon^2}{h^2}\right)^2 \frac{Z^2}{s^4}\left[(1-F_1)^2 + \frac{S_v}{Z^2}\right] \qquad (44)$$

If one lets $F_1 = F/Z$, one obtains the form given by Brockway (6, p. 238).

$$I_{(\theta)} = \left(\frac{8\pi^2 m\epsilon^2}{h^2}\right)^2 \left[\frac{(Z-F)^2}{s^4} + \frac{S_v}{s^4}\right] \qquad (45)$$

By referring to equation (26), it is seen that the first term of equation (45) is equal to $|f_{(\theta)}|^2$ which is the intensity of elastically scattered waves from an atom.

S_v is equal to (25, p. 30)

$$S_v = 1 - \int_0^{X_0} X^2 dX \left[\left(\frac{\phi(x)}{X}\right)^{\frac{1}{2}} - v\right]^2 \left[\left(\frac{\phi(x)}{X}\right)^{\frac{1}{2}} - \frac{v}{2}\right] \quad (46)$$

where $\underline{v}$ is

$$v = \frac{4\pi b}{\lambda} \sin \theta/2 \quad (47)$$

and $\underline{b}$ is the characteristic atomic radius for incoherent radiation which is proportional to $(Z)^{-\frac{2}{3}}$. $\phi(x)/X$ is a dimensionless electric potential function which is equal to (25, p. 1-15)

$$\left(\frac{\phi(x)}{X}\right)^{\frac{1}{2}} = \left[\frac{\psi^2 4\pi a^3}{Z}\right]^{\frac{1}{3}} \quad (48)$$

The procedure in calculating incoherent scattering is to calculate $\underline{v}$ for some value of θ, and then by using tables prepared by Bewilogua (5, p. 740-744) S_v may be obtained. The total intensity (coherent and incoherent) from an atom is given by equation (45) and for a molecule by equation (49) below.

$$I_{(\theta)} = \frac{1}{r^2}\left[\frac{8\pi^2 m \epsilon^2}{h^2}\right]^2 \left[\sum_i \sum_j f_i f_j \frac{\sin s r_{ij}}{s r_{ij}} + \sum_i \frac{S_v}{s^4}\right] \quad (49)$$

where

$$f_i = \frac{(Z-F)_i}{s^2}$$

TEMPERATURE EFFECT. James (16, p. 737-754) has studied the thermal vibrations of atoms in gaseous molecules. His theoretical treatment dealt with the case of x-ray diffraction, but it has been found to apply also to electron diffraction. It was found that the effect of thermal vibrations on interatomic distances could be taken account of by the factor

$$e^{\left[-8\pi^2 \delta r_{ij} \left(\frac{\sin\theta/2}{\lambda}\right)^2\right]} = e^{(-a_{ij}s^2)} \qquad (50)$$

where the δr_{ij} is the mean square of the change in the distance r_{ij}. The equation for the total scattered intensity per unit solid angle from a non-rigid molecule is thus

$$I_{(\theta)} = K\left[\sum_i \sum_j f_i f_j \frac{\sin s r_{ij}}{s r_{ij}} e^{(-a_{ij}s^2)} + \sum_i f_i^2 + \sum_i \frac{S-u}{s^4}\right] \qquad (51)$$

where K represents the constant $\left[\frac{8\pi^2 m e^2}{h^2}\right]^2 \frac{1}{r^2}$.

EXPERIMENTAL

Pentafluorosulfur hypofluorite (SOF_6), first prepared by Dudley, Cady and Eggers (12, p. 1553-1556), is the major product of the catalytic reaction between silver difluoride and thionyl fluoride at 200°C.; the minor product of the reaction is thionyl tetrafluoride (SOF_4). SOF_6 has an odor like oxygen difluoride and is an extremely strong oxidizing agent. It is a gas at ordinary conditions (f.p. is -86°C. and the b.p. is -35.1°C.). Dudley, Cady and Eggers (12, p. 1553-1556) suggested that the molecule has a structure like SF_6 with one of the fluorines replaced by an (OF) group and confirmed this structure by chemical means and by infrared spectroscopy.

Electron diffraction photographs of SOF_6 were made by Drs. Dudley and Hedberg in the apparatus at the California Institute of Technology. This apparatus operates essentially as the apparatus described by Brockway (6, p. 231-266) except that a mechanical device, called a sector, is incorporated in order to modify the scattered intensity uniformly with angle in such a way as to permit easier microphotometry of the photographic plates. The diffraction photographs consisted of a series of concentric diffraction rings (with the position of the

undiffracted electron beam as center) which died off rapidly in intensity with increasing scattering angle.

The reduction of the data, represented by photographs of diffraction patterns, has as its ultimate object the preparation of a function or curve which is everywhere proportional to the intensity of scattered electrons arising from the structure of the molecule. The problem of reduction, then, is essentially the problem of converting the blackness of the plates to a scattered intensity curve. The conversion may be accomplished by measuring the density of the photographic plates as a function of scattering angle and then determining the relationship between the measured density and scattered electron intensity. The procedure used to obtain the SOF_6 scattering data in useful form from the photographic plates required many steps. The following account is presented in detail; subsequent work with other molecules may well differ somewhat as shorter and more convenient operations are worked out.

The SOF_6 plates, carefully selected, were placed on a recording densitometer and a trace of each made while being rotated about the center of the diffraction halos in order to even out the graininess of the emulsion. Since density of plate is proportional to log

(I_o/I), where $\underline{I}_o$ is the intensity of the impinging densitometer beam and $\underline{I}$ is the emergent intensity, it would seem convenient to adjust the densitometer such that $\underline{I}_o = 100$ for clear plate and $\underline{I} = 0$ for complete absorption fall at extreme edges of the chart paper. For darker plates, however, this scale is too insensitive, particularly at larger distances from the center of the plate where the ring amplitudes are decreased, and it is helpful to increase the gain of the amplifier such that the $\underline{I}_o$ line is moved off the chart paper. With reference to Figure XIX (a typical trace of an SOF_6 plate) it may be seen that this amounts to magnifying the undulations of the trace. A still further magnification of the trace undulations may be achieved by increasing the gain of the amplifier in the other direction, that is, by displacing the $\underline{I} = 0$ base line from the chart in the other direction. Each of these three techniques was employed with the SOF_6 plates.

With the SOF_6 traces prepared, the problem of reduction began. First, a scale of the electron diffraction variable $\underline{s}$ $(= \frac{4\pi}{\lambda} \sin \theta/2)$ was established and affixed to the trace (the wavelength λ of the electrons for the SOF_6 experiment was 0.0620 A). This was accomplished by first computing the scattering

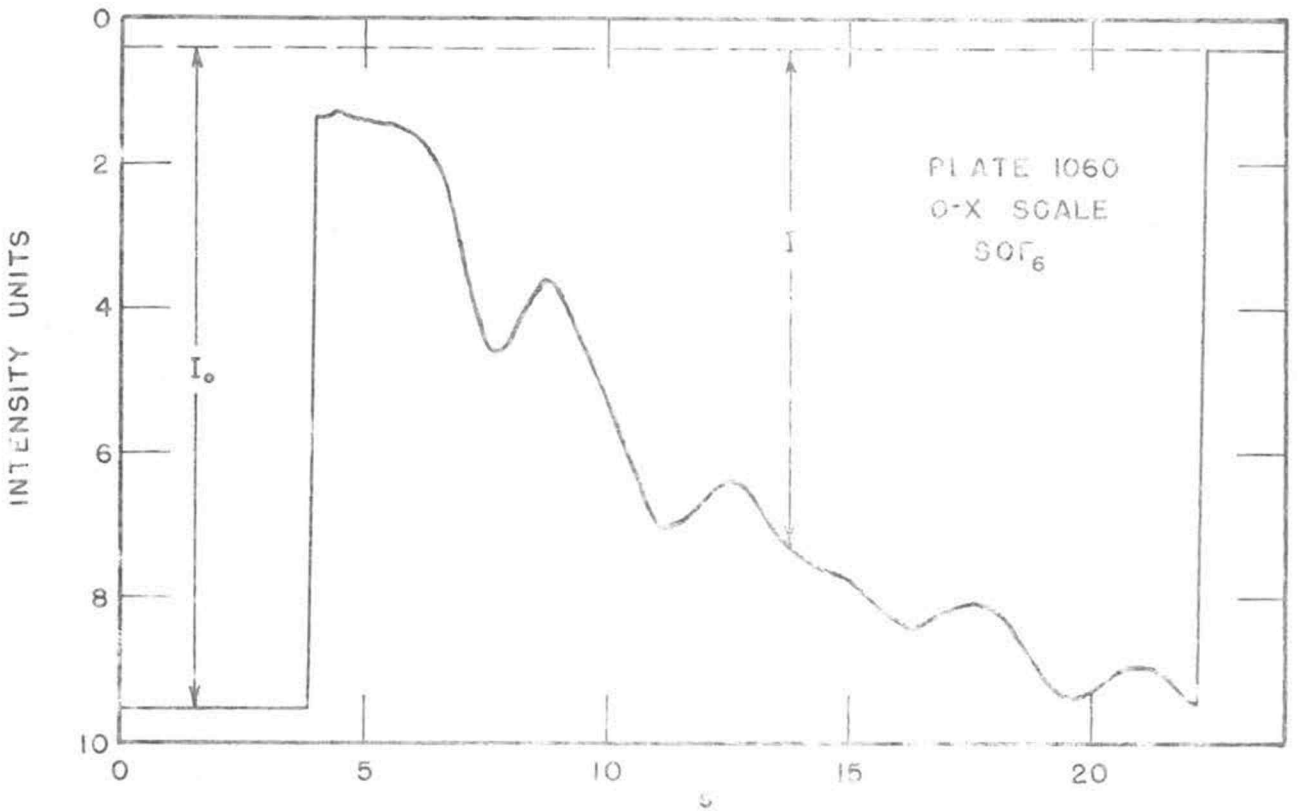

FIGURE XIX

TYPICAL DENSITOMETER PLOT WITH s SCALE INCLUDED

angles θ corresponding to each of a set of selected $\underline{s}$ values (the set ran from $1 \leqq \underline{s} \leqq 45$ in intervals of $\frac{1}{4}\,\underline{s}$) and then establishing the connection between these $\underline{s}$ values and linear distance on the trace through use of 1) the relationship $\underline{r}_p = L \tan\theta$ and 2) the relationship $r_p/r_t = 1/13.490$; $\underline{r}_p$ and $\underline{r}_t$ were distances on the plate and trace, respectively, measured from the position of the undiffracted beam. The distance from the scattering point to the photographic plate is designated by $\underline{L}$ and is equal to 96.27 mm.

The next step was to evaluate photographic densities from the individual densitometer traces at intervals closely enough spaced on the continuous trace to yield a satisfactory amount of data. Rather arbitrarily, the interval chosen was $\frac{1}{4}\,\underline{s}$. Since as mentioned previously

$$D \cong \log (I_o/I)$$

where $\underline{D}$ is photographic density it was convenient to make a logarithmic rule such that $\log (I_o/I)$ could be read directly from the traces having zero per cent and 100 per cent transmission (0-100 scale) identified with complete absorption and clear plate respectively. The same logarithmic rule could be and was used with the traces in which the 100 per cent transmission point had been

amplified off the chart paper (0-X scale). Since the scale on the rule is log (100/I) = 2 - log I, the amplification amounts to displacing all points $\underline{I}$ of the trace to proportionally larger values $\underline{I}'$ and these values $\underline{I}'$ are measured by the rule as 2 - log I' = 2 - log n - log I. Thus, in order to convert readings obtained using the rule from the 0 - X scale to density it was simply necessary to add a constant to all readings. The constant was evaluated by comparing readings from the rule for 7-10 corresponding points on traces made from a given plate on both the 0 - 100 and 0 - X scales; the average of the differences was taken as the constant. To obtain densities from the traces made on the X - X scale a more elaborate procedure was required since these traces bore no reference point (such as the zero or 100 per cent transmission base lines). This procedure amounted to establishing the scale of transmission ($= I/I_o$) for the X - X traces by comparing them at selected points with the 0 - 100 scale traces from the same plate for which, of course, the transmissions were known. The transmissions at 10 selected points on an X - X trace were measured on an arbitrary scale and these values differenced by pairs (1-6, 2-7, 3-8, etc.). These differences in actual transmission had to be equal to the corresponding differences derived from the 0 - 100 trace.

For each combination difference the ratio of the number of true transmission units from the 0 - 100 scale to the number of scale divisions on the X - X scale, or $\Delta T/\Delta$ S.D. , was formed. The average of these ratios was taken as representing the relationship between transmission and the arbitrary scale of the X - X trace. The transmissions from the X - X trace were then obtained by measuring from a reference base line and using the established ratio. The logarithims of reciprocal transmissions were then computed to yield photographic densities.

Following the above described measurements of photographic densities from the several plates the results were averaged into a single set of density data. Since the density of a photographic plate exposed to electrons is proportional to the intensity of the electron rays striking the plate over a considerable range of density (see Figure XX) this averaging procedure amounted to formulation of a curve of scattered electron intensity striking the plate (I_p) as a function of the variable $\underline{s}$. The actual procedure was accomplished by simply adding the photographic densities of the various plates at corresponding values of $\underline{s}$ and dividing by the number of plates provided that each of the plates had a range of densities falling only on the linear part of the response

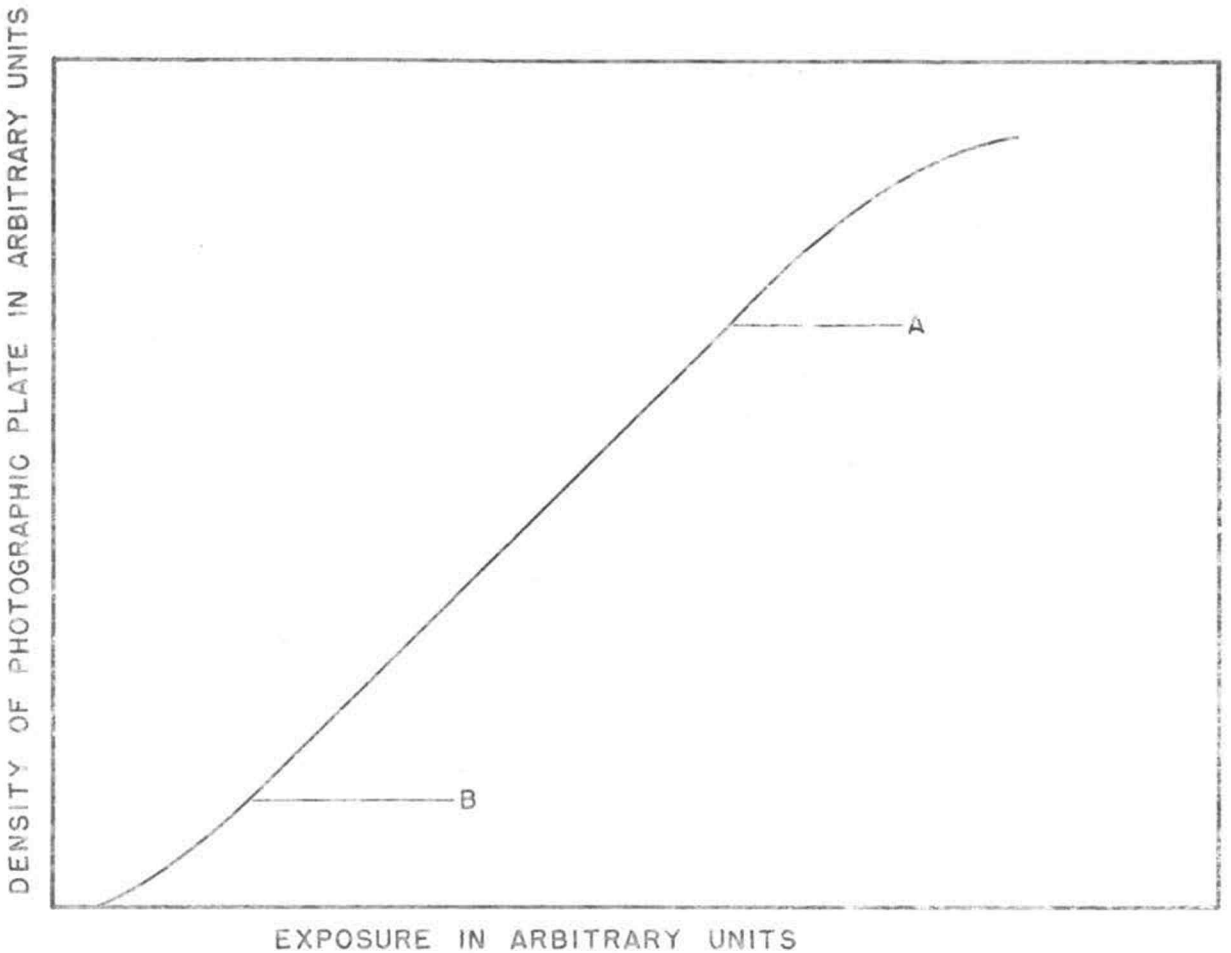

FIGURE XX

PHOTOGRAPHIC PLATE DARKENING VERSUS EXPOSURE TIME

curve shown in Figure XX, that is, in the range between points A and B. Plates with densities falling outside this range were also used but a correction had to be made for non-linearity of response. This correction was made by choosing a relatively light plate for which the density was surely everywhere proportional to exposure ($0.2 \leqq D \leqq 1.5$, as found from past experience with this photographic emulsion) and dividing the density values point by point into the density values for each of the more heavily exposed plates. These ratios were constant so long as the heavier plate density values lay on the linear part of the response curve. Deviations from constancy were used as factors to correct the density values of the more heavily exposed plates. Karle and Karle (18, p. 957-962) give a more detailed account of this procedure. Table V gives the individual plate intensities (I_p) and the composite plate intensities for all the SOF_6 plates used over the range of data, that is, $4.5 \leqq s \leqq 45$. Plate 1039 was not used in the composite curve for two reasons: it did not have the same slope as the other curves and the data appeared to be slightly displaced (about 1/8 of an s unit) to larger values of s. The calculations described below were done on the composite curve and the data from plate 1039 separately and the curve combined as a final step.

TABLE V

AVERAGING SEPARATE PLATE INTENSITIES TO OBTAIN I_p

s	1060 O-X	1074 O-X	1072 X-X	1074 X-X	I_p
4.5	2.001				2.001
5.0	1.886				1.886
5.5	1.818				1.818
6.0	1.737				1.737
6.5	1.560				1.560
7.0	1.245				1.245
7.5	1.068				1.068
8.0	1.082				1.082
8.5	1.155				1.155
9.0	1.152				1.152
9.5	1.080				1.080
10.0	0.974				0.974
10.5	0.870				0.870
11.0	0.818				0.818
11.5	0.827	0.826	0.8356		0.8295
12.0	0.849	0.845	0.8637		0.8526
12.5	0.860	0.858	0.8783		0.8654
13.0	0.841	0.842	0.8533		0.8454
13.5	0.800	0.802	0.8045		0.8022
14.0	0.774	0.776	0.7817		0.7772
14.5	0.766	0.765	0.7656		0.7655
15.0	0.754	0.756	0.7579		0.7560
15.5	0.738	0.742	0.7438		0.7413
16.0	0.727	0.728	0.7212		0.7254
16.5	0.727	0.726	0.7227		0.7252
17.0	0.733	0.730	0.7322		0.7317
17.5	0.737	0.736	0.7396		0.7375
18.0	0.730	0.730	0.7319		0.7306
18.5	0.706	0.710	0.7087		0.7082
19.0	0.680	0.682	0.6779		0.6800
19.5	0.665	0.666	0.6595		0.6635
20.0	0.670	0.667	0.6605		0.6658
20.5	0.683	0.676	0.6774		0.6788
21.0	0.686	0.683	0.6855		0.6848
21.5	0.676	0.676	0.6780		0.6767
22.0	0.660	0.660	0.6609		0.6603
22.5		0.648	0.6487		0.6484
23.0		0.640	0.6392		0.6396
23.5		0.636	0.6360		0.6360
24.0		0.634	0.6330		0.6335

TABLE V - Cont.

s	1074 O-X	1072 X-X	1074 X-X	I_p	1039 X-X
24.5	0.630	0.6331		0.6316	
25.0	0.629	0.6310		0.6300	
25.5	0.627	0.6290		0.6280	
26.0	0.624	0.6268		0.6254	
26.5	0.619	0.6227	0.6290	0.6202	
27.0	0.612	0.6134	0.6124	0.6126	
27.5	0.604	0.6059	0.6056	0.6052	
28.0		0.5999	0.6000	0.6000	
28.5		0.5999	0.5989	0.5994	
29.0		0.6013	0.6003	0.6008	
29.5		0.6030	0.6010	0.6020	
30.0		0.6006	0.5984	0.5995	
30.5		0.5943	0.5933	0.5938	
31.0		0.5873	0.5881	0.5877	0.6515
31.5		0.5816	0.5830	0.5823	0.6468
32.0		0.5803	0.5811	0.5807	0.6459
32.5		0.5806	0.5811	0.5808	0.6468
33.0		0.5800	0.5811	0.5806	0.6472
33.5		0.5803	0.5801	0.5802	0.6450
34.0		0.5793	0.5780	0.5786	0.6418
34.5		0.5750	0.5751	0.5750	0.6382
35.0			0.5727	0.5727	0.6341
35.5			0.5704	0.5704	0.6313
36.0			0.5687	0.5687	0.6299
36.5			0.5673	0.5673	0.6290
37.0			0.5676	0.5676	0.6296
37.5			0.5684	0.5684	0.6305
38.0			0.5687	0.5687	0.6307
38.5			0.5682	0.5682	0.6291
39.0			0.5671	0.5671	0.6268
39.5			0.5658	0.5658	0.6245
40.0			0.5645	0.5645	0.6236
40.5			0.5647	0.5647	0.6245
41.0			0.5663	0.5663	0.6260
41.5			0.5674	0.5674	0.6271
42.0			0.5677	0.5677	0.6268
42.5			0.5677	0.5677	0.6263
43.0			0.5665	0.5665	0.6244
43.5			0.5662	0.5662	0.6223
44.0			0.5642	0.5642	0.6207
44.5			0.5641	0.5641	0.6191
45.0			0.5632	0.5632	0.6175

The total scattered intensity per unit solid angle is related to the electron intensity striking the photographic plate by equation (52) (2, p. 1311-1317).

$$I_p = I_t \cdot \alpha(s) \cdot P(\theta) \tag{52}$$

where

$\alpha(s)$ is the sector function (calibrated by direct measurement)

I_t is the total scattered intensity per unit solid angle = $I(\theta)$

I_p is the electron intensity striking the plate

$P(\theta)$ is $\cos^3\theta$ where θ is the scattering angle

The $P(\theta)$ is necessary because the photographic plate is normal to the undiffracted beam instead of being everywhere equidistant from the scattering point. The $\alpha(s)$ function arises from the presence of the sector in the apparatus. The sector is a device, cut in the shape of a heart, which rotates rapidly around an axis perpendicular to its plane and coincident with the undiffracted beam. The purpose of the sector is to reduce the scattered electron intensity at low angles relative to that at high angles. The angular opening of the sector

is proportional to $\underline{r}^3$, measured on the sector, except at very small scattering angles where the opening is larger. The function $\alpha(s)$, then, expresses the relationship between angular openings on the sector and the variable $\underline{s}$ on the plate.

If $\underline{I}_t$ from equation (51) is substituted in equation (52), one obtains (neglecting the constant since only relative intensities are of interest)

$$\frac{I_p}{\alpha(s)\,P(\theta)} = \sum_{ij}{}' \frac{(Z-F)_i(Z-F)_j}{s^4} e^{(-a_{ij}s^2)} \frac{\sin s r_{ij}}{s r_{ij}} + \sum_i \frac{(Z-F)_i^2}{s^4} + \sum_i \frac{S_v}{s^4} \qquad (53)$$

where the prime indicates that $i \neq j$. Of the summed terms it is the first which is of interest in connection with the molecular structure. If equation (53) is multiplied through by $\underline{s}^4$ and rearranged, one obtains what has been called the molecular scattering equation (2, p. 1311-1317) and (28, p. 671-690)

$$I_m = \sum_{ij}{}' \frac{(Z-F)_i\,(Z-F)_j}{s r_{ij}}\, e^{(-a_{ij}s^2)}\, \underline{\sin s r_{ij}}$$

$$= \frac{s\,I_p}{\phi_{(s)}\,P(\theta)} - B_t \qquad (54)$$

where $\phi_{(s)} = \frac{\alpha(s)}{s^3}$ differs only slightly from constancy and

$$B_t = \sum_i \left[(Z-F)_i^2 + S_{-v}\right]$$

is the theoretical background. In order to obtain a curve corresponding to only the molecular scattering, the operations suggested by equation (54) were applied to the I_p data for SOF_6 in the following way. Each density value (Table V) was multiplied by the quantity

$$\frac{s^3}{\alpha(s)} \cdot \frac{1}{\cos^3\theta}$$

and plotted on large-size graph paper. Then the background function B_t was prepared by simply drawing a smooth curve through the undulations of the curves and subtracting it point by point. Finally, the two curves carried through to this point (I_p and 1039, Table V) were

combined and multiplied by $\underline{s}$ to give a composite molecular scattering curve $\underline{I}_m$. This manner of handling B_t deserves a word. The actual background on the photographic plate may, and nearly always does, differ considerably from the theoretical background because of miscellaneous experimental effects, such as scattering from apparatus pinholes, etc. Fortunately, the experimental background seems to be a smooth function which has only the effect of boosting the overall density of the plate and can be easily taken account of as indicated.

In practice the molecular scattering curve $\underline{I}_m$ does not lend itself well to analysis (28, p. 671-690). A more convenient curve may be prepared by dividing $\underline{I}_m$ through by a function which converts the variable coefficients $(Z - F)_i$ to essentially constant coefficients. This was done for SOF_6 by dividing by

$$f_S \cdot f_F \cdot s^3$$

(the subscript refers to sulfur and fluorine atoms) using the atomic scattering factors calculated by Ibers and Hoerni (15, p. 405-408). The relationship existing between the function given by Ibers and Hoerni and equation (54) is

$$f_{i(\theta)} = \frac{K(Z-F)_i}{s^2}$$

such that

$$f_F \cdot f_S \cdot s^3 = \frac{K'(Z-F)_F(Z-F)_S}{s} \qquad (55)$$

where K and K' are constants. Equation (54) reduces to

$$I_s = \sum_{ij}{}' \frac{K_{ij}}{r_{ij}} e^{(-a_{ij}s^2)} \sin s r_{ij} \qquad (56)$$

The coefficient K_{ij}/r_{ij} is exactly constant for all terms involving sulfur and fluorine, but deviates slightly from constancy for the sulfur-oxygen, fluorine-fluorine, and fluorine-oxygen terms. For example, the deviation for sulfur-oxygen terms is the small deviation of the ratio

$$\frac{(Z-F)_O}{(Z-F)_F}$$

from constancy. The experimental curve for SOF_6 resulting from this treatment is presented as Table VI. This curve includes data from $0.5 \leqq \underline{s} \leqq 4.5$ not obtained in the densitometric procedure (the region was blocked off by the central beam stop) but by visual estimation of ring amplitudes and diameters from a plate made without a beam stop.

TABLE VI

SOF_6 EXPERIMENTAL INTENSITY I

s	I_s	s	I_s
0.5	1930	20.5	290
1.0	2500	21.0	957
1.5	1130	21.5	776
2.0	-710	22.0	127
2.5	-1110	22.5	-274
3.0	-410	23.0	-525
3.5	430	23.5	-440
4.0	695	24.0	-324
4.5	360	24.5	41
5.0	322	25.0	233
5.5	592	25.5	432
6.0	950	26.0	610
6.5	841	26.5	604
7.0	-608	27.0	145
7.5	-1228	27.5	-258
8.0	-629	28.0	-431
8.5	840	28.5	-202
9.0	1775	29.0	239
9.5	1797	29.5	670
10.0	684	30.0	706
10.5	-748	30.5	363
11.0	-1421	31.0	-97
11.5	-842	31.5	-374
12.0	88	32.0	-301
12.5	714	32.5	19
13.0	685	33.0	265
13.5	25	33.5	272
14.0	-217	34.0	228
14.5	-104	34.5	92
15.0	-113	35.0	-111
15.5	-350	35.5	-252
16.0	-667	36.0	-299
16.5	-378	36.5	-314
17.0	225	37.0	-142
17.5	830	37.5	102
18.0	909	38.0	282
18.5	293	38.5	248
19.0	-618	39.0	172
19.5	-1086	39.5	-74
20.0	-723	40.0	-263

TABLE VI - Cont.

s	I_s	s	I_s
41.0	-16	43.5	-38
41.5	227	44.0	-102
42.0	369	44.5	-138
42.5	408	45.0	-278
43.0	160		

ELUCIDATION OF THE MOLECULAR STRUCTURE OF SOF_6

The problem of elucidating the structure of a gaseous molecule from an experimental intensity curve is the problem of discovering the lengths and number of interatomic distances giving rise to the curve; the connection between the curve and the molecular geometry is given by equation (56). An obvious procedure, but indirect, would involve calculation of theoretical intensity curves using equation (56) for various models of the molecule; the calculated curve most closely agreeing with the experimental curve would correspond to the model having the most nearly correct parameter values. A more direct method would seem to be one by which the experimental curve could be analyzed for the number and magnitudes of the distances going into it. Both of these methods are used in practice, the direct method for the purpose of establishing preliminary distance values from which a reasonable model of the molecule can be deduced. The more sensitive indirect method is then used for refining the parameter values.

The direct method involves calculation of a radial distribution function from the experimental intensity curve. This function has as ordinate a quantity related to the probability of finding two atoms a distance r apart

and as abscissa the variable r; distances corresponding to internuclear separations thus appear as peaks on the curve. The theory of the calculation may be summarized as follows. A function $r^2D(r)$ may be defined as representing the product of the scattering powers of two volume elements a distance r apart. The total scattered intensity from a molecule will then be expressed by (26, p. 659-664)

$$I_s = K\int_0^\infty r\, D(r) \sin sr\, dr \qquad (57)$$

which upon inversion becomes

$$r\, D(r) = K'\int_0^\infty I_s \sin sr\, ds \qquad (58)$$

Substitution of I_s from equation (56) into (58) and performing the integration reveals that the peaks of the radial distribution curves are Gaussian in form. In a calculation using experimental values I_s, the integration of equation (58) is done numerically (26, p. 659-664) using the approximate relation

$$r D(r) = \sum_s I_s \sin sr \qquad (59)$$

where the constant has been neglected.

The first step in the elucidation of the SOF_6 structure was to calculate a suitable radial distribution function according to equation (59). The first calculation was done using $I_s \cdot \exp(-as^2)$ with $\underline{a} = 6 \times 10^{-4}$ in place of I_s in order to give better convergence of the Fourier series. The calculation was programmed for the Alwac III-E digital computer (the programming is described in the last part of this thesis) and carried out at intervals $\Delta s = 0.5$ over the range $0.5 \leqq \underline{s} \leqq 45.0$. The resulting preliminary curve (shown in Figure XXI) contains two obvious errors largely arising from errors in positioning the background to obtain I_m: 1) positive values of rD(r) at $\underline{r} < 1.0$ A cannot correspond to any interatomic distance and 2) negative values of rD(r) have no interpretation. Some not-so-obvious errors due to background positioning are also present which take the form of spurious peaks in the ranges of $\underline{r}$ which might well contain real peaks. Identification of such spurious peaks is difficult, but

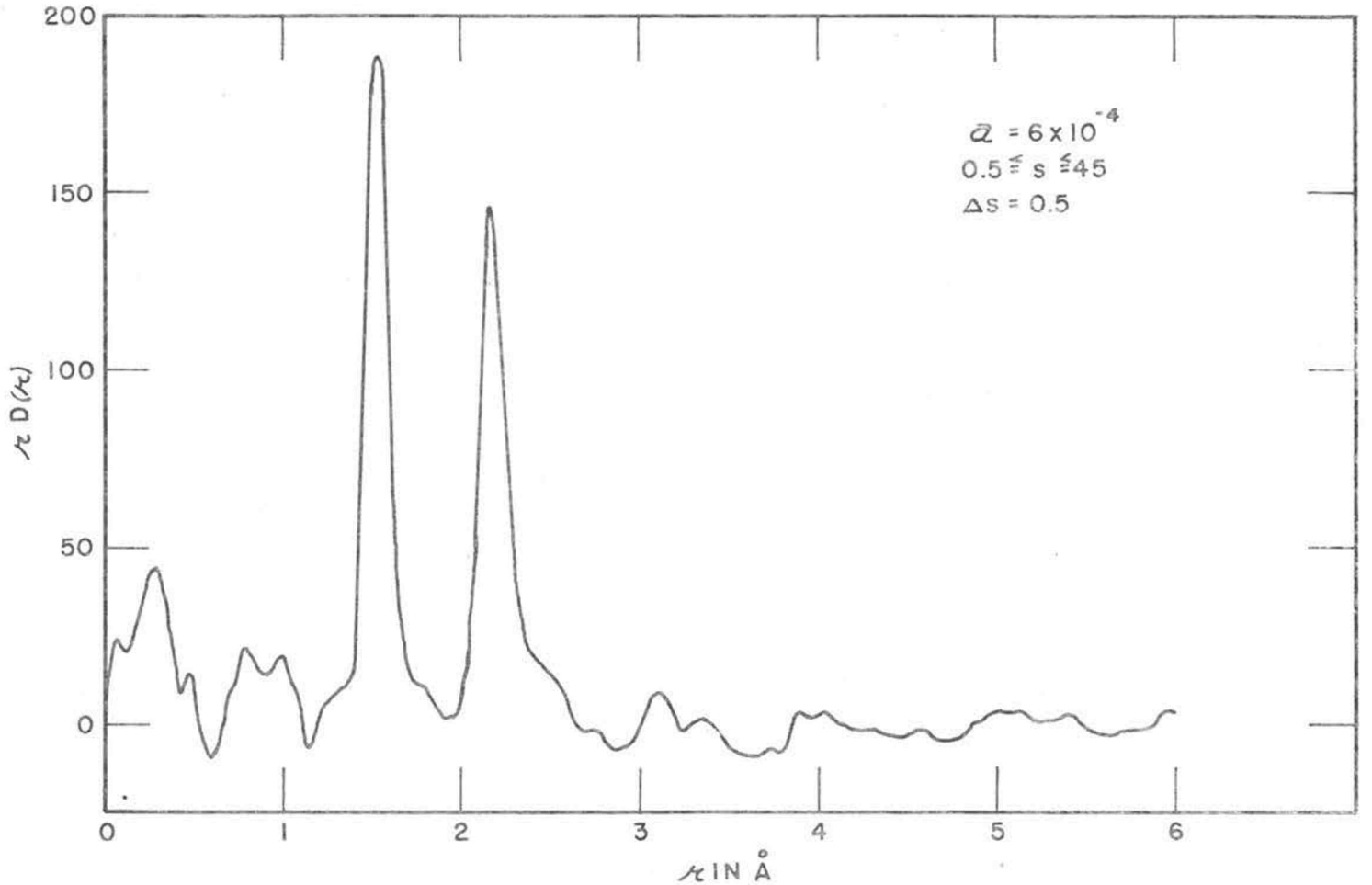

FIGURE XXI

EXPERIMENTAL RADIAL DISTRIBUTION CURVE I FOR SOF_6

may often be accomplished by computing a second radial distribution function with more rapid damping of I_s: spurious peaks tend to disappear while real peaks simply become shorter and broader. After identifying certain of the errors in the preliminary rD(r) curve for SOF_6, the connection between these errors and the background of the I_m curve was established, a corrected background introduced and a second I_s curve prepared. The radial distribution curve corresponding to this second I_s curve is shown in Figure XXII (the numerical results are given in Table VII) and it is seen to be much improved. Figure XXIII shows the experimental intensity curve II and Table VIII gives the numerical values of these data.

The next step was the deduction of the approximate geometry of the SOF_6 molecule from the distance spectrum given by the radial distribution curve. On inspection it was clear that a model of SOF_6 consisting of five fluorine atoms and an O-F group bonded to the sulfur atom in an octahedral configuration could qualitatively account for all peaks of the curve. For example, assuming the approximately octahedral configuration shown in Figure XXIV, a $S\text{-}O\text{-}F_6$ bond angle of 108°, and a staggered configuration of F_6 relative to F_1 and F_2, the large peak at 1.53 A may be assigned to all the bond distances of

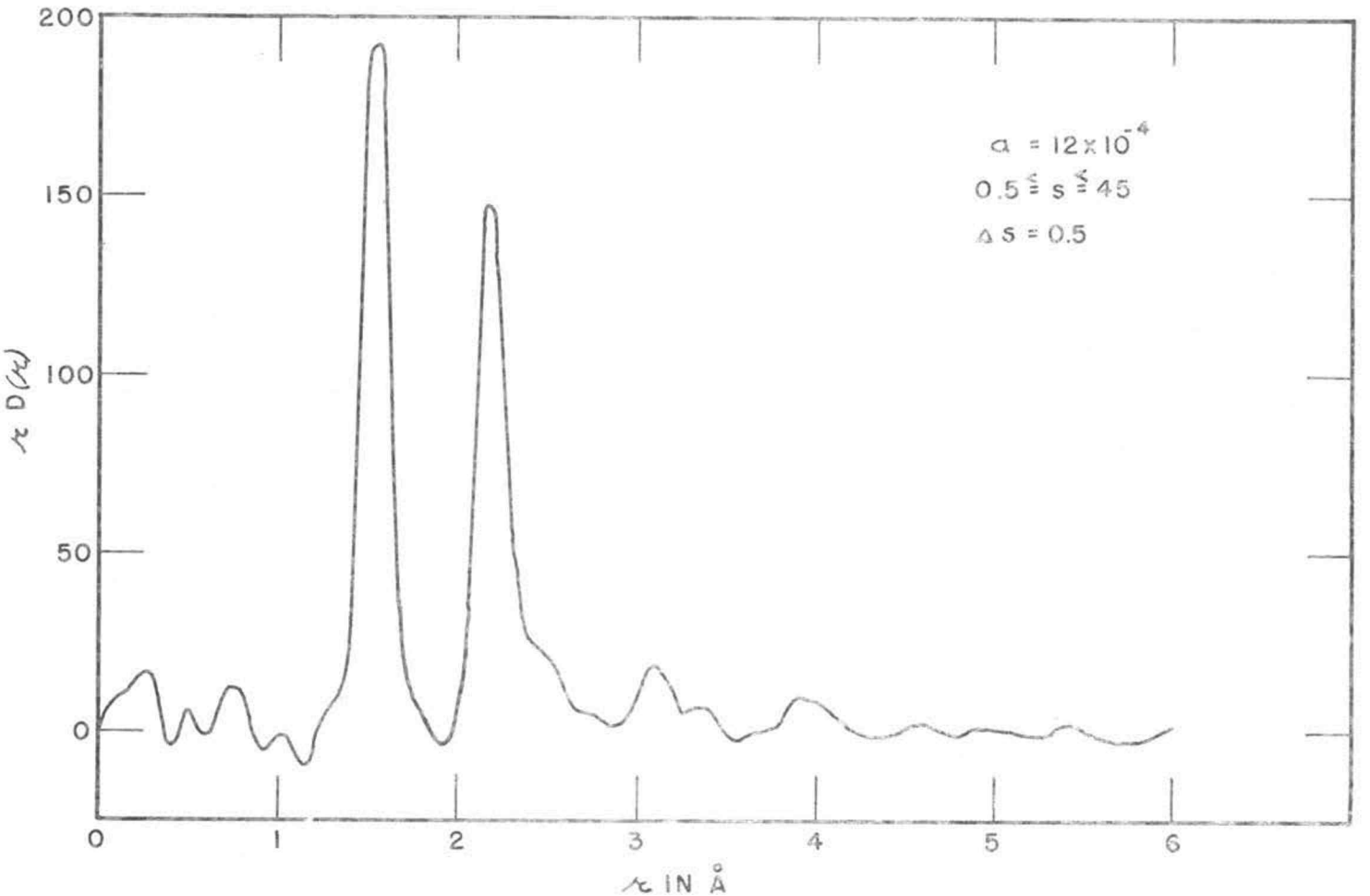

FIGURE XXII

EXPERIMENTAL RADIAL DISTRIBUTION CURVE II FOR SOF_6

TABLE VII

EXPERIMENTAL RADIAL DISTRIBUTION CURVE FOR SOF_6

r in Å	rD(r) in Arbitrary Units	r in Å	rD(r) in Arbitrary Units	r in Å	rD(r) in Arbitrary Units
0.05	7.2	2.05	36.1	4.05	7.5
0.10	9.6	2.10	96.1	4.10	4.8
0.15	10.9	2.15	145.3	4.15	2.2
0.20	14.4	2.20	145.3	4.20	0.0
0.25	16.9	2.25	106.0	4.25	-1.5
0.30	13.7	2.30	62.9	4.30	-1.6
0.35	3.3	2.35	36.4	4.35	-1.6
0.40	-4.4	2.40	25.6	4.40	-1.0
0.45	0.7	2.45	22.8	4.45	0.0
0.50	6.0	2.50	21.3	4.50	1.0
0.55	0.8	2.55	17.3	4.55	2.5
0.60	-0.8	2.60	11.4	4.60	2.9
0.65	6.7	2.65	6.8	4.65	1.3
0.70	10.8	2.70	5.9	4.70	-0.4
0.75	12.5	2.75	6.0	4.75	-1.5
0.80	9.7	2.80	3.9	4.80	-1.0
0.85	0.0	2.85	1.9	4.85	0.7
0.90	-5.9	2.90	2.1	4.90	1.2
0.95	-4.3	2.95	4.6	4.95	1.0
1.00	-1.2	3.00	9.9	5.00	0.9
1.05	-1.5	3.05	16.0	5.05	0.2
1.10	-7.5	3.10	18.8	5.10	-0.2
1.15	-9.4	3.15	16.6	5.15	-0.6
1.20	-1.9	3.20	10.4	5.20	-1.4
1.25	3.7	3.25	5.6	5.25	-1.2
1.30	6.7	3.30	5.8	5.30	0.3
1.35	11.2	3.35	7.3	5.35	1.8
1.40	29.0	3.40	6.3	5.40	2.6
1.45	94.5	3.45	2.8	5.45	1.9
1.50	181.1	3.50	-1.3	5.50	0.4
1.55	192.3	3.55	-2.4	5.55	-1.1
1.60	119.4	3.60	-1.2	5.60	-2.3
1.65	48.9	3.65	-0.3	5.65	-2.5
1.70	19.0	3.70	0.7	5.70	-2.7
1.75	9.4	3.75	1.0	5.75	-3.3
1.80	4.7	3.80	2.3	5.80	-3.0
1.85	-0.7	3.85	7.2	5.85	-2.4
1.90	-4.6	3.90	10.3	5.90	-1.1
1.95	-3.8	3.95	9.3	5.95	0.9
2.00	4.1	4.00	8.6	6.00	0.9

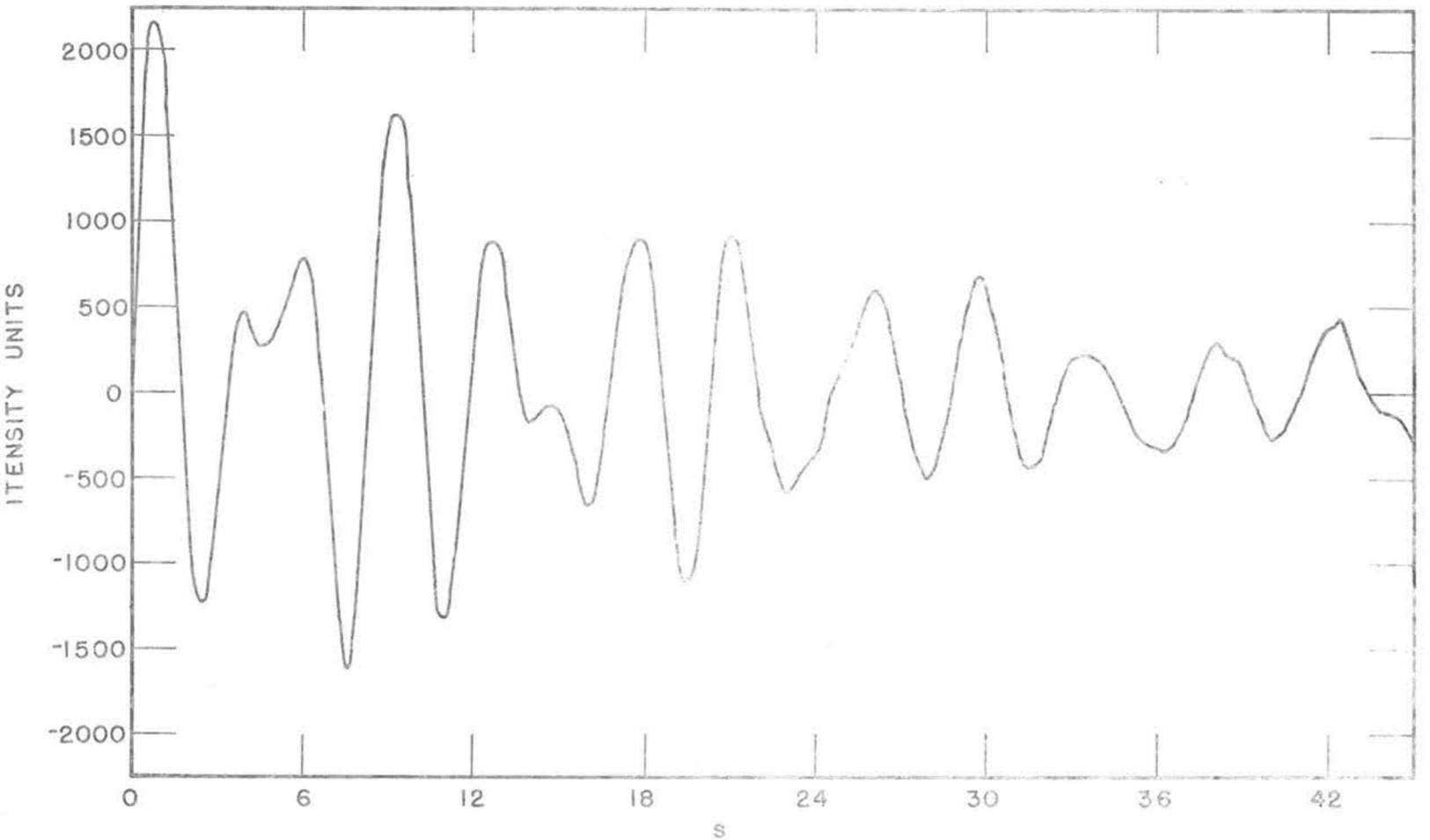

FIGURE XXIII

EXPERIMENTAL INTENSITY CURVE FOR SOF_6

TABLE VIII

SOF_6 EXPERIMENTAL INTENSITY II

s	I_s	s	I_s
0.5	2110	21.0	915
1.0	2026	21.5	730
1.5	434	22.0	78
2.0	-870	22.5	-325
2.5	-1220	23.0	-576
3.0	-550	23.5	-492
3.5	215	24.0	-378
4.0	465	24.5	-17
4.5	260	25.0	173
5.0	289	25.5	371
5.5	551	26.0	576
6.0	796	26.5	539
6.5	466	27.0	78
7.0	-771	27.5	-326
7.5	-1633	28.0	-500
8.0	-1010	28.5	-271
8.5	614	29.0	171
9.0	1522	29.5	602
9.5	1617	30.0	639
10.0	589	30.5	297
10.5	-742	31.0	-159
11.0	-1332	31.5	-432
11.5	-706	32.0	-354
12.0	250	32.5	-29
12.5	878	33.0	221
13.0	814	33.5	233
13.5	126	34.0	194
14.0	-161	34.5	63
14.5	-84	35.0	-133
15.0	-108	35.5	-270
15.5	-350	36.0	-312
16.0	-661	36.5	-323
16.5	-401	37.0	-147
17.0	215	37.5	101
17.5	817	38.0	282
18.0	892	38.5	248
18.5	273	39.0	172
19.0	-642	39.5	-74
19.5	-1116	40.0	-263
20.0	-758	40.5	-206
20.5	251	41.0	-16

TABLE VIII - Cont.

s	I_s	s	I_s
41.5	227	44.0	-102
42.0	369	44.5	-138
42.5	408	45.0	-278
43.0	160		
43.5	-38		

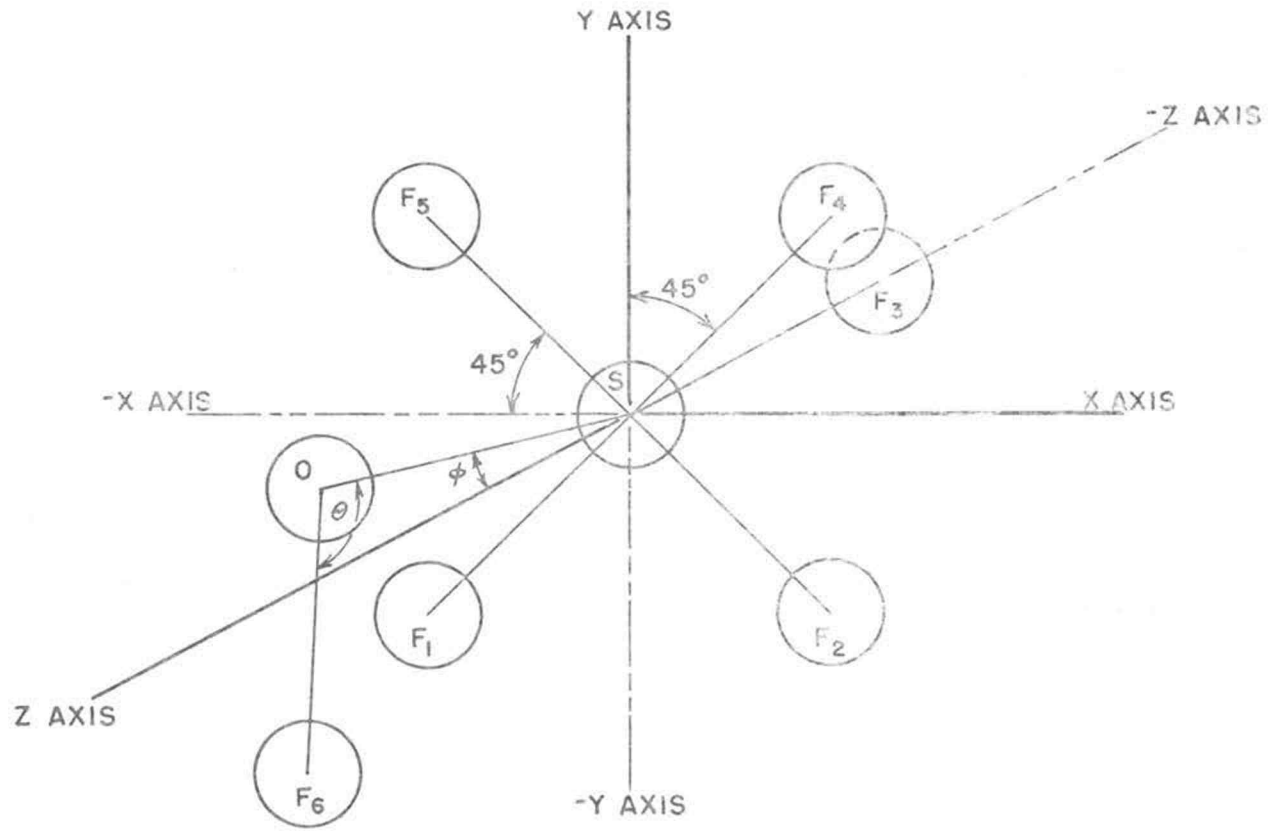

FIGURE XXIV

COORDINATE SYSTEM USED FOR SOF_6

the molecule (the different bond distances are too close to be resolved), the peak at 2.18 A is due to the interactions $F_3 \cdots F_{1,2,4,5}$, $F_6 \cdots F_{1,2}$, $F_1 \cdots F_{2,5}$, $F_2 \cdots F_{1,4}$, $O \cdots F_{1,2,4,5}$, and $S \cdots F_6$, the peaks at 3.10 and 3.35 A are due to $F_6 \cdots F_{4,5}$, $F_1 \cdots F_4$, $F_2 \cdots F_5$, and $O \cdots F_3$, and the peak at 3.90 A is due to $F_6 \cdots F_3$.

Having established the configuration of the molecule as octahedral, it remained to discovered values of the structural parameters giving an acceptable fit to the radial distribution and experimental curve. Investigation disclosed that a symmetrical model (all bond angles except the S-O-F_6 angle equal to 90°) could not be made to give as good a fit as slightly distorted models. The number of parameters necessary for the description of distorted models is, of course, much greater than for a symmetrical model and the structural problem for SOF_6 was thus more difficult than it might have been. Indeed, small distortions of quite different types could certainly be found which give about equal quality fits. Because of this complexity, the work of elucidating the SOF_6 structure was devoted to obtaining a good fit to the data for a distorted model which preserved as much symmetry as possible. The parameters to be adjusted were thus held to a managable number.

The procedure was to calculate and compare theoretical radial distribution curves for various models of the molecule with the experimental radial distribution curve, and for those cases where apparently good agreement was obtained, to calculate the more structure sensitive theoretical intensity curves for comparison with the experimental intensity curve II (see Figure XXIII). The calculation of a theoretical radial distribution curve first required calculation of the several interatomic distances corresponding to the model having the desired parameter values; second, calculation of individual Gaussian peaks corresponding to each of the distance terms; and third, summation of the several Gaussian peaks to give the desired result. The calculation of the interatomic distances was achieved by establishing x,y,z coordinates for each atom in the particular model of the SOF_6 molecule and solving the usual distance equations expressed in terms of these coordinates. The geometrical parameters chosen for investigation were the bond distances $S\text{-}F_3$, $S\text{-}F_1$ ($= S\text{-}F_2 = S\text{-}F_4 = S\text{-}F_5$), S-O, and $O\text{-}F_6$, the bond angles ϕ and θ (see Figure XXIV); the not-so-obvious coordinates are $\underline{x} = 0$, $\underline{y} = A \sin\phi$, $\underline{z} = A \cos\phi$ for oxygen and $\underline{x} = 0$, $\underline{y} = -(B \cos\chi - A \cos\phi)$, $\underline{z} = A \cos\phi + B \sin\chi$ for fluorine (6) where $\underline{A}$ is the S-O distance, $\underline{B}$ is the $O\text{-}F_6$ distance and $\chi = \theta - (90 - \phi)$.

There also exist vibration parameters (the a_{ij} terms) but no attempt was made to investigate them. They were included in the calculation at reasonable values in terms of Dr. Hedberg's past experience, changes occasionally being made when it seemed in order to obtain a better fit. The calculation of the Gaussian peaks corresponding to the individual distances was done as follows. The equation for the Gaussian curve is (2, p. 1311-1317)

$$h = h_{\Delta r=0}\, e^{-\frac{(\Delta r_{ij})^2}{4a_{ij}}} \tag{60}$$

where Δr_{ij} is the displacement of the distance r_{ij} from equilibrium. If the area beneath the curve is to be equal to nZ_iZ_j/r_{ij} where n is the number of distances of length r_{ij} and the Z's are the atomic numbers, one may write (2, p. 1311-1317)

$$\text{Area} = \int_{-\infty}^{\infty} h\, d(\Delta r)$$

$$= \frac{nZ_iZ_j}{r_{ij}} \frac{1}{\sqrt{\pi a_{ij}}} \int_{-\infty}^{\infty} e^{-\frac{(\Delta r_{ij})^2}{4a_{ij}}}\, d(\Delta r_{ij}) \tag{61}$$

$$= \frac{nZ_iZ_j}{r_{ij}}$$

from which the peak height $h_{\Delta r=0}$ is given by

$$h_{\Delta r=0} = \frac{n Z_i Z_j}{\mu_{ij}} \frac{1}{\sqrt{\pi a_{ij}}} \qquad (62)$$

For each Gaussian a $h_{\Delta r=0}$ was calculated according to equation (62) omitting the factor $1/\sqrt{\pi}$ which was common to all. These quantities were placed on a convenient arbitrary scale and the individual peaks plotted out at 0.05 A intervals from equation (60) and summed to give the theoretical rD(r).

A total of 20 models of the SOF_6 molecule covering the parameter ranges (see Figure XXIV)

$$2^\circ \leqq \phi \leqq 10^\circ$$
$$107^\circ \leqq \Theta \leqq 112^\circ$$
$$90^\circ \leqq \angle F_3\text{-}S\text{-}F_{1,2,4,5} \leqq 93^\circ$$
$$90^\circ \leqq \angle F_3\text{-}S\text{-}F_{1,2} \leqq 94^\circ$$
$$88^\circ \leqq \angle F_3\text{-}S\text{-}F_{4,5} \leqq 90^\circ$$
$$1.53 \leqq S\text{-}O \leqq 1.65$$
$$1.525 \leqq S\text{-}F_{1,2,4,5} \leqq 1.54$$
$$1.51 \leqq S\text{-}F_3 \leqq 1.58$$
$$1.42 \leqq O\text{-}F_6 \leqq 1.50$$

were tested by calculation of theoretical radial distribution curves, either wholly or in part. A number of these gave curves in good agreement with the observed

curves, and for them theoretical intensity curves were also calculated (these rather lengthy calculations were carried out by the Alwac III-E digital computer; the programming is discussed in the last section of this thesis) using the equation (see also equation (54))

$$s I_s = \sum_{ij}{}' \frac{n Z_i Z_j}{r_{ij}} e^{(-a_{ij} s^2)} \sin s r_{ij} \qquad (63)$$

where n is a weighting factor and has a numerical value equal to the number of interatomic distances with exactly the same r_{ij}. The atomic numbers of the atoms may replace the (Z-F) terms when the atoms comprising the molecule are not too different. Comparison of these theoretical intensity curves with the observed intensity curve provided a sensitive check on the quality of the model.

Two of the best fits were given by models 19 and 29, for which the various calculations described above are presented in detail: the parameters, atomic coordinates, and interatomic distances are given in Tables IX and X, the relative Gaussian peak height and vibration factor constants in Tables XI and XII, the numerical data for the individual Gaussian peaks and theoretical radial distribution curves in Tables XIII and XIV, the theoretical

TABLE IX

MODEL 19 COORDINATES AND INTERATOMIC DISTANCES

Values of Parameters

$\phi = 7^{\circ}$

$\ominus = 108^{\circ}30'$

$F_3\text{-}S\text{-}F_{1,2}$ angle = 92°

$F_3\text{-}S\text{-}F_{4,5}$ angle = 90°

S-O = 1.65 Å

$S\text{-}F_3$ = 1.51 Å

$S\text{-}F_{1,2,4,5}$ = 1.54 Å

$O\text{-}F_6$ = 1.43 Å

Atom	x	y	z
S	0	0	0
F_1	-1.0883	-1.0883	0.0537
F_2	1.0883	-1.0883	0.0537
F_3	0	0	-1.5100
F_4	1.0889	1.0889	0
F_5	-1.0889	1.0889	0
O	0	0.2011	1.6377
F_6	0	-1.0896	2.2533

TABLE IX - Cont.

Distance Type	Interatomic Distance (Å)
$F_6 \cdots F_3$	3.918
$S \cdots F_6$	2.503
$F_6 \cdots F_{4,5}$	3.318
$F_6 \cdots F_{1,2}$	2.454
$O \cdots F_{4,5}$	2.158
$O \cdots F_{1,2}$	2.314
$O \cdots F_3$	3.154
$F_3 \cdots F_{1,2}$	2.194
$F_3 \cdots F_{4,5}$	2.157
$F_1 \cdots F_2$	2.178
$F_1 \cdots F_5$	2.178
$F_2 \cdots F_4$	2.178
$F_4 \cdots F_5$	2.178
$F_1 \cdots F_4$	3.079
$F_2 \cdots F_5$	3.079

TABLE X

MODEL 29 COORDINATES AND INTERATOMIC DISTANCES

Values of Parameters

$\phi = 2^{\circ}$

$\theta = 108^{\circ}$

$F_3\text{-}S\text{-}F_{1,2,4,5}$ angle $= 90^{\circ}$

$S\text{-}O = 1.64$ Å

$S\text{-}F_{1,2,3,4,5} = 1.53$ Å

$O\text{-}F_6 = 1.43$ Å

Atom	x	y	z
S	0	0	0
F_1	-1.0819	-1.0819	0
F_2	1.0819	-1.0819	0
F_3	0	0	-1.5300
F_4	1.0819	1.0819	0
F_5	-1.0819	1.0819	0
O	0	0.0490	1.6390
F_6	0	-1.2865	2.1281

TABLE X - Cont.

Distance Type	Interatomic Distance (Å)
$F_3 \cdots F_6$	3.877
$S^3 \cdots F_6$	2.487
$F_6 \cdots F_{4,5}$	3.363
$F_6 \cdots F_{1,2}$	2.396
$O \cdots F_{4,5}$	2.219
$O \cdots F_{1,2}$	2.266
$O \cdots F_3$	3.170
$F_3 \cdots F_{1,2,4,5}$	2.164
$F_1 \cdots F_{2,5}$	2.164
$F_2 \cdots F_{1,4}$	2.164
$F_1 \cdots F_4$	3.060
$F_2 \cdots F_5$	3.060

TABLE XI

MODEL 19 NORMALIZATION OF PEAK HEIGHTS

Distance	Normalization Constant $k_{sx}=0$	Peak Height in Arbitrary Units	$a_{ij} \times 10^4$
$S\text{-}F_{1,2,4,5}$	11837.0	30.00	10
$S\text{-}F_3$	3018.9	7.65	10
S-O	2456.8	6.23	10
$O\text{-}F_6$	1592.9	4.04	10
$F_1 \cdots F_5$ $F_2 \cdots F_4$ $F_4 \cdots F_5$	2882.6	7.31	15
$F_1 \cdots F_2$	962.0	2.44	15
$F_3 \cdots F_{4,5}$	1940.1	4.92	15
$F_3 \cdots F_{1,2}$	1908.1	4.84	15
$O \cdots F_{4,5}$	1724.5	4.37	15
$O \cdots F_{1,2}$	1607.1	4.07	15
$F_6 \cdots F_{1,2}$	1007.3	2.55	45
$S \cdots F_6$	980.0	2.48	35
$F_1 \cdots F_4$ $F_2 \cdots F_5$	1177.3	2.98	25
$O \cdots F_3$	510.6	1.30	25
$F_6 \cdots F_{4,5}$	718.1	1.82	45
$F_3 \cdots F_6$	267.2	0.68	60

TABLE XII

MODEL 29 NORMALIZATION OF PEAK HEIGHTS

Distance	Normalization Constant $k_{sr}=0$	Peak Height in Arbitrary Units	$a_{ij} \times 10^4$
$S\text{-}F_{1,2,3,4,5}$	14906.8	37.50	10
S-O	2471.0	6.22	10
$O\text{-}F_6$	1592.9	4.01	10
$F_3 \cdots F_{1,2,4,5}$ $F_1 \cdots F_{2,5}$ $F_2 \cdots F_{1,4}$	7741.9	19.47	15
$O \cdots F_{1,2}$	1642.0	4.13	15
$O \cdots F_{4,5}$	1676.3	4.22	15
$F_6 \cdots F_{1,2}$	1007.5	2.54	45
$S \cdots F_6$	978.2	2.46	35
$F_1 \cdots F_4$ $F_2 \cdots F_5$	1184.2	2.98	25
$O \cdots F_3$	508.1	1.28	25
$F_6 \cdots F_{4,5}$	718.1	1.81	45
$F_3 \cdots F_6$	352.9	1.32	35

TABLE XIII

MODEL 19 NORMALIZED GAUSSIAN PEAKS PLUS THE SUM OF PEAKS
(THEORETICAL rD(r))

r	$S\text{-}F_{1,2,4,5}$	$S\text{-}F_3$	S-0	$0\text{-}F_6$	rD(r)
1.35				1.1	1.1
1.40	.1	.5		3.1	3.7
1.45	4.6	3.3		3.5	11.4
1.50	20.2	7.5		1.3	29.0
1.55	29.3	5.1	.7		35.1
1.60	13.4	1.0	3.3		17.7
1.65	1.3		6.2		7.5
1.70			3.3		3.3
1.75			.7		.7

r	$F_1 \cdot F_5$ $F_2 \cdot F_4$ $F_4 \cdot F_5$	$F_1 \cdot F_2$	$F_3 \cdot F_{4,5}$	$F_3 \cdot F_{1,2}$	$0 \cdot F_{1,2}$	$0 \cdot F_{4,5}$	$F_6 \cdot F_{1,2}$	$S \cdot F_6$	rD(r)
2.05	.5	.1	.5	.1		.5			1.7
2.10	2.5	.8	2.4	1.2		2.4			9.3
2.15	6.3	2.1	4.8	3.7		4.3			21.2
2.20	7.0	2.3	3.6	4.7	.8	3.2			21.6
2.25	3.4	1.1	1.4	2.7	2.2	1.4	.1		12.3
2.30	.7	.2	.2	.5	4.0	.2	.7	.1	6.6
2.35					3.1		1.4	.5	5.0
2.40					1.1		2.2	1.2	4.5
2.45					.1		2.5	2.1	4.6
2.50							2.2	2.5	4.7
2.55							1.4	2.1	3.5
2.60							.7	1.2	1.9
2.65							.1	.5	.6
2.70								.1	.1

TABLE XIII - Cont.

r	$F_1 \cdot F_4$ / $F_2 \cdot F_5$	$O \cdot F_3$	$F_6 \cdot F_{4,5}$	$F_6 \cdot F_3$	rD(r)
2.90	.1				.1
2.95	.6				.6
3.00	1.5	.1			1.6
3.05	2.6	.5			3.1
3.10	2.8	1.0			3.8
3.15	1.7	1.3	.4		3.4
3.20	.8	1.0	.9		2.7
3.25	.2	.5	1.4		2.1
3.30		.1	1.8		1.9
3.35			1.8		1.8
3.40			1.3		1.3
3.45			.7		.7
3.50			.2		.2
3.75				.1	.1
3.80				.3	.3
3.85				.5	.5
3.90				.7	.7
3.95				.5	.5
4.00				.3	.3
4.05				.1	.1

TABLE XIV

MODEL 29 NORMALIZED GAUSSIAN PEAKS
PLUS SUM OF PEAKS
(THEORETICAL rD(r))

r	$S-F_{1,2,3,4,5}$	$S-0$	$0-F_6$	rD(r)
1.35			.8	.8
1.40	.5		3.1	3.6
1.45	9.1		3.4	12.5
1.50	29.1		1.2	30.3
1.55	32.7		.4	33.1
1.60	12.5	3.0		15.5
1.65	1.2	6.2		7.4
1.70		2.6		2.6
1.75		.4		.4

r	$F_3 \cdot F_{1,2,4,5}$ $F_1 \cdot F_{2,4}$ $F_2 \cdot F_{1,5}$	$0.F_{1,2}$	$0.F_{4,5}$	$F_6 \cdot F_{1,2}$	$S \cdot F_6$	rD(r)
2.00	.3					.3
2.05	2.6					2.6
2.10	10.9		.4			11.3
2.15	19.1	.6	1.8			21.5
2.20	14.2	1.8	3.8	.2		19.0
2.25	6.4	3.7	3.5	.7		14.3
2.30	.9	3.4	1.5	1.4		7.2
2.35		1.5	.2	2.2	.6	4.5
2.40		.5		2.5	1.4	4.4
2.45				2.1	2.2	4.3
2.50				1.5	2.5	4.0
2.55				.7	2.0	2.7
2.60				.1	1.1	1.2
2.65					.3	.3

r	$F_1 \cdot F_4$ $F_2 \cdot F_5$	$0.F_3$	$F_6 \cdot F_{4,5}$	$F_6 \cdot F_3$	rD(r)
2.90	.3				.3
2.95	1.0				1.0
3.00	1.9				1.9
3.05	2.9	.3			3.2
3.10	2.5	.7			3.2
3.15	1.3	1.2	.1		2.6
3.20	.5	1.1	.5		2.1
3.25		.7	1.0		1.7
3.30		.1	1.5		1.6
3.35			1.8		1.8
3.40			1.7		1.7

TABLE XIV - Cont.

r	$F_1 \cdot F_4$ / $F_2 \cdot F_5$	$0 \cdot F_3$	$F_6 \cdot F_{4,5}$	$F_6 \cdot F_3$	rD(r)
3.45			1.1		1.1
3.50			.6		.6
3.55			.2		.2
3.75				.4	.4
3.80				.8	.8
3.85				1.2	1.2
3.90				1.2	1.2
3.95				.8	.8
4.00				.4	.4

radial distribution curves are plotted in Figures XXV and XXVI, the numerical data for the theoretical intensity curves in Tables XV and XVI, and finally, the theoretical intensity curves in Figures XXVII and XXVIII. In all models giving good fits the average S-F bond length was found to be about 1.53 A, in agreement with the values found in other compounds, and, although little can be said about the relatively weakly scattering O-F and S-O linkages, they appear to be of normal length. The S-O-F_6 bond angle in the better models is 3-4° larger than the normal oxygen angle, a not-too-surprising circumstance in view of the possible steric effects occasioned by the proximity of the F_6 and $F_{1,2}$ atoms. The diffraction results suggest that the F_6 and $F_{1,2}$ atoms are in staggered configuration.

In conclusion it may be said that the diffraction results for SOF_6 are in agreement with the hypofluorite structure proposed by Dudley, Cady and Eggers (12, p. 1553-1556), and that the bond distances and bond angles are about normal. Because the number of structural parameters for the molecule prohibited exhaustive investigation it was not possible to evaluate error limits for the various distances and angles; undoubtedly many models, differing slightly from the best found in this

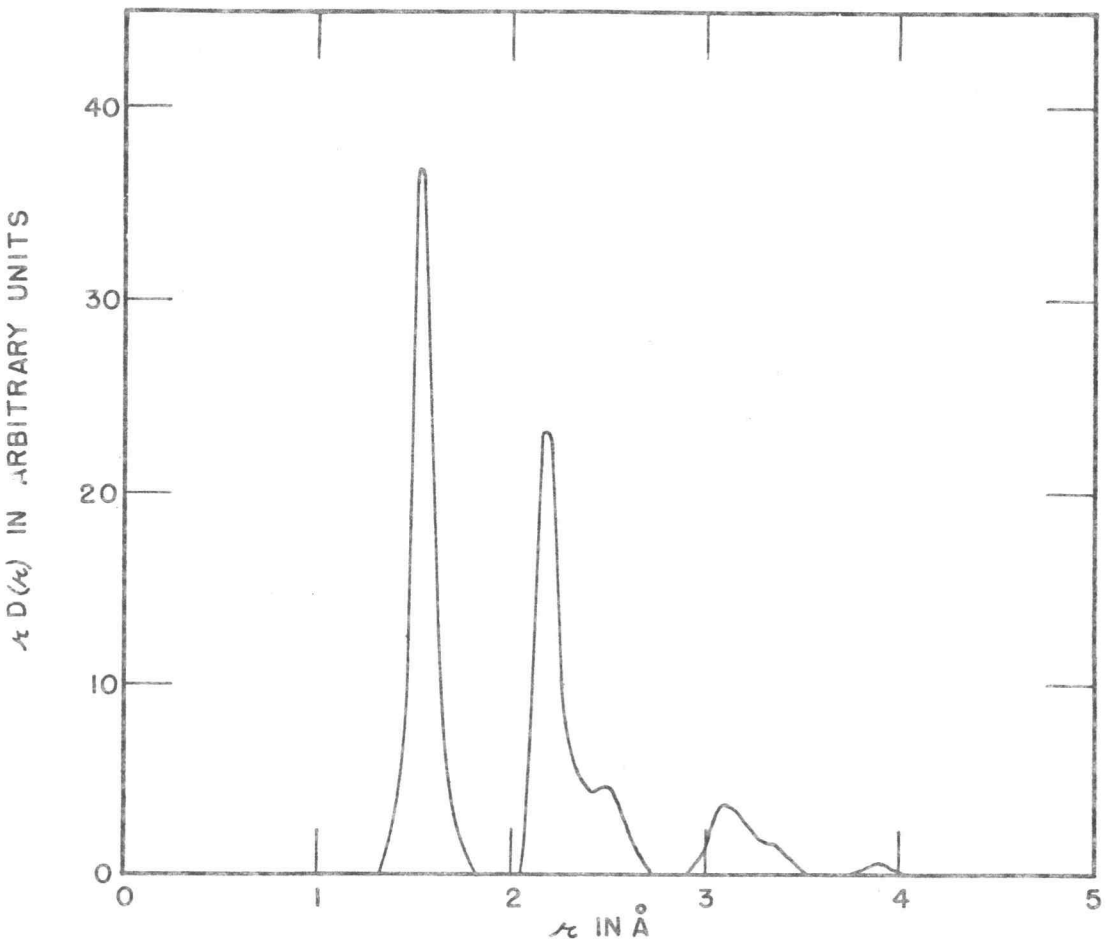

FIGURE XXV

MODEL 19 - THEORETICAL $r\,D(r)$ CURVE FOR SOF_6

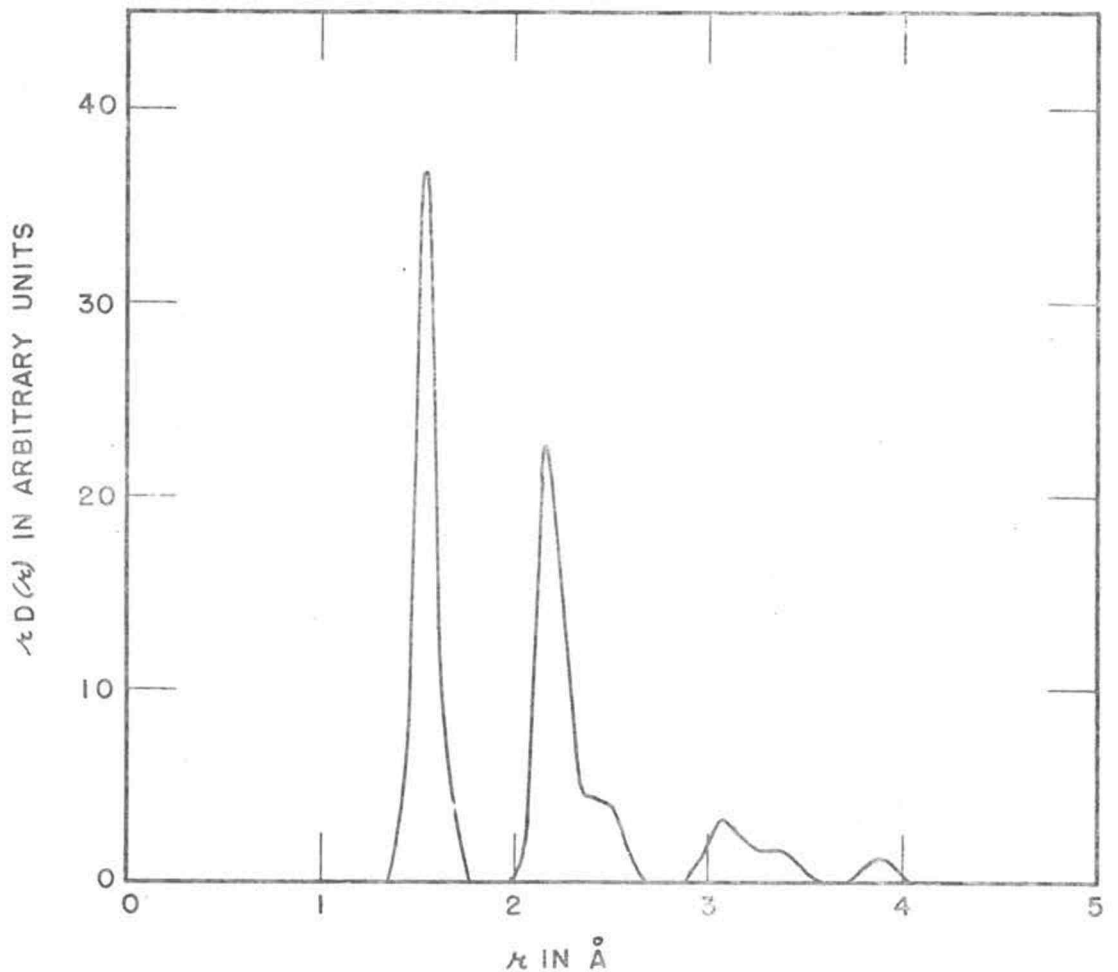

FIGURE XXVI

MODEL 29 - THEORETICAL rD(r) CURVE FOR SOF_6

TABLE XV

MODEL 19 THEORETICAL INTENSITY CALCULATION

s	Arbitrary Intensity Units	s	Arbitrary Intensity Units
0.5	1054	20.5	124
1.0	997	21.0	361
1.5	180	21.5	273
2.0	-450	22.0	31
2.5	-585	22.5	-125
3.0	-381	23.0	-147
3.5	-58	23.5	-106
4.0	142	24.0	-48
4.5	143	24.5	1
5.0	131	25.0	31
5.5	273	25.5	64
6.0	396	26.0	114
6.5	126	26.5	120
7.0	-493	27.0	17
7.5	-798	27.5	-143
8.0	-380	28.0	- 213
8.5	317	28.5	-115
9.0	686	29.0	69
9.5	594	29.5	193
10.0	169	30.0	175
10.5	-366	30.5	43
11.0	-638	31.0	-103
11.5	-436	31.5	-161
12.0	30	32.0	-101
12.5	376	32.5	10
13.0	385	33.0	77
13.5	153	33.5	72
14.0	-42	34.0	39
14.5	-78	34.5	21
15.0	-90	35.0	8
15.5	-178	35.5	-26
16.0	-230	36.0	-72
16.5	-117	36.5	-83
17.0	131	37.0	-32
17.5	351	37.5	55
18.0	355	38.0	112
18.5	86	38.5	91
19.0	-284	39.0	3
19.5	-459	39.5	-85
20.0	-269	40.0	-108

TABLE XV - Cont.

s	Arbitrary Intensity Units	s	Arbitrary Intensity Units
40.5	-54	43.0	-14
41.0	26	43.5	-36
41.5	74	44.0	-42
42.0	66	44.5	-34
42.5	26	45.0	-11

TABLE XVI

MODEL 29 THEORETICAL INTENSITY CALCULATION

s	Arbitrary Intensity Units	s	Arbitrary Intensity Units
0.5	1056	20.5	111
1.0	1005	21.0	361
1.5	193	21.5	285
2.0	-446	22.0	42
2.5	-601	22.5	-114
3.0	-399	23.0	-130
3.5	-46	23.5	-101
4.0	164	24.0	-74
4.5	131	24.5	-39
5.0	102	25.0	12
5.5	272	25.5	89
6.0	418	26.0	159
6.5	153	26.5	140
7.0	-469	27.0	0
7.5	-818	27.5	-165
8.0	-447	28.0	-223
8.5	286	28.5	-118
9.0	733	29.0	70
9.5	654	29.5	195
10.0	173	30.0	173
10.5	-402	30.5	45
11.0	-653	31.0	-82
11.5	-417	31.5	-137
12.0	31	32.0	-106
12.5	344	32.5	-28
13.0	372	33.0	43
13.5	170	33.5	77
14.0	-26	34.0	73
14.5	-53	34.5	48
15.0	-61	35.0	10
15.5	-198	35.5	-39
16.0	-293	36.0	-85
16.5	-146	36.5	-89
17.0	156	37.0	-32
17.5	387	37.5	54
18.0	378	38.0	108
18.5	92	38.5	91
19.0	-296	39.0	17
19.5	-476	39.5	-63
20.0	-284	40.0	-101

TABLE XVI - Cont.

s	Arbitrary Intensity Units	s	Arbitrary Intensity Units
40.5	-74	43.0	3
41.0	-3	43.5	-35
41.5	60	44.0	-53
42.0	78	44.5	-47
42.5	50	45.0	-19

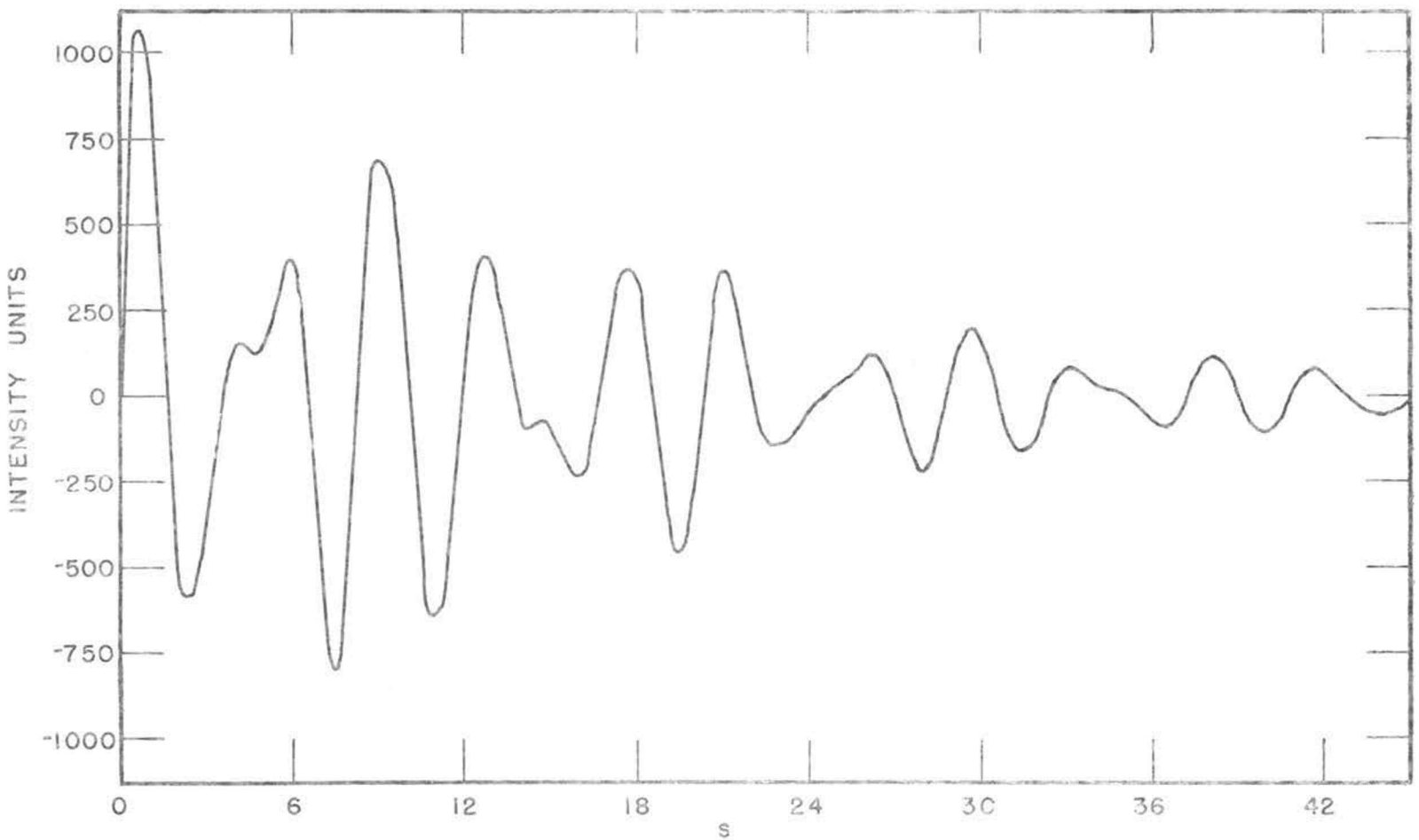

FIGURE XXVII

MODEL 19 - THEORETICAL INTENSITY CURVE

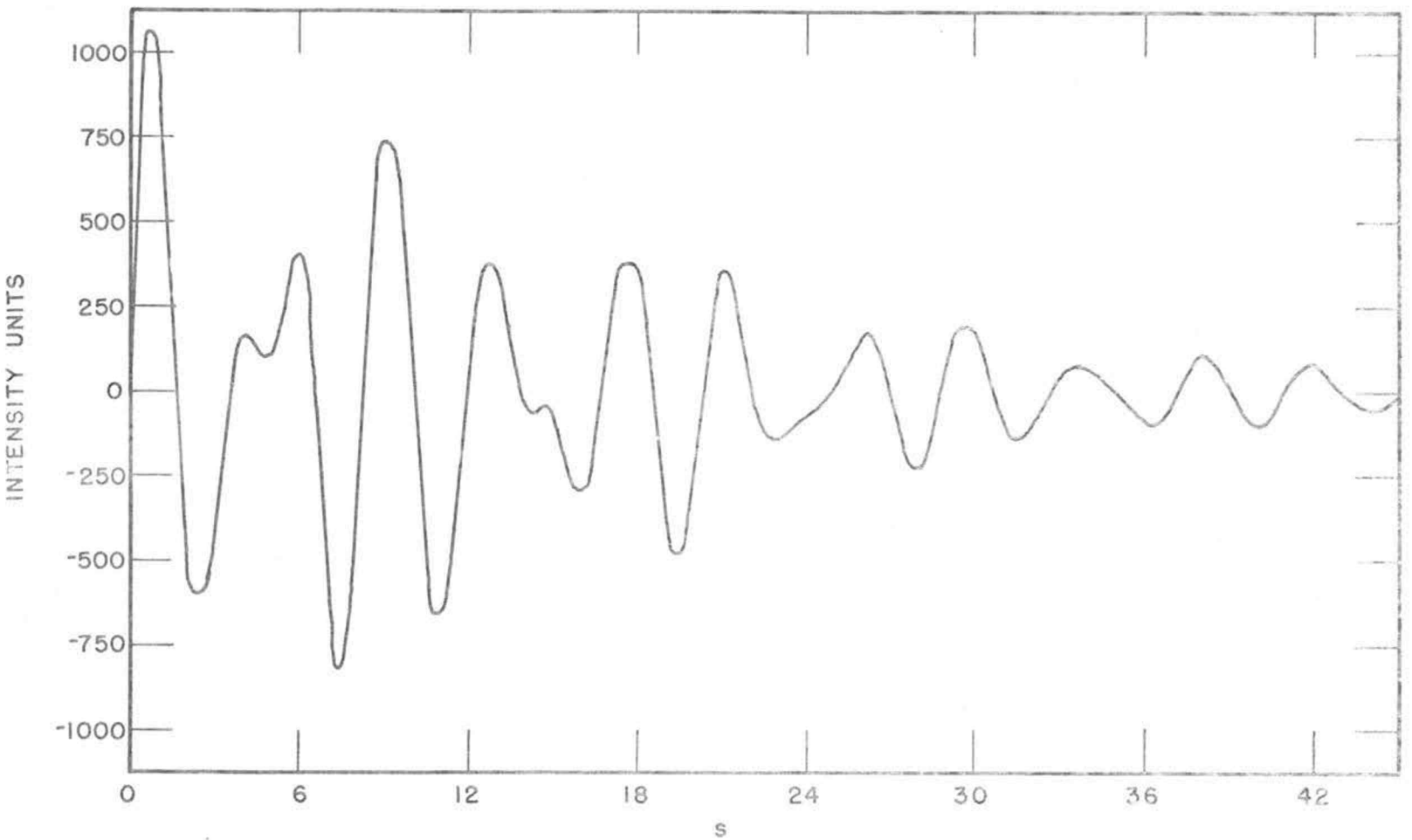

FIGURE XXVIII

MODEL 29 - THEORETICAL INTENSITY CURVE

study would also provide good fits to the experimental data. It is even possible, though very unlikely, that a model grossly dissimilar to the natural octahedral structure could be found which would provide an acceptable fit to the experimental data. Such a model, however, would surely correspond to a bizarre structure and would be ruled unlikely on chemical grounds.

ELECTRON DIFFRACTION PROGRAMS
USING THE ALWAC III-E DIGITAL COMPUTER

The computer for which the electron diffraction calculations were written is the Alwac III-E (1, p. 1-93) and (19, p. 1-19), an electronic digital computer capable of handling 16,000 instructions. These instructions are called words and are stored in cells (in each cell, two words may be stored) which are grouped into channels consisting of 32 cells per channel. The Alwac has two types of channels: 1) working storage and 2) main storage. All computers must use some type of a circulating loop; in the Alwac the working storage represents this loop. There are four working storage channels from which the Alwac obtains its instructions. The main storage, more commonly referred to as the memory, has 256 channels.

The 256 available words in working storage are numbered hexadecimally from 00 to ff (this counting system will be explained later). The main storage channels are numbered from 00 to ff; however, the individual words in main storage do not receive any cell number till they are transferred to working storage at which time they receive the numbers associated with that working storage channel. The cell numbers (2 numbers per

cell because 2 words can be placed in a cell) for the working storages are:

Working Storage I;	00 to 1f and 80 to 9f
Working Storage II:	20 to 3f and a0 to bf
Working Storage III:	40 to 5f and c0 to df
Working Storage IV:	60 to 7f and e0 to ff

Figure XXIX shows the cell numbering in working storage I. Any main storage channel may be transferred to any working storage channel and any working storage channel may be transferred to any main channel. When a channel transfer is desired, one instructs the Alwac to copy a main channel to a particular working storage channel, for example working storage III. The instruction, of course, must be given in a language understood by the computer. The code number 85 is recognized as "copy" (a transfer is just a copy operation) from main channel X to working storage III. Of course, one must also tell the Alwac which main channel it is supposed to transfer, hence this channel number must accompany the instruction. As do many computers, the Alwac III-E uses the radix 2 (binary) system for all of its operations, however, in order to simplify coding the computer is coded using the radix 16 (hexadecimal) system. Since four binary digits exactly comprise one hexadecimal digit, an easy conversion exist between radix 2 and radix 16. For example, the

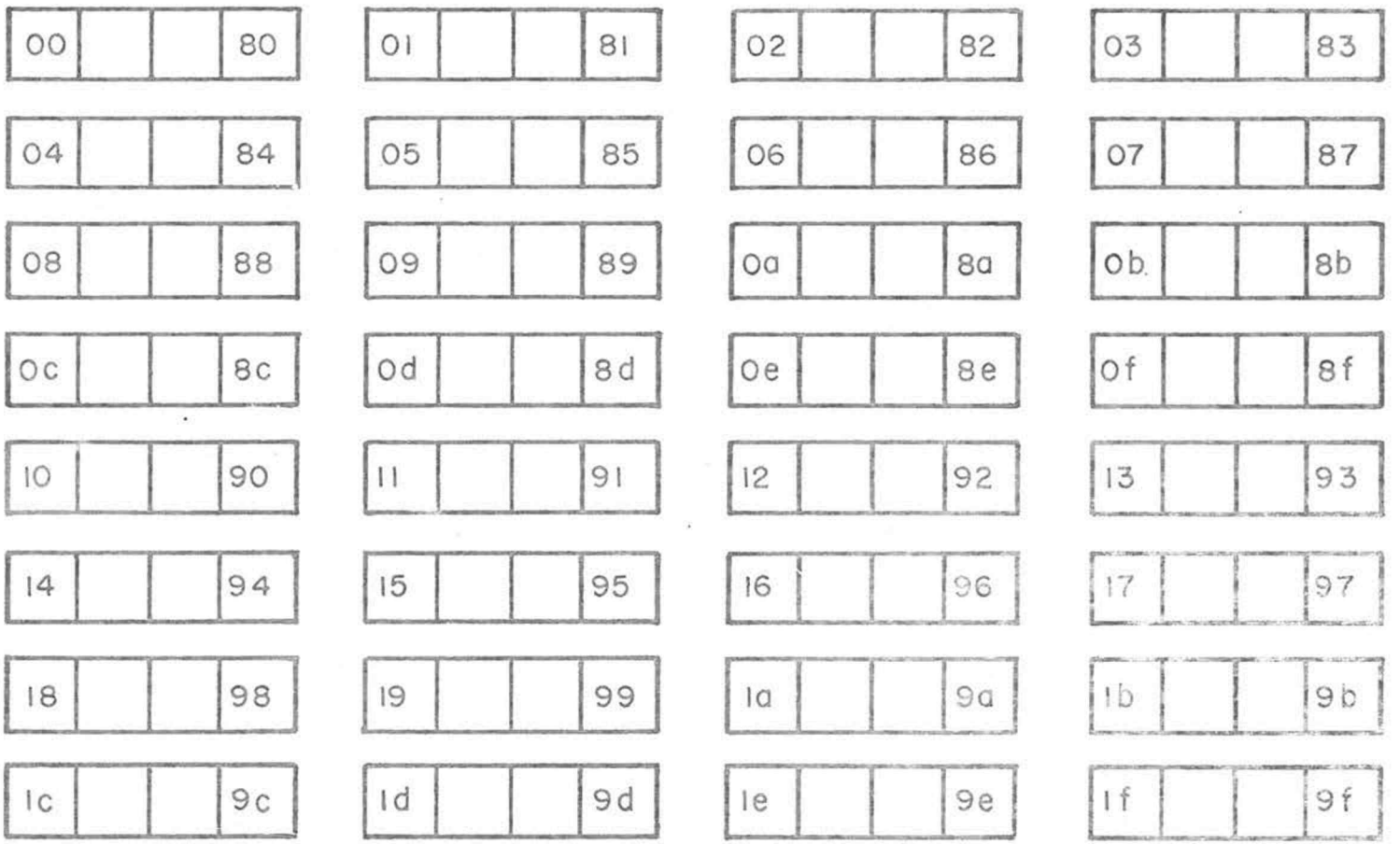

FIGURE XXIX

WORKING STORAGE I - ALWAC III-E

decimal number 30, which has 11110 as the binary equivalent, is represented in hexadecimal language as 1e. Thus to transfer main channel 1e to working storage III, one enters the single word 851e. The Alwac interprets the word 851e as 1000 0101 0001 1110, since it converts immediately to binary. This example typifies many of the Alwac operations.

The Alwac has four registers which are used in the computations. The A register is the accumulator and it holds sums, differences and remainders. The B register holds multiplicands, dividends and quotients. The combined (AB) register (not considered one of the four registers) is a double length accumulator with B being the least significant part and A the most significant part. The D register holds multipliers, divisors, and keywords (used when Alwac subroutines are used). Finally the E register, which is only a half-register, is a counting register when cyclical operations are being used.

RADIAL DISTRIBUTION PROGRAMS

In electron diffraction there are two main calculations to be performed. These are: 1) radial distribution calculation, and 2) intensity calculation.

Since the radial distribution calculation is performed first it will be discussed first. The radial distribution function is given by

$$r D(r) = \sum_{r_{min}}^{r_{max}} \sum_{s_{min}}^{s_{MAX}} I_s e^{(-as^2)} \sin sr \qquad (64)$$

where

$\underline{I}_s$ is the experimental intensity curve

$\underline{a}$ is the temperature factor and is a constant for any calculation

$\underline{s} = \frac{4\pi}{\lambda} \sin \theta/2$ and is the angle variable

$\underline{r}$ is the distance in $\underline{r}$ space and is in Angstrom units

The calculation is accomplished by summing all contributions I_s at a given $\underline{r}$, then changing the $\underline{r}$ and repeating the operation until all $\underline{r}$ values have been included. Since a normal calculation will have at least 120 values of $\underline{r}$ and a minimum of 90 values of $\underline{s}$ and I_s, one can immediately see this is a rather extensive calculation. It thus becomes important to have an optimum program to conserve computer time.

The terms $I_s \cdot \exp(-as^2)$ are the same for each cycle over $\underline{r}$ so it is profitable to devise a special program (which is called the data input routine) to

compute and then store these products, normally 90-150 in number, for use later. Since electron diffraction intensity curves and the variable s are always expressed in decimal, the routine must also convert these to binary. The Alwac III-E already has a subroutine which performs this input conversion. It is called the decimal typewriter input (DTI) and must be copied to working storage IV for operation. To actuate the DTI routine, two pieces of information must be included in a keyword: 1) the binary scaling of the number and 2) the word address in the main routine to which the Alwac should return when the subroutine calculation is finished. Since the DTI recognizes decimal points, the scaling gives the number of significant figures (expressed in powers of 2) to the right and to the left of the decimal point. Finally, the DTI also recognizes the sign given to a number. The result of the DTI is placed in the (AB) register after which the number is dealt with by the main routine. Table XVII gives the data input routine for the radial distribution calculation. The 6304 command tells the Alwac that main channel 63 will be involved and the 04 denotes a routine is to be fed into the machine. After the Alwac has accepted all 32 cells (64 words), it will store the routine in channel 63. In performing a

TABLE XVII

DATA INPUT ROUTINE FOR
RADIAL DISTRIBUTION CALCULATIONS

```
6304
871e5b08 f1012800 4860871e 67000000
11601000 870b411a 1714570b 00020000
0014000c e71aa10a 8c707904 00080000
4917570b e717a106 a70c6103 00000000
c30b5713 2f0c5b15 4903f502 00200000
c30f5707 11600019 17101b00 00000000
5a201160 a10ce71b 00000000 00000000
481c1718 a30c570f 000e001c 0014001c
3a00
63 2f16a5a7
```

routine, Alwac starts in cell 00 (this is not strictly true because the Alwac may be instructed to begin a program anywhere in the four working storages, but will follow the order given) reading first the left hand word then the right hand word, proceeds to cell 04, works thus down the column to 1c where it jumps to cell 01. The process continues until a 1b command (stop command) is reached.

The data input routine operates essentially as follows. First the DTI is called down to working channel IV and loaded with the keyword for a from the main routine. The Alwac will ask for input of a in decimal, the number being terminated by a space (the only way the DTI can recognize the termination of a number), and finally a (in binary now) is stored in cell 17 to be used shortly. The next few commands are necessary to perform the proper cycling necessary to correctly store the eventual product $I_s \cdot \exp(-as^2)$. The DTI is now loaded with the keyword for s from the main routine, the number s_{min} is entered in the computer and s stored. The cycle is repeated for the I_s corresponding to the s just previously given and at the completion of which the Alwac will ask for one character. This character is just a dummy character to allow a carriage return to be punched

where preparing tapes of $\underline{s}$ and I_s data: when tapes are checked it is much simpler to check a column of numbers than it is to check a row of numbers. The next step is to square $\underline{s}$ and then multiply s^2 by a. as^2 is made negative and the exponential subroutine is copied to working storage IV. The exponential subroutine is loaded in a fashion similar to the DTI. Exp $(-as^2)$ is placed in the (AB) register by the subroutine and this quantity is immediately multiplied by I_s. The result is stored in cell 40. The DTI is again called down and the routine jumps back to cell 14 in preparation for computation of a new value of $I_s \cdot \exp(-as^2)$. This time the result is placed in cell 41. The cycling is continued 32 times, that is, until $I_s \cdot \exp(-as^2)$ data have completely filled working storage III. At this point, the Alwac leaves the cycle, copies working storage III to main channel 68 and then types out the number 68 to signify that channel 68 now has data in it. The routine jumps back to cell 10 (for proper $\underline{E}$ register counting) and the first cycle starts over again. After 32 more $I_s \cdot \exp(-as^2)$ values have been calculated and stored in working storage III, the contents of the storage are copied to main channel 69. The number 69 is then typed out by the Flexowriter. This procedure continues until all data are in main memory.

The data input routine, the data output routine and the rD(r) routine (to be discussed shortly) all assume the data $I_s \cdot \exp(-as^2)$ are stored in main channel 68-6f (8 channels) and each routine will start storing or extracting information from channel 68. The latter two routines will stop after:

1) the number 8 has been counted down to zero by the E register
2) s_{max} has been reached (data output) or r_{max} has been reached (rD(r))

The data input routine, however, is stopped only by restriction 1; there is no provision for use of restriction 2. Now, only on rare occasion will all eight channels be used; therefore, this routine will normally have to be stopped by pushing the clear button. Furthermore, the data will not leave working storage III until all 32 cells have been filled, and again only on rare occasion will the data $I_s \cdot \exp(-as^2)$ exactly fill the last channel used. Therefore, in preparing a tape of $\underline{s}$ and I_s values, one must type enough $\underline{s}$ and I_s values (let $I_s = 0$ for the extra data) to completely fill the last channel.

As mentioned earlier, each time working storage III is copied to a main channel by the data input routine,

the main channel number is typed out. The reason for this is the following. Remembering that the routine asks for $\underline{s}$, I_s, and then a dummy character, and also that an input to the DTI is terminated by a space, one can see that the space following I_s can not be checked by typing out the tape. If a space has been forgotten after one value of I_s, the DTI would then interpret that value of I_s, the carriage return, and the next $\underline{s}$ value all as I_s. This type of error is extremely easy to make and, of course, ruins the calculation. Since one always fills the last channel used, it is only necessary to watch the tape near the end of the tape and as soon as the last piece of data goes into the machine, the main channel where the data is stored should be typed out. This serves as a check on the correctness of the tape.

In any one molecular structure determination, there usually will be only one or two experimental intensity curves (I_s), but this curve may be run with several damping factors $\underline{a}$. It is convenient, therefore, to prepare a tape of $\underline{s}$ and I_s only, and to type the $\underline{a}$ value into the routine each time. The following procedure is used in preparing a tape for the data input routine.

1) Depress the punch on button.
2) Press the tape feed button until 3-4 inches of tape is available.
3) Type s_{min}, terminate with a space.
4) Type I_s corresponding to the $\underline{s}$ in step 3, terminate with a space.
5) Type carriage return.
6) Repeat steps 3,4 and 5 until all $\underline{s}$ and I_s values are on tape.

One must be sure that the number of $\underline{s}$ and I_s values is 32 times the number of main channels to be used.

The following is the procedure for using the data input routine. It is assumed that the data input routine is stored in main channel 63 and a tape of the data is available.

1) Place tape of data ($\underline{s}$ and I_s) in the tape reader.
2) Push the clear button.
3) The Alwac will ask for five characters: type 6300 followed by carriage return.
4) The Alwac will ask for one character (and continue to do so until a space is given): type in the $\underline{a}$ value in decimal.
5) The Alwac will ask for one character: push

the start read button.

6) After all data is in, push the clear button.

It is useful to have some sort of additional check on the data just stored by the data input routine. For this reason, a data output routine for radial distribution calculations was devised. This program simply types out the $\underline{s}$ values followed by the corresponding values of $I_s \cdot \exp(-as^2)$ with sign. In order to do this, the Alwac has to convert the stored binary number to a decimal number. There is available a subroutine called the decimal typewriter output (DTO) which uses keyword notation similar to the DTI. However, the DTO uses valuable computer time in converting binary numbers to decimal. If only the decimal equivalent is wanted (no decimal point), there is a command (f5cX where X is the number of digits to be typed) which does this conversion much faster. In this data output routine, both the DTO (for $\underline{s}$ values where decimal points are desired) and the decimal equivalent ($I_s \cdot \exp(-as^2)$ where the decimal point is not needed) are used. The routine requires the entering of s_{max}, Δs, and s_{min} at the beginning (these must correspond to the values used in the data input routine) following which it causes Alwac to type out the stored data. The process begins with the contents of the first

cell of main channel 68 and stops when $s = s_{max}$. The overall cycling procedure is similar to the data input routine. Table XVIII gives this routine.

The following is the procedure for using the data output routine (stored in main channel 64) for radial distribution calculations.

1) Press clear button.
2) The Alwac will ask for five characters: type 6400 followed by carriage return.
3) The Alwac will ask for one character: type s_{max} followed by space.
4) The Alwac will ask for one character: type Δs followed by space.
5) The Alwac will ask for one character: type s_{min} followed by space.

In steps 3, 4 and 5 the decimal numbers are used. The machine will stop when finished.

The most complicated of all programs is the radial distribution calculation. This uses two working storages for the program plus a third working storage each time an answer is typed out. The equation which is actually calculated is

$$r\,D(r) = \sum_{r} \sum_{s} I'_s \sin sr \qquad (65)$$

TABLE XVIII

DATA OUTPUT ROUTINE
FOR RADIAL DISTRIBUTION CALCULATION

```
6404
871e5703 11600000 f5c4791b 00030000
5b081160 020e0209 f702791f 00200000
000e000c 570b7840 611e491f 00000000
48201704 0e00a114 651d1d1a 00080000
570f8270 41130c00 570b1798 80000000
c30f5707 eb173200 570f1790 00002710
871fc30b d5001102 1b000000 01680000
5b05791f 00000000 00000000 00000000
3a00
64 9decae27
```

where

$$I_s' = I_s \cdot \exp(-as^2)$$

The program computes rD(r) at each r value by summing over all s; at the conclusion of this operation, a new r is generated by adding Δr to the first value and the operation repeated. If there were 90 s values and 120 r values (these are reasonable numbers) there will be 10,800 computation of sine alone. At an average of 250 milliseconds per computation of sine by the available sin-cos subroutine, this one calculation would take 45 minutes. It was thus important to try and shorten this computation. Consider the trigonmetric identities

$$\begin{aligned} \sin(x + y) &= \sin x \cos y + \cos x \sin y \\ \sin(x - y) &= \sin x \cos y - \cos x \sin y \end{aligned} \tag{66}$$

by addition

$$\sin(x + y) = 2 \sin x \cos y - \sin(x - y) \tag{67}$$

Letting $x = rs$ and $y = r \cdot \Delta\phi$ one obtains

$$\sin r(s + \Delta\phi) = 2 \sin rs \cos r \cdot \Delta\phi - \sin r(s - \Delta\phi) \tag{68}$$

and letting $s + \Delta\phi = s_n$ equation (68) becomes

$$\sin rs_n = 2 \sin rs_{n-1} \cos r \cdot \Delta\phi - \sin rs_{n-2} \tag{69}$$

Equation (69) is a recursion formula which allows $\sin sr_n$ (for r = constant) to be calculated from the two previous sine terms. This represents a large saving of time compared with the subroutine since a single multiplication (sin-cos term) requires 17 milliseconds and addition and subtraction only a couple milliseconds. When the absolute value of $\sin rs_n$ becomes small, there is a possibility that equation (69) will promote significance thus causing rather large errors if used for a long enough time; therefore, each $\sin rs_n$ that is calculated, after storing, is given a positive sign and compared with the number 0.01. If the absolute value of $\sin rs_n$ is less than 0.01, the program calls down the sin-cos subroutine and calculates this particular $\sin rs_n$ via the subroutine.

The program generates r_{min} and computes $\cos r_{min}$ via the cosine subroutine, $\sin r_{min}s_{n-2}$ and $\sin r_{min}s_{n-1}$ via the sine subroutine and stores the results. Then $\sin r_{min}s_n$ (where s_n is s_{min} for the first cycle) is computed, compared with 0.01, multiplied by I_s' and this result stored. The cycle then repeats for $r_{min}s_{n+1}$ and the result added to the previous $I_s' \cdot \sin r_{min}s_n$. The cycle continues until all $\underline{s}$ values and I_s' values have been used. The program then calls down a small output routine to working storage III (this is not the same

output routine discussed earlier) which causes Alwac to type out r_{min} and the corresponding rD(r) value. The program then jumps back and generates a new $\underline{r}$ (now $r_{min} + \Delta r$), calculates cos $(r_{m+1} \cdot \Delta \lambda)$, sin $r_{m+1} s_{n-2}$, sin $r_{m+1} s_{n-1}$ and cycling repeats. Table XIX gives the radial distribution calculation.

The following is the procedure for using the rD(r) program (stored in main channel 60, 61 and 62). This assumes the values of I_s' are already stored.

1) Push clear button.
2) The Alwac will ask for five characters: type 6000 followed by carriage return.
3) The Alwac (using the DTI) will ask for six pieces of data which are entered in this order:
   a) Δr followed by space
   b) r_{max} followed by space
   c) r_{min} followed by space
   d) $\Delta \lambda$ followed by space
   e) s_{max} followed by space
   f) s_{min} followed by space

The Alwac will stop when $\underline{r} = r_{max}$.

Before proceeding to the intensity calculation some minor points should be cleared up. At the bottom

TABLE XIX

ROUTINE FOR RADIAL DISTRIBUTION CALCULATION

```
6004
8361871e 1d051b00 c32a4123 84705733
572e5b0c 413de73c e73ca108 c32f4139
11604840 a1085b0d 5b0e11e4 e732a303
00140088 11600011 a10c000e 67384139
17848706 a102c532 572ac43a c5384939
28004937 793f4923 7923613d 2c006527
793c613a 673d673d 49231702 1d2c4123
493c673b 49235736 572bc322 e73c1120
6104
a1085b24 49377923 00000000 00000000
11e40028 613d4923 00000000 000028f5
a10cc539 653e1db1 00000000 00080000
572f4139 17075722 00060000 00000000
e660a302 179e8562 00000000 00200000
61371121 11400000 00020000 00000000
00000000 00000000 00000000 00000000
00000000 00000000 00000000 00000000
6204
871f5b48 5a000000 00000000 00000000
793c1160 00000000 00000000 00000000
0214034c 00000000 00000000 00000000
5b547937 00000000 00000000 00000000
11600000 00000000 00000000 00000000
060a0058 00000000 00000000 00000000
7941f702 00000000 00000000 00000000
11900000 00000000 00000000 00000000
3a00
60 6c195ed6
61 4288fb55
62 59ffe087
```

of each of the programs shown in Tables XVII, XVIII and XIX, there is a 3a00 command followed by a series of hexadecimal numbers. In Table XVII, it is 63 2f16a5a7. The 3a00 is a tally (via tape) command which tells the Alwac to add all the numbers in the channel to be given, as channel 63. The number 2f16a5a7, then, is the sum of all the numbers in channel 63. This is very useful in that it provides a quick check by the operator to see if the program is still in main memory. Another check is the manual tally of any channel: the operator (after pushing the clear button) types "tally" then a space, followed by, for example, 6064 and a carriage return. The Alwac will type out the tallys of main channels 60 through 64. Many times the tallys will not check when one wishes to do a calculation and the routines must be placed in main memory. Since all programs are on tape (with the correct main channel on the tape also) it is only necessary to place the proper tape in the tape reader, press the clear button, and press the start read button. When the program is in the computer, press the stop read.

Lastly, a few words should be said about the toggle switches on the control panel. For all the programs so far described, all switches should be in the normal position (this is not the case for all the tapes which are used in

electron diffraction calculations).

INTENSITY CALCULATION PROGRAMS

The intensity calculation, like the radial distribution calculation, is composed of three separate programs: 1) the data input routine, 2) the data output routine and 3) the intensity calculation. The calculation to be carried out has been developed earlier in this thesis and is given by

$$s I_s = \sum_{ij} \frac{A_{ij}}{r_{ij}} e^{(-a_{ij} s^2)} \sin s r_{ij} \qquad (70)$$

where $A_{ij} = nZ_iZ_j$. The programs will be discussed the order given above.

The data input routine for the intensity calculation is more complicated than the data input discussed in the rD(r) section: it actually consists of two routines called the normal and single input routines. When all new data are to be used, a tape will normally be prepared and one will use the normal routine; however, other times only one or two parameters may be changed from a previous model and to avoid the inconvenience of preparing a whole new tape for such a minor change the single input routine can be used. Another factor leading

to complications of the routine is the fact that the numerical values of the molecular parameters may have a range of 10^7 so that different scaling factors must be loaded into the DTI for s, a, r, A and a quantity n (n is the number of different interatomic distances. The number of different r values may or may not equal the number of different a or A values in one particular model). Briefly, the routine accepts a set of decimal numbers, most of which are values of structural parameters for the molecule but some of which are used to control the routine, converts these decimal numbers to binary, stores them in working storages II and III, and finally copies working storages II and III to main channels 56 and 57. The following denotes the location of the various quantities in the working storages.

cell 20	s_{min}
cell 21	s_{max}
cell 22	Δs
cell 23	n
cells 24-37	r
cells 38-4b	a
cells 4c-5f	A

There are 20 cells each for r, a and A and the location of a given r and its associated a and A must correspond;

that is, if r goes to cell 24, the corresponding a and A values are respectively in cells 38 and 4c. The intensity calculation uses the number n to determine which cell to find r and its corresponding a and A, so if the data are not placed correctly on the tape serious errors will result. To determine where the first values of r, a, and A are located, subtract (n-1) from 37, 4b and 5f. The next r, a and A values are found in the next higher cell numbers, the last r, a and A always filling cells 37, 4b and 5f respectively. Anything may be placed in the remaining cells because they are not used, but normally zeros are placed there.

The following is the procedure for preparing a tape for use with the data input routine (the routine is stored in main channel 51).

1) Type 5100 followed by carriage return.
2) Type in the decimal numbers in the following order: s_{min}, space, s_{max}, space, $\Delta\nu$, space, n, space, then 20-n zeros each followed by a space, then the values of r_{ij} terminating each with a space. Follow a similar procedure for a and A.

When the normal data input routine is desired (data on tape) the input procedure is as follows.

1) Put data tape in the tape reader.
2) Place jump switches 1 and 2 in the normal position.
3) Press the clear button.
4) Press the start read button.

The Alwac will stop when all data is stored.

The single input routine requires the operator to type in the cell number, scaling, decimal number, and finally a carriage return. The single input routine may be selected instead of the normal input routine by correctly setting the jump switches on the computer control panel: the sequence of commands for the normal input is thus jumped over and the single input sequence entered (the single input routine begins in word 8e).

The procedure for using the single input routine (stored in main channel 51) is the following.

1) Place jump switch 1 to jump.
2) Press the clear button.
3) The Alwac will ask for five characters: type 5100 followed by carriage return.
4) The Alwac will ask for two characters: type the cell number to be corrected.
5) The Alwac will ask for two characters. If the quantity to be corrected is

a) s_{min}, s_{max}, Δs , type 0e

b) n, type 10

c) r, type 12

d) a, A, type 14

6) The Alwac will ask for one character repeatedly until a space is received (DTI): type the decimal number.

7) The Alwac will ask for one character: type carriage return. The entry of one piece of new data has been achieved at this point and the computer is ready to accept an additional entry. The procedure is repeated beginning with step 4.

8) With the last piece of data to be placed in the computer and anytime before step 7, place jump switch 2 to jump. On pressing the carriage return key, these changes and the unchanged data are copied to main channels 56 and 57. The machine now stops.

Step 8 is important because if something goes wrong during an intensity calculation, usually all data in working storages II and III are ruined. With the data also stored in main memory, one only has to copy it back to working storages II and III and proceed. Table XX gives the data input routine for intensity calculations.

TABLE XX

DATA INPUT ROUTINE FOR INTENSITY CALCULATION

```
5104
871e138e 4923570d 00280000 490b5b0b
57105b0c 5b091160 48601795 11600000
11600000 00120011 8b568d57 00000000
00000014 00140000 1b002800 00000000
00030000 48381705 f102a710 f101150a
48231784 57025b1d 611f490f 118e0000
5b1c1160 11600000 2800f102 0000000f
00100001 00140006 a710611b 49000000
3a00
51 9dfbf18c
```

The data output routine for intensity calculations serves the same function as the data output routine for the rD(r) calculation; that is, as a check to see if the data are properly stored. Like the data input just discussed, the data output is in two parts. These are called the normal and single output routine.

The normal routine for the data output simply types out, in decimal, the data stored in working storages II and III with the aid of the DTO. The same variation in the numerical values occur here so different scaling factors must be loaded into the DTO for each s, n, r, a and A. This is accomplished by the main routine. The following is the procedure for using the normal data output routine (stored in main channel 52) for intensity calculations.

1) Set jump switches 1 and 2 to normal.
2) Press the clear button.
3) The Alwac will ask for five characters:
   type 5200 followed by carriage return.

The Alwac will stop when the last piece of data has been typed out.

The single output routine is normally used after the single input routine has been used. As in the data input, the single output routine is more complicated to

use because the cell number of the data desired and the cell number of the correct scaling factor must be given to the routine. The cell number for the scaling factor will only vary between s, n, r, a and A. The following is the procedure for using the single output routine of the data output routine.

1) Set jump switch 1 to jump.
2) Press the clear button.
3) The Alwac will ask for five characters: type 5200 followed by carriage return.
4) The Alwac will ask for three characters: type the data cell number as the first two characters and a space as the third character.
5) The Alwac will ask for two characters. Type one of the following:
   a) 1b if s_{max}, s_{min} or $\Delta \nu$ is desired
   b) 1c if n is desired
   c) 1d if r is desired
   d) 1e if a is desired
   e) 1f if A is desired

   The desired piece of data will be typed out immediately and the process may be repeated by returning to step 4.

6) Press the clear button to stop the routine. Table XXI gives the data output routine for intensity calculations.

The intensity calculation evaluates equation (70) for $s_{min} \leqq \underline{s} \leqq s_{max}$ as follows. First, s_{min} is multiplied by the first $\underline{r}$ stored in working storage II (the $\underline{r}$ with the smallest cell number) and then the sine subroutine is used to evaluate $\sin s_{min} r_{ij}$. The sine subroutine places the result in the (AB) register where it is immediately divided by r_{ij}. This result is stored for later use. s_{min} is squared, multiplied by the a_{ij} corresponding to the r_{ij} used (the a_{ij} with the smallest cell number), and the product given a negative sign. $\text{Exp}\ (-a_{ij}s^2)$ is computed by the exponential subroutine and the result multiplied by $\sin s_{min} r_{ij}$. This product is multiplied by the A_{ij} corresponding to the previous r_{ij} and a_{ij} and the result is stored. The cycle now repeats using the next r_{ij}, a_{ij} and A_{ij} values (respectively stored in cells 37-(n-2), 4b-(n-2) and 5f-(n-2)); this result is added to the previous result and the sum stored. The cycle continues until all data have been used. The DTO is then called down and s_{min} typed out, a d500 instruction is given which types out the sign of sI_s, and finally a f5c4 instruction which types out the decimal

TABLE XXI

DATA OUTPUT ROUTINE FOR INTENSITY CALCULATION

```
5204
871f1302 f5025b09 2800f103 7913f702
570fc30f 791f1160 a5044d96 11020000
78204909 00000000 2800f102 0000000a
781b3600 7913f702 4d8e7900 00050000
79056117 1710570f 670b3a00 01680000
4905a708 17841b00 00037900 00010000
00141101 00140000 00141160 020e040d
0210020d 0212050d 0014060d 0314020d
3a00
52 e4fabb02
```

equivalent (no decimal point). One is not interested in absolute peak heights, only relative peak heights, so the decimal equivalent is quite satisfactory. After output, the routine cycles back and repeats the above process for $s_{min} + \Delta s$, continuing to cycle until $s = s_{max}$ after which the Alwac stops. Table XXII gives the intensity calculation program.

The following is the procedure for using this routine (stored in main channel 50).

1) Press the clear button.
2) The Alwac will ask for five characters: type 5000 followed by carriage return.

The Alwac will stop when $\underline{s} = s_{max}$.

The radial distribution program is a versatile, reasonably efficient, and quite general program and it meets all foreseeable requirements. Any possible work toward improving this program will doubtless be aimed at improving its efficiency, that is, at cutting down computer time. The intensity program, however, while versatile, is not so efficient as might be hoped nor is it as general as will be required for some work. A program general enough to meet almost all needs will have to permit the use of variable coefficients (corresponding to $(Z-F)_i(Z-F)_j$ in place of the A_{ij}'s)

TABLE XXII

ROUTINE FOR INTENSITY CALCULATION

```
5004
28004917 c30511e4 c1001160 791ff702
7920871f 00000009 55000006 79206122
5b0c1160 5705ea38 a112e713 49206721
020e0210 c513870b e660a102 1d001b00
2800f783 4120e720 61174917 00000000
57234120 a10a0000 17940e00 00000000
e6380000 e64ca106 eb1ba320 09c40000
87065b05 2f0c5b06 d500f5c4 01680000
3a00
50 fb084171
```

and the inclusion of an additional factor, a cosine term, to take account of the phase shifts which may occur in the scattering process when the molecules contain atoms of quite different atomic numbers.

BIBLIOGRAPHY

1. Allen, P. W. and L. E. Sutton. Tables of interatomic distances and molecular configurations obtained by electron diffraction in the gas phase. Acta Crystallographica 3:46-72. 1950.

2. Bastiansen, O., Lise Hedberg and Kenneth Hedberg. Reinvestigation of the molecular structure of 1,3, 5,7-cyclooctatetraene by electron diffraction. The Journal of Chemical Physics 27:1311-1317. 1957.

3. Beek, Allen (ed.). Elementary coding manual, Alwac III-E. Hawthorne, California, n.d. 93 numb. leaves.

4. Bethe, H. Zue theorie des durchgangs schneller korpuskularstrahlen durch materie. Annalen der Physik, Series 5, 5:325-400. 1930.

5. Bewilogua, L. Uber die inkoharente streuung der rontgenstrahlen. Physikalische Zeitschrift 32: 470-744. 1931.

6. Brockway, L. O. Electron diffraction by gas molecules. Review of Modern Physics 8:231-266. 1936.

7. Compton, A. H. and S. K. Allison. X-rays in theory and practice. 2d ed. New York, D. Van Nostrand, 1935. 828 p.

8. Cruft Electronics Staff (ed.). Electronic circuits and tubes. New York, McGraw-Hill, 1947. 994 p.

9. Davisson, C. and C. H. Kunsman. The scattering of low speed electrons by platinum and magnesium. The Physical Reviews 22:242-258. 1923.

10. Davisson, C. and L. H. Germer. Diffraction of electrons by a crystal of nickel. The Physical Reviews 30:705-740. 1927.

11. Debye, P. Zerstreuung von rontgenstrahlen. Annalen der Physik, Series 4, 46:809-823. 1915.

12. Dudley, F. B., G. H. Cady and D. F. Eggers, Jr. Pentafluorosulfur hypofluorite and thionyl tetrafluoride. Journal of the American Chemical Society 78:1553-1556. 1956.

13. Glauber, Roy and Verner Schomaker. The theory of electron diffraction. The Physical Reviews 89: 667-671. 1953.

14. Heisenberg, W. Uber die inkoharente streuung von rontgenstrahlen. Physikalische Zeitschrift 32: 737-740. 1931.

15. Ibers, James A. and Jean A. Hoerni. Atomic scattering amplitudes for electron diffraction. Acta Crystallographica 7:405-408. 1954.

16. James, R. W. Uber den einflub der temperatur auf die streuung der rontgenstrahlen durch gasmolekule. Physikalische Zeitschrift 33:737-754. 1932.

17. James, R. W. and G. W. Brindley. Some numerical values of the atomic scattering factors. Zeitschrift fur Kristallographie 78:470-476. 1931.

18. Karle, J. and I. L. Karle. Internal motion and molecular structure studies by electron diffraction. II. Interpretation and method. The Journal of Chemical Physics 18:957-962. 1950.

19. Logistics Research Inc. (ed.). Descriptions of Operation-Alwac III-E, electronic digital computer. Hawthorne, California, n.d. 22 numb. leaves.

20. Morse, Philip M. Unelastische streuung von kathodenstrahlen. Physikalische Zeitschrift 33: 443-445. 1932.

21. Mott, N. F. The scattering of electrons by atoms. Proceedings of the Royal Society of London, Series A, 127:658-665. 1930.

22. Mott, N. F. and H. S. W. Massey. The theory of atomic collisions. 2d ed. London, Oxford University Press, 1949. 388 p.

23. Pauling, Linus and J. Sherman. Screening constants for many electron atoms. The calculation and interpretation of X-ray term values and the calculation of atomic scattering factors. Zeitschrift fur Kristallographie 81:1-29. 1932.

24. Pinsker, Z. G. Electron diffraction. London, Butterworths Scientific Publications, 1953. 443 p.

25. Pirenne, M. H. The diffraction of X-rays and electrons by free molecules. Cambridge, England, Cambridge University Press, 1946. 160 p.

26. Shaffer, P. A., Jr., Verner Schomaker and Linus Pauling. The use of punched cards in molecular structure determination. II. Electron diffraction calculations. The Journal of Chemical Physics 14: 659-664. 1946.

27. Sproull, Wayne T. X-rays in practice. New York, McGraw-Hill, 1946. 615 p.

28. Waser, Jurg and Verner Schomaker. The fourier inversion of diffraction data. Reviews of Modern Physics 25:671-690. 1953.

29. Wierl, R. Elektronenbeugung und molekulbau. Annalen der Physik, Series 5, 8:521-564. 1931.